The University Of Southampton 1991

FACULTY OF ENGINEERING AND APPLIED SCIENCE

DEPARTMENT OF MECHANICAL ENGINEERING

THE WELDABILITY OF CHROMIUM HARDENED HIGH STRENGTH COPPER NICKEL ALLOY

by

Nicholas Joseph Brooksbank Walton

To Alison.

Acknowledgements.

The author wishes to thank Professor Roy A. Farrar, who supervised this work, to whom he is indebted for much helpful advice, encouragement and constructive criticism. Additionally, the willing cooperation and cheerful assistance of many members of the Mechanical Engineering workshop staff and the Engineering Materials laboratory staff are much appreciated.

Table of contents.

List of figures.

List of tables.

THE UNIVERSITY OF SOUTHAMPTON

Abstract

FACULTY OF ENGINEERING AND APPLIED SCIENCE

DEPARTMENT OF MECHANICAL ENGINEERING

Master of Philosophy

THE WELDABILITY OF CHROMIUM HARDENED HIGH STRENGTH COPPER NICKEL ALLOY

by Nicholas Joseph Brooksbank Walton

The as cast microstructures of chromium hardened high strength cupronickel alloys have been investigated using optical and scanning electron microscopy, energy dispersive analysis of X-rays and microhardness measurements. Fracture surfaces, and the closely adjacent matrix regions of cracks produced during welding, were examined using these techniques. A Theta dilatometer was used to conduct heat treatments intended to reveal the existence of low melting point grain boundary films. The effects of prolonged, high temperature heat treatment on the microstructure were observed. Weld tests were conducted to establish the effect of preheat temperature on cracking susceptibility.

The as cast alloy structures were found to be very heterogeneous, exhibiting severe dendritic chemical segregation (coring), undissolved original alloy additions and widespread shrinkage porosity. High temperature heat treatment caused chromium enrichment of second phase grain boundary particles, with consequent denudation of chromium in the narrow zone immediately adjacent to the boundaries. A minor reduction in the propensity for cracking during welding was produced with increasing preheat temperature.

The pronounced structural inhomogeneity is considered to cause a sufficiently wide disparity between the matrix and grain boundary strength and ductility, such that cracking along the grain boundaries becomes inevitable as contractional welding stress develops.

A model is proposed to explain the invariable occurrence of cracking in a narrow region parallel to, but separated from the fusion zone.

THE WELDABILITY OF HIGH STRENGTH COPPER-NICKEL-CHROMIUM ALLOY

1 Introduction.

Current naval practice is to use Nickel Aluminium Bronze alloys (NAB) for safety critical applications in the seawater systems of submarines. Cast components in these systems such as pumps, large valves, garbage ejector parts, condenser tube headers and access plates, water boxes and other large fresh / salt water heat exchanger components must be manufactured with high integrity where their application is such that failure would cause uncontrollable flooding, total immobilisation of the vessel or serious hazard to personnel.

Previous experience has shown that the weld repair of casting defects causes preferential corrosion in the heat affected zone (HAZ), by the sensitisation of the Kappa phase; thus leading to a reduction in the reliable life of components. This corrosion necessitates the costly revalidation or replacement of components several times during the design life of a submarine. In addition to the costs incurred when casting replacement parts and in conducting an inspection, the time taken to dismantle components for inspection and for the subsequent reassembly causes the vessel to be non-operational for considerable periods. NAB is therefore unable to meet the extended commission periods now required of ships of the fleet.

Replacement of the NAB components with castings manufactured using an alloy which would last the design life of the vessel would lead to large cost savings, decreased refitting time and increased overall efficiency. After conducting a survey during the 1970s, of all the

corrosion resistant casting alloy materials currently available, the Ministry of Defence Naval Architect decided the most suitable material with which to replace NAB castings in the seawater systems of submarines was a chromium hardened 70%Copper 30%Nickel alloy similar to that defined as CN1 in BS1400. Cast cupronickel alloys are compatible with the wrought Cu-Ni pipework and are resistant to fouling by marine growth. Additionally they have superior shock resistance in comparison with NAB. The alloy, originally developed by The International Nickel Company and given the designation IN768, was re-designated Naval Engineering Standard 824 (NES824) [1]. The NES listings of standards are replacing the previous Director General Ships documents.

The mechanical properties of the chromium hardened high strength copper nickel (HSCN) alloy defined in NES824 are broadly similar to those of NAB. Both of them are superior to those of plain 70/30 Cupronickel, Table 1.1, which could be used as an alternative to NAB but would lead to a considerable increase in the bulk and weight of cast components.

Alloy	0.2% Proof Stress MPa	UTS MPa	%Elong on 5.65/So
Cu-31%Ni-1%Fe-1%Mn	170	417	42
HSCN (Minimum values)	300	480	18
NAB	250	620	15

Table 1.1
Mechanical properties of 70/30 Cupronickel, HSCN & NAB.

The materials used to manufacture HSCN are mainly costly imported strategic metals but the quantity required for submarine use is small, in the order of 200 tonnes annually [2]. Consequently production costs are high with little scope for cost saving. For these reasons the desirability of producing sound castings at the first attempt is acute. Castings for submarine systems may be both physically large (1000 kg) and of complex geometric shapes. In this context there is a need for minor casting defects, of the type which may be considered inevitable in the production of a large a complex cast component, to be successfully repaired by welding after manufacture, in order that the casting should not have to be scrapped. Additionally, weld repair may become necessary due to wear and tear throughout the long service of a cast component. It is therefore vital that the alloy should be weldable.

Currently the weldability of HSCN has been found to be highly variable [3,4,5,6,7,8,9]. The alloy suffers from weld induced cracking in the HAZ which invariably occurs on the grain boundaries and this severely limits the use of the current alloy.

The work described in this thesis therefore seeks to explore the microstructure and reasons for cracking in the HSCN materials.

2. Review of Literature

It is not intended to confine this review specifically to the chromium hardened high strength cupronickel alloy referred to in the Introduction Section 1 of the work. Other more generalised aspects of weld cracking in metal alloys will be included where these are thought to be relevant to understanding the behaviour observed in HSCN.

2.1 Cracking in welds.

A sound basis of general information from which the discussion of potential weld cracking problems may be progressed is presented in the work of Baker and Newman [10].

If cracking is to occur in a metal, then initially strain must take place. In weld cracking, the critical strain is normally extremely localised, produced by differential expansion and contraction resulting from the intense heating and cooling involved during welding. The solid material adjacent to, or already deposited in the weld undergoes a cycle in which it is rapidly heated and then cooled while at the same time being plastically strained. The weld metal being deposited in the current run is also subjected to plastic strain as it cools. Thus the degree of success with which a material accommodates any strain imposed, will depend upon its hot ductility, and in particular, the hot ductility within a localised region and at a specific time and temperature during the welding cycle.

Baker and Newman [10] state that low ductility, either during or following welding, may be attributable to a number of conditions as follows:-

1. The presence of a thin liquid film between the solid metal grains, produced either by low melting point constituents concentrated at the grain boundaries, or where liquid films persist between the grains during the solidification process.

2. The presence of brittle films of solid material between the more ductile metal regions, e.g. as with sulphides in steels.

3. A reduction in the intrinsic ductility of the alloy system within a particular range of temperature, encompassed by the wider range between melting point and ambient temperature. This is considered to be caused by a change in the mode of plastic deformation which takes place with changing temperature.

4. Low intrinsic ductility resulting from phase changes in the material.

5. The introduction of gases into the metal during welding. A well known example of this is the effect which hydrogen has on both the weld metal and the heat affected zone (HAZ) in ferritic steels.

In some cases, the formation of micro-cracks during welding may be attributable to more than one of these mechanisms acting simultaneously.

In the parent metal HAZ, adjacent to the fusion boundary, high temperatures are achieved. This may result in the production of a localised liquid grain boundary film caused by melting of various types of inclusion, phases or segregated elements. The strain imposed during welding may be sufficient to produce cracks in these locally melted regions. In addition to ferritic steels, this problem is known to occur in face centred cubic (fcc) materials such as austenitic steels and nickel based

alloys.

In the context of weld cracking, high temperature may be regarded as that > 0.5 T_m where T_m is the solidus temperature in Kelvin; for HSCN this temperature range begins at 440°C (solidus approx. 1150°C).

Hemsworth et al [11] recognised two main types of high temperature cracking. The temperature ranges, with respect to the melting point, in which each of these occur are illustrated in Fig 2.1.

Type 1 cracking, caused by intergrannular films.

This is associated with the formation of a second phase film, distributed along surfaces in three dimensions. The film may be formed from elements deliberately added as part of the alloy (an intrinsic film), or from impurity elements which have become concentrated there by segregation (an extrinsic film). It may be intrinsically brittle, and thus crack when the thermally induced stress is developed. Alternatively, the film may melt and this is termed HAZ liquation cracking. It occurs where an alloy is heated to just below the solidus temperature of the bulk metal matrix, but at which temperature, pockets of liquid exist. Notable characteristics of HAZ liquation cracking are the jagged edges and varied opening widths of such cracks which may indicate locally enhanced pockets of melted material. The depth of penetration of liquation cracking, beyond the fusion boundary and into the HAZ, will depend on the melting range of the liquating phases. Additionally, cracking may penetrate further into the HAZ because it is linked also with the so called ductility dip phenomenon. Both types of cracking have been observed to occur in the same metal specimen. Examples of cracking caused by intrinsic films are found in aluminium - magnesium alloys and in boron and niobium hardened steels, notably boron

treated AISI 304 steel. Extrinsic films which cause this type of cracking are formed by the impurities sulphur and phosphorus.

Type 2 cracking:- The Ductility Dip phenomenon.

This occurs at boundaries which are essentially free from inclusions and liquated films and is associated with a reduction in the intrinsic ductility of the material. It is termed 'ductility-dip' cracking and it may be categorised into three sub groupings, according to where the cracks occur :-

a) In the heat affected zone.
b) In primary (single bead) weld metal.
c) In the weld metal reheated by multi-pass weld runs.

Ductility dip cracks have distinct metallographic features characterised by crack edges accurately following the grain boundaries and crack width varying gradually and with geometric regularity. Slip bands or thermal faceting or both will be evident on the otherwise uncontaminated fracture surfaces; these distinctive features are clearly shown in the fracture surface of a AISI 316 steel illustrated by Hemsworth [11]. Hadrill and Baker [12] observed Type 2 cracking occurring in a fully austenitic 25 Cr-20 Ni steel, although the cause of the reduction in ductility at elevated temperature was not determined. Rollanson [13] reported similar micro-cracking in multi-run weld deposits made on an 18 Cr-12 Ni-1 Nb alloy.

2.2 Grain boundaries

Grain boundaries in metal alloys are the interfaces between regions which differ in crystallographic orientation, composition or dimensions of the crystal lattice. They are non-equilibrium planar structural

defects and have high energy, typically 0.2 to 1.0 $J.m^{-2}$. In consequence, a polycrystalline material will always try to reduce the grain boundary area in order to reduce its free energy.

The concentration of solute present at the grain boundaries in cast metals is usually rather high because it becomes concentrated there during the solidification process. When welding is carried out, some regions in the HAZ achieve very high temperature such that the boundaries will tend to become mobile. Duvall and Owczarski [14], in their work on a nickel based high temperature alloy, showed that it is possible for the most mobile grain boundaries to break away from the concentration of solute, leaving it behind as a network in the matrix, outlining the former position of the boundaries. In such a case, the migrated boundaries will be freed from impurity and other solute contamination. Conversely, if the contaminated boundary is so firmly pinned that it is unable to break free, then it will continue to be subject to any effects which the contamination may cause.

Evans and Jones [15] studied the hot ductility of a series of extremely fine grained annealed Fe-Ni alloys, with tensile tests conducted at temperatures where these alloys were in the austenitic condition. They reported that good ductility and the low incidence of grain boundary cracking in a 36% Ni alloy, was always associated with grain boundary movement during testing, whereas in regions where grain boundary movement was not observed, cracking was severe.

Pinning of grain boundaries by large particles and shrinkage pores was commonly observed, after heat treatment, within the HSCN alloys investigated in the current work. The reduction in grain boundary mobility indicated by this is considered to be a highly significant contributory factor in developing the embrittlement

apparent in this fcc material.

Cracks along grain boundaries nucleate at a number of sites including grain corners and triple points, second phase or other particles and the serrations and ledges produced by the intersection of sub-boundaries and slip planes with the boundaries. Here, grain boundary sliding is the critical mechanism for crack nucleation and subsequent growth. Evans and Jones [15] proposed that if the boundary were sufficiently mobile it could move away from the features at which cracks nucleate; conversely, cavities which develop to a size sufficient to prevent grain boundary mobility, will produce embrittlement. The limiting case for this mobility would be where the boundary must move a distance equal to the diameter of a developing crack or cavity in the time taken for this defect to form. This work indicated that, at a constant temperature and strain rate, grain boundary mobility decreased rapidly with the addition of alloying elements and it was concluded that high ductility is associated with grain boundary mobility occurring as strain takes place.

In the current work, grain boundary micro-void formation was observed to take place during heat treatment at high temperature. These cavities may be expected to significantly inhibit boundary mobility in addition to reducing interfacial cohesive strength.

Davies and Evans [16] conducted an investigation into creep deformation at high temperature in which the nucleation of grain boundary cavities, leading to intergrannular cracking, took place. During the welding process, localised high rates of strain, similar to creep deformation at elevated temperature, will occur. Gittings and Williams [17] proposed that at high creep rates, cavity growth takes place by sliding at the boundaries which undergo maximum shear stress i.e. those oriented at

angles close to 45° to the stress axis. At lower strain rates the controlling factor is vacancy diffusion.

In work on intergrannular failure observed in a Mg-0.8%Al alloy which displayed ductility dip behaviour at 300°C, Evans [18] concluded the minimum ductility coincided with the maximum void growth rate. The rate of void growth was found to be proportional to the rate of grain boundary sliding.

Grain boundary sliding, whereby a pair of grains shear at their common interface, may occur either by movement taking place in a zone of finite width around the boundary or by shear confined completely to the interface. This mode of deformation becomes important at temperatures $> 0.45\ T_m$ [19] and is considered to contribute significantly to the promotion of intercrystalline weakness in metals at high temperature. Contamination by other elements is known to affect the rate of sliding e.g. small additions of lead (5 to 10 ppm) have been found to increase the sliding rate in copper by factors of 5 to 20 [19].

Where boundary sliding occurs in a narrow width zone, the tendency for sliding to take place will be affected by the strength. In a material hardened by short range spinodal decomposition or precipitation of a second phase, localised depletion of the alloy constituent which produces the hardening will have a pronounced effect. If a second phase exists at the boundaries, as is observed in HSCN, there is often also a zone free of precipitates adjacent to the boundary. In his review of grain boundary sliding, Stevens [19] noted a correlation between the strain occurring at high temperature and the ratio of precipitate depleted zone width to spacing of grain boundary precipitates.

Thomas and Nutting [20] suggested an explanation for

the observed relationship between grain boundary precipitate free zones and brittleness in age hardened aluminium alloys. They proposed that all plastic deformation will be confined to the soft precipitate free zones, with no dislocation movement occurring in the very strong, precipitation hardened matrix regions. As this takes place, the soft zone rapidly work hardens, loses ductility and then fracture takes place in a brittle manner. Starke [21] observed that narrow precipitate zones are present in most commercial alloys of this type. They are the result of solute depletion caused by heterogeneous precipitation of particles on, or preferential segregation of solute to the grain boundaries during cooling.

2.2.1 Summary of grain boundary effects.

Alloy structures in which a very strong matrix is developed are particularly susceptible to the nature of their grain boundary interfacial regions. This is the case in HSCN. In particular, the degree of grain boundary mobility is important as this factor invariably influences the resulting hot ductility. Grain boundary mobility is affected by the existence of impurity or other films. Additionally, particles and voids affect both the grain boundary mobility and cohesive strength. Factors which affect the rate of grain boundary sliding when under stress are similarly important as this movement eventually leads to the formation of cracks thus enhancing development of the brittle condition. The boundary sliding rate is increased by the existence of impurity films and of precipitate free zones adjacent to the boundaries.

2.3 High strength copper nickel

Copper nickel alloys display a marked reduction in ductility with increasing temperature, the true cause of

which is undetermined. Although the subsequent hot working of castings, after manufacture, is not normally conducted, this ductility dip phenomenon causes serious problems in the production of high quality castings in which weld repair may be an essential requirement.

A number of investigations into the cracking which commonly occurs when welding 70-30 and other Cu-Ni alloys have been reported [22-26].

Lee et al [22] proposed micro-segregation of low melting point impurities at the principal and sub grain boundaries to be the cause of hot cracking in a simple binary cast Cu-Ni alloy. In particular, the detrimental effects of segregated sulphur and phosphorus were noted and the possibility of a synergistic effect, produced by other impurities in combination with these, was also considered. The alloys which Lee used generally contained greater impurity levels than those specified as the maximum permissable in NES 824; in particular, they contained up to six times the maximum permitted P level and twice that for S, Pb and Te. It is assumed that these increased impurity levels will cause them to be more susceptible to grain boundary embrittlement than HSCN. In the course of his work, Lee additionally found that the cracking sensitivity of Cu Ni could be controlled by choice of welding parameters. He employed the Varestraint Test [23] which involves making a single weld pass using the tungsten inert gas process. The results indicated that reducing travel speed and increasing arc voltage both produced a significant increase in the cracking susceptibility. This would appear to suggest a strong correlation with nominal heat input and hence slower cooling times.

Holsberg [24] conducted work on a number of high strength 70-30 cupronickels, including a 2.8% Cr hardened alloy. This alloy displayed high temperature ductility

dip behaviour on cooling with minimum ductility at 770°C. Using the Varestraint testing method [23], he observed that all cracking took place in the melted region with none in the HAZ. In consequence he proposed that the cracking problem could be solved by use of the correct filler metal, subsequently reporting success in producing welds free from cracks in this Cr hardened material. Petersen [25] also reported that crack free welds could be produced in HSCN providing that the Cr content was less than 3.75% Cr; however, the levels of impurities present in the alloys used were not defined.

Scott [5] conducted a study into the weldability of a series of both cast and wrought niobium hardened HSCN alloys. While several forms of cracking were observed, the most serious and common form was sub solidus ductility dip type cracking in the HAZ of welds. This occurred in the HAZ, parallel to the fusion zone and 1 mm to 3 mm from it, no melting was observed. Cracking took place in the range of temperature between 600°C and 800°C at which the ductility minima exists. A very wide variation in cracking susceptibility of the various alloys used was reported, with no cracking being observed in the wrought material. Detailed chemical analysis of a number of impurities present in trace concentrations failed to indicate a significant element causing the cracking. Special alloys were manufactured containing known specific combinations of six impurities. This work produced an unexpected result whereby an alloy with high concentration of all six impurities displayed a better resistance to hot cracking than alloys with high concentrations of only three of the impurities. The possibility of a synergistic effect in which a favourable interaction between impurities takes place is suggested by this. Scott additionally conducted specific tests to show that post weld heat treatment caused cracking during the heating process in the temperature range 620°C to 630°C.

Savage et al [26] conducted weldability studies on 70-30 Cu-Ni and found the impurity antimony to be beneficial to weldability when in isolation in the alloy. However, when present in combination with phosphorus, a detrimental effect was produced as were the combinations of Sb-Fe and P-Fe. The majority of cracks observed in this work were initiated in the partially melted region and observed to contain traces of low melting point material deposited after the crack had opened. However, the cracks had also propagated well beyond the fusion zone indicating that although fusible films may be the cause, an intrinsic weakness at the grain boundaries also existed.

The findings of Scott and Savage are contradictory. While Scott demonstrated conclusively that cracking in a Nb hardened HSCN took place at the relatively low temperature of 620°C - 630°C and hence could not be caused by a fusible film, the work conducted by Savage on binary cupronickel alloys indicated clearly that cracking is caused by films melting at the grain boundaries immediately adjacent to the weld fusion zone. Savage concluded that weldability is impaired by the presence of minor alloying elements which lower the effective solidus temperature. Where these cracks were subsequently filled by molten material after initiation, the composition of the fused film was determined by an electron probe microanalyser.

Although the alloys investigated by Scott and Savage were not identical, the results are considered to indicate the very complex nature of the cracking problem and the probability that a number of independent factors are involved in producing the brittle condition.

If solute atoms are the cause of ductility dip cracking, then this is brought about by the segregation of such atoms to the grain boundaries. Evidence for this

type of segregation in copper based alloys has been obtained by Gavin [27] and by Kanno [28], for the elements Bismuth and Sulphur respectively, both using the sensitive Auger electron spectroscopy technique on intergrannular fracture surfaces.

Kanno investigated the hot ductility of a Cu - 0.7%Cr alloy, adding 0.15%Zr in order to establish the effect of this element. A significant improvement in hot ductility, occurring at temperatures in the region of 600°C, was produced by the Zr addition. Kanno considered six potential causes of intergrannular failure, specifically discounting all of these except the segregation of impurities to the grain boundaries. He observed very fine, sparsely distributed grain boundary precipitates and, due to this, discounted both precipitate fracture and decohesion at the precipitate interface as possible causes of intergrannular fracture.

This possible cause of embrittlement cannot be discounted in HSCN where the large and widespread Cr rich grain boundary precipitate particles are likely to contribute significantly to development of the brittle condition.

Kanno concluded that the improvement in hot ductility, brought about by the addition of Zr, is caused by the interaction of Zr with S to form zirconium sulphide. The formation of particles of this compound significantly reduces the concentration of S distributed in the form of a grain boundary film. Kanno detected the compound using Auger spectroscopy.

In the current work, S was not detected at the grain boundaries using EDAX analysis, although the chemical analysis provided by the manufacturers indicated the presence of this impurity. This was considered to indicate that the S present was distributed in a very thin film. Additionally, if Zr is to improve the hot ductility

of HSCN by combining with S, then it must first be dissolved into solution in the alloy. This was not found to occur with Zr existing in the form of undissolved original alloy additions.

In recent work on the weldability of thirty four individual cast HSCN alloys, Plumb [29] reported a general proclivity for improvement in welding response linked to reducing the impurity content. However, he also observed specific notable exceptions to this trend, where both very poor weldability was found in alloys with low impurity content and good weldability was found in alloys with high impurity content. Rigorous and repeated chemical analysis using a range of techniques, including glow discharge mass spectrometry, failed to indicate either a single element, or group of impurity elements which could be identified as consistently causing poor weldability. The breadth of Plumb's investigation is considered to indicate clearly the existence of additional factors, other than the impurity levels in the alloys, which significantly enhance the cracking susceptibility of HSCN.

Gavin et al [27] studied the effects of a number of a number of trace impurities detected in a commercial purity Cu-10%Ni alloy. He found the presence of tramp impurity elements decreased the intermediate temperature ductility of the alloy, with bismuth giving the most severe reduction and sulphur the least. The compositional limits could be specified for individual impurities, when isolated in simple alloys. However, these limits did not hold when the elements were present in combination in moderate amounts; in this event the effect of different impurities on ductility is found to be cumulative. Gavin developed a so called Bismuth Equivalent expression which is intended to enable the prediction of the ductility of an alloy containing a number of impurities :-

$$BiEquiv = Bi + 0.7Te + 0.4Pb + 0.2Se + 0.1S$$

where the composition of each element is given in ppm by weight.

Having calculated the Bismuth Equivalent value for an alloy, the minimum ductility may be determined from the graph of ductility vs bismuth impurity content Fig 2.2.

A discrepancy between the predicted and observed ductility values of commercial purity alloys suggests that an interaction between the impurity and alloying elements could be responsible for the excessively low ductility measured in the commercial alloy. Gavin also considered the possibility that precipitation of second phase compounds at the grain boundaries is likely to produce stress concentrating points and thus enhance the tendency for intergrannular cracking to occur at intermediate temperatures. The effect of individual elements in complex alloys is different from the effect observed for the same element in a simple (binary) alloy. The reason for this is unclear but may be due to differences in grain boundary structure, in diffusion properties or, as stated previously, to alloying and impurity element interactions.

At temperatures greater than 780°C Gavin observed recrystallisation occurring primarily at grain boundaries. This caused grain boundary cracks to become blunted thus producing an improvement in ductility at this elevated temperature. In the current work, weld induced cracking was invariably observed in a zone adjacent to, but separated from the weld fusion zone Fig 2.3. Recrystallisation in the narrow band between the fusion zone and the cracked region may account for this.

The work of Chubb and Billingham [30] showed clearly the effect which the additions of nickel have on the hot ductility of copper Fig 2.4. Their investigation of

nickel additions in the range 6-30 wt% Ni indicated a ductility minimum at 970K (700°C) in a binary Cu-30% Ni alloy. This was considered to be a consequence of nickel delaying the stress relieving recovery processes of grain boundary migration and recrystallisation. These workers with Gavin [27], also conducted detailed studies into the effect of trace impurities on the intermediate temperature ductility of a fine grained Cu-10% Ni alloy Fig 2.2. In this study, sulphur was reported to be relatively unharmful when in concentrations up to 750 ppm wt.

2.3.1 Summary of effects reported in cupronickels.

These numerous studies of various cupronickel and similar fcc alloys indicate that cracking is brought about by a number of discrete causes all of which are associated with the grain boundaries. These include :-

a) gross chemical segregation, often found in casting alloys where the constituent metals differ widely in melting point,

b) sluggishness in the rate of recrystallisation,

c) the presence of impurities, especially in the form of intergrannular films, but also as particles,

d) the presence initially or development under stress of grain boundary voids.

The cracking mechanism in HSCN, which operates at elevated temperature, is likely to be due to a number of causes operating simultaneously. It appears to be enhanced by increasing the rate of heat input during welding.

2.4 Proposed aims for the current study.

The review of literature in sections 2.1, 2.2 and 2.3 combined with consideration of the materials and other resources available, indicate that it would be appropriate to concentrate current investigation on the following aspects of HSCN alloy.

1. The macrostructure, the hardness and details of the microstructure in the as cast condition, with particular emphasis on the presence of impurities in the form of particles or inclusions.

2. The behaviour of the alloy at high temperature.

3. The existence of low melting point films.

4. The effect of welding parameters and the influence of plate temperature, both below and above ambient temperature, before welding.

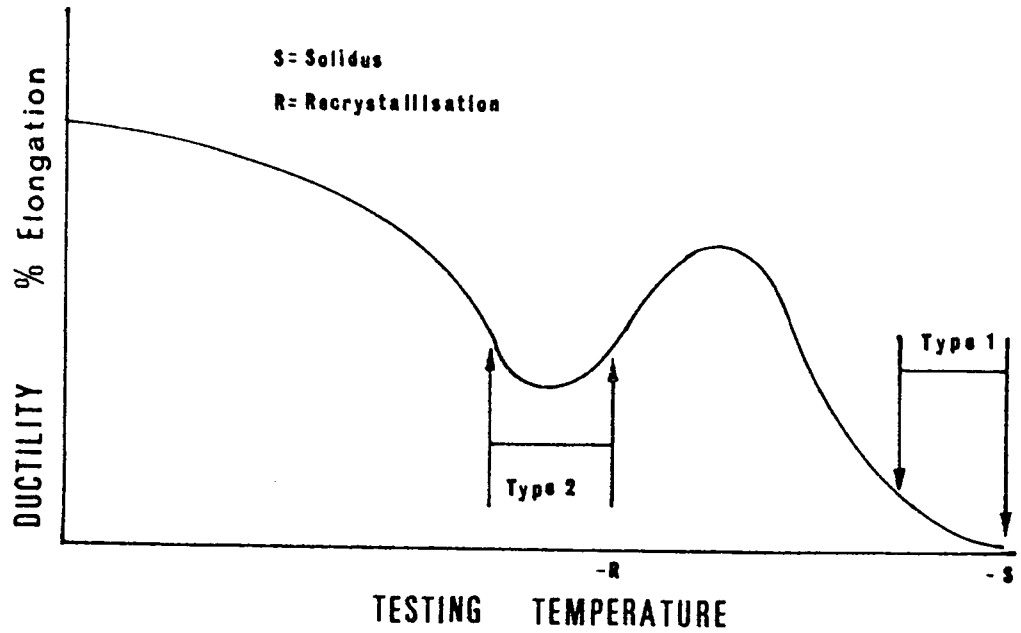

Fig 2.1 Temperature ranges in which Type-I and Type-II cracking occur (After Hemsworth)

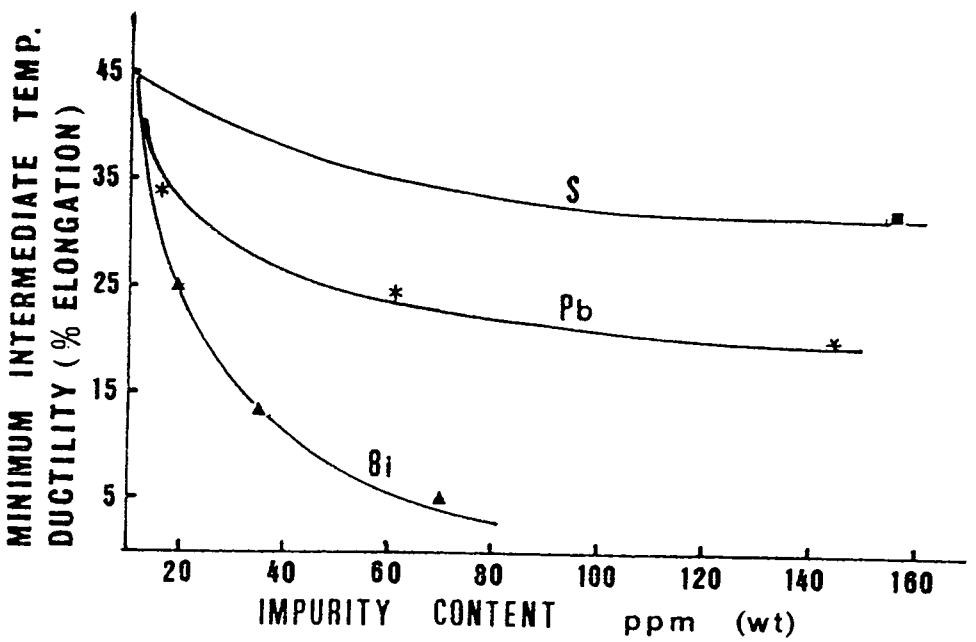

Fig 2.2 The effect of bismuth on the minimum intermediate temperature ductility of copper - 10% nickel alloy (After Gavin)

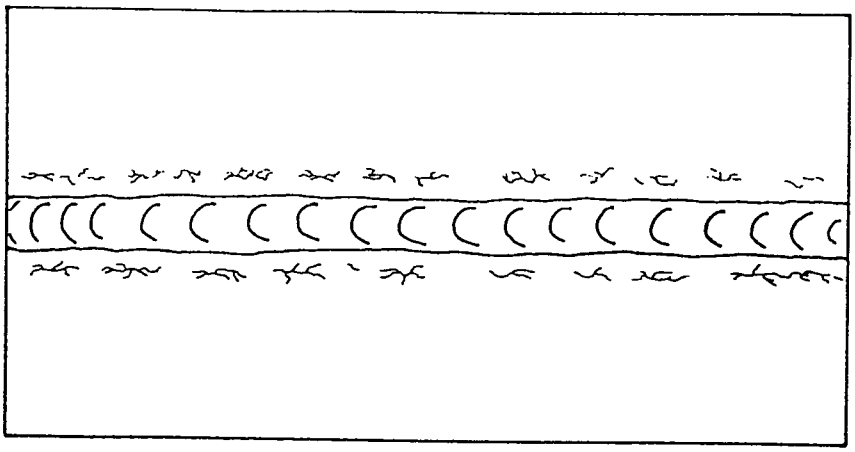

POSITION OF WELD INOUCED CRACKS

Fig 2.3

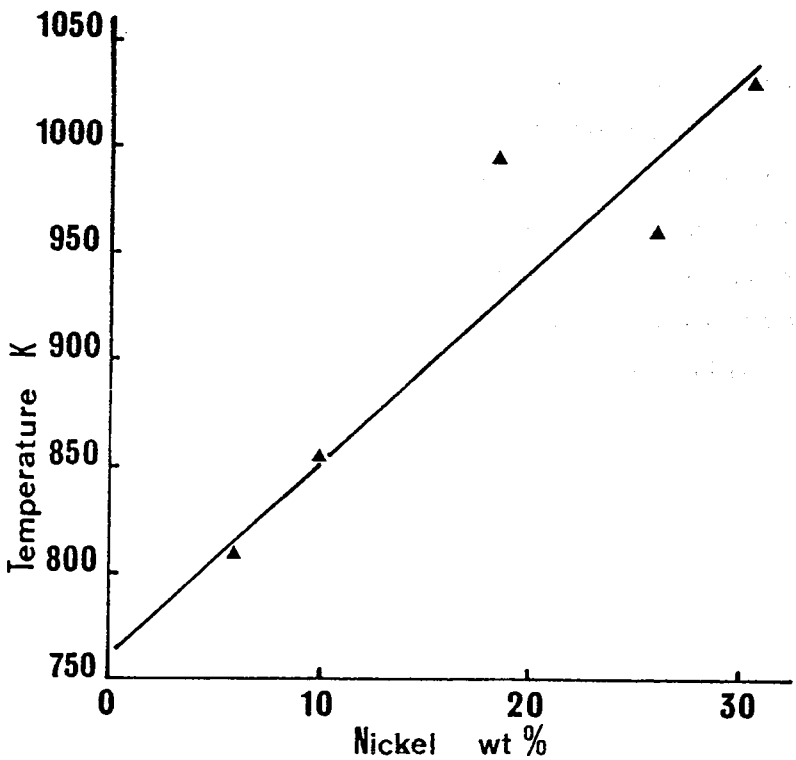

Fig 2.4 The effect of nickel on the temperature at which recrystallisation was first observed in binary Cu-Ni alloys (after Chubb and Billingham)

3 Experimental methods.

3.1 Materials

The work was conducted using cast alloy materials manufactured by the four foundries listed below in Table 3.1 to the specification NES 824, the chemical composition of which is listed in Table 3.2.

Supplier	Cast Number
Vickers Shipbuilders and Engineers Ltd. (VSEL)	CN4710
Wesley Brothers Ltd. (WBL)	3794
Aluminium Pressure Vessels (Paramount) Ltd. (APV)	RYG
Rosyth Naval Dockyard (RD).	RD 466

Table 3.1 List of manufacturers

The bulk of this material consisted of weld test plates 320 mm x 250 mm x 40 mm supplied by WBL. In consequence, the majority of the experimental work was conducted on this alloy with lesser amounts on two test plates supplied by VSEL. The alloy supplied by APV consisted of a valve body casting which had received a standard stress relieving heat treatment. The cast alloy manufactured by Rosyth Dockyard and reputed to be weldable [31], was supplied near the close of the period of experimental work and consisted of only a very small piece, 2 cm x 1.5 cm x 1 cm.

Commercial founders have expressed unwillingness to enter into contracts undertaking the production of HSCN alloys having very low and rigidly defined impurity levels, therefore a list of desirable, but not mandatory, impurity levels have been specified as Target Levels [1]. These are listed in Table 3.3. A chemical analysis for each alloy was supplied by the manufacturer. In addition

to these, the WBL alloy was analysed by the Admiralty Materials Laboratory at Holton Heath, Dorset. These analyses are listed in Table 3.4. The mechanical properties of the alloys are listed in Table 3.5.

3.2 Metallography.

Sections were cut from the test plates after discarding the first 10 mm from the plate end. These were polished to a 1um diamond finish, etched in dilute alcoholic ferric chloride and examined using the light microscope and a Cambridge Stereoscan 150 scanning electron microscope (SEM). Sections from weldments were selected to include HAZ cracks where these were discernible and were treated in a similar manner. Weldment sections, exhibiting surface breaking cracks, were opened mechanically by bending about the weld root. Additionally, small sections of the as cast material were prepared by grinding to a 600 grit finish, notching with a hacksaw and fracturing mechanically. The fracture surfaces were examined using the stereoscopic microscope and SEM.

Carbon extraction replicas of the three alloys were produced by first deeply etching the polished specimen surface with alcoholic ferric chloride and then applying an acetate film softened by acetone [32]. The acetate sheet was subsequently removed and sputter coated with carbon. The aim of employing this technique was to isolate the very small grain boundary precipitate particles from the matrix material, in order to accurately determine their chemical composition. Accurate chemical analysis of the particles while in the matrix is not possible owing to their small size (0.3um) compared with the normal spread of the electron beam in a solid sample. The technique was not totally successful due to damage sustained by the delicate carbon films when dissolving the acetate sheet. While the chemical composition of

extracted material was successfully measured by carrying out analyses in the discernible grain boundary regions, the particles themselves were not visible.

An extraction technique using well annealed very high purity aluminium as the extracting medium was also used [33]. This revealed zirconium particles, very small silica particles and a region showing the high degree of chemical segregation at a dendrite core.

3.3 Chemical Analysis.

Microstructural features observed by SEM were chemically analysed using the energy dispersive analysis of X-Rays (EDAX) technique. The dendritic segregation, ie coring, was measured and mapped using this technique. Additionally, the size and chemical composition of particles at the grain boundaries and within the bulk matrix were measured, within the limitation due to electron beam spread described below.

3.3.1 EDAX analysis accuracy.

The EDAX 9100 series, energy dispersive X-Ray analysis system uses a focused beam of incident electrons to excite the X-Ray spectrum within the sample being examined. The main advantage of this technique is that the beam of electrons may be focused, with great precision, by magnetic lenses, enabling localised analysis to be carried out. The electron beam may be finely focused to a spot 1um in diameter on the surface of the specimen, but spatial resolution is limited by spreading of the beam within the sample. When operating at 30 kV the electron beam will penetrate the specimen exciting a pear-shaped volume approximately 2 um in diameter. In consequence, the point count data will represent the average chemical composition within this volume. This limits the accuracy

of all spot analysis [34]. Additionally, counting statistics set a fundamental limit on the precision with which X-Ray intensities may be measured. Count times of 60 to 100 seconds were used which exceeded the times of 10 to 40 seconds normally sufficient to detect the major constituents. The detection limit for minor elements, and especially impurities, is determined by whether a peak may be distinguished from the continuous background X-Ray spectrum caused by decelerating incident electrons and a realistic figure for this detection limit is 0.5% to 0.7%. The sensitivity is worse for heavy elements ($Z > 30$) eg Zr, and for light elements ($Z < 12$) eg C,B. Silicon ($Z=14$) is close to the light element sensitivity limit and the concentrations observed for this constituent were often found to be higher than the values expected based on the bulk analyses data.

It is assumed that the greatest degree of segregation in HSCN will exist in the grain boundary region which may be far less than 2-3 um wide. In consequence the detection of very narrow films of impurities will not be possible using this technique, unless they are of sufficiently different composition to the matrix, when small indications may be possible.

3.4 Hardness Measurement.

Vickers hardness measurements were taken on polished and etched surfaces of bulk section specimens using a 10 kg applied load. Microhardness measurements were taken with a Matsuzawa Zeiki MHT-1 machine using a 50 gm applied load and surveys across individual cored dendrites were conducted using this equipment. Microhardness measurements across a weld section were also taken, from within the weld metal, across the HAZ to the parent plate.

3.5 Grain Size.

Grain size measurements were taken, using simple optical means, on the weld test plates where sections were polished and etched prior to measuring the rather coarse macrostructure.

3.6 Dilatometer tests.

Small cylindrical specimens, 7 mm in diameter and 10 mm long, were machined from the WBL and VSEL alloys. A flat surface was ground along the specimen and polished to enable subsequent examination. The specimens were heated to various temperatures under a vacuum of 10^{-4} torr or greater using a Theta dilatometer.

In this device the specimen was supported in the centre of a radio frequency inductive furnace between the tips of fixed and sensing fused silica rods. The temperature was monitored by a Pt / Pt-Rh thermocouple, the hot junction being joined by spot welding to the specimen surface Fig 3.1. During the heating cycle changes in length were monitored by a Dilaflex (Theta Industries patented) frictionless sensor Fig 3.2, the output from this device being linked to a chart recorder. The recorder pen movement magnification control was set to 1000 times magnification causing the full chart span to be used at a specimen temperature of 1180°C. With this magnification setting a step reduction in length of 3 um would be clearly discernible.

Initially hollow specimens were used. Subsequently, when the nature of the grain boundary effects produced by the heat treatments became apparent, solid samples were used to increase the volume of material for examination.

3.7 Weld Tests.

The test plates and flange of the valve casting were skimmed to remove residual sand and heavy oxide film from the as cast surface and weld preparations 10 mm deep with a 90° included angle were milled into the material. The plates were clamped to a steel beam prior to welding in order to ensure a high degree of restraint during the MMA welding process which was carried out with the plate initially at ambient temperature. Welds were made using direct current with the 3.25 mm diameter Stubbs 387 CR electrode positive (reversed polarity). The electrodes were baked at 100°C for one hour immediately before use to remove moisture. The welding current used was in the range 100-140 amperes with arc voltage of 22-25 volts. These settings produced energy input rates of 1.1 to 2.3 kJ per mm.

Subsequently the weld test blocks were sectioned and polished for examination using the light microscope and SEM.

3.8 Weld preheat temperature tests.

A series of welds were made, using a similar weld preparation, at initial and interpass temperatures of 0°C, 20°C, 100°C and 200°C. Subsequently the degree of weld cracking induced was measured sequentially on three different planes within the weld. The cracking susceptibility was defined as the length of cracking / the total length of sample measured.

Element.	Percentage by weight.	
	Not less than	Not more than
Ni	29.0	32.0
Cr	1.6	2.0
Fe	0.5	1.0
Mn	0.5	1.0
Si	0.2	0.4
Zr	0.05	0.15
Ti	0.1	0.2
Cu	Balance	
Impurity		
Pb	--	0.003
P	--	0.005
Bi	--	0.001
S	--	0.005
C	--	0.020
Co	--	0.020
B	--	0.001

Table 3.2. NES 824 (Issue 2) Chemical composition.

Impurity	Percentage by weight
	Not more than
Pb	0.0015
Bi	0.0005
S	0.003
C	0.006
Se	0.0005
Te	0.0005
As	0.001
Zn	0.003

Table 3.3 HSCN Impurity element target levels.

Element	VSEL4710 Cast 4710	WBL3794 Cast 3794	WBL3794 By Adm. Mat.Lab.	APV RYG
Ni	31.0	30.42	31.95	29.6
Cr	1.92	1.83	1.79	1.8
Fe	0.74	0.79	0.82	0.7
Mn	0.84	0.76	0.71	0.8
Si	0.29	0.33	0.32	0.2
Zr	0.11	0.07	0.005	0.05
Ti	0.095	0.07	0.004	0.13
Cu	Balance	Balance	Balance	Balance
Impurities				
Pb	0.004	<.001	0.0002	<.005
P	<.002	0.002	0.0017	<.002
Bi	<.0005	<.001	0.00005	***
S	0.001	0.001	<.001	<.004
C	0.002	0.005	0.006	0.01
Co	0.005	0.002	<.01	0.05
B	0.0008	<.001	<.0005	***
Se	***	<.00003	<.0002	***
Te	***	<.00003	<.0001	***
As	<.0005	0.00005	<.0002	***
Zn	***	<.001	<.0001	***
Nb	***	<.001	***	***

*** Not determined

Table 3.4 Chemical analyses of alloys used.

Alloy	0.2% Proof Stress MPa	UTS MPa	% Elongation
NES824 (Min. values)	300	480	18
WBL3794	340	536	22
VSEL4710	354	536	22
APV RYG	320	488	23

Table 3.5 Mechanical properties of alloys used.

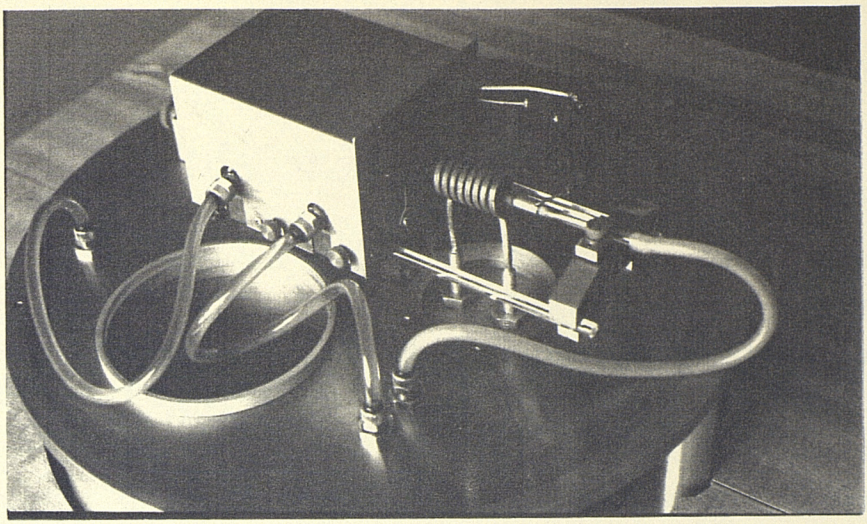

Fig 3.1 Theta dilatometer furnace and specimen

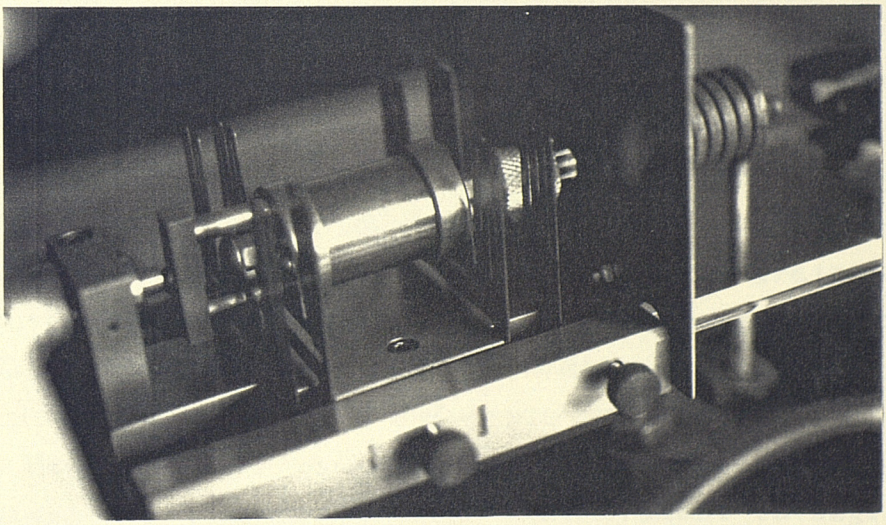

Fig 3.2 Theta dilatometer Dilaflex sensor

4 Results.

4.1 Chemical segregation (coring)

The alloys were found to exhibit both pronounced chemical segregation and widespread shrinkage porosity, both being a consequence of the high pouring temperature used to achieve acceptable fluidity in production. Fig 4.1 shows an overview of the as cast macrostructure, while Fig 4.2 shows a general view of the coring and the shrinkage porosity found in all three casts. Cast RYG had received a 450°C stress relieving heat treatment which had caused recrystallisation to commence; it is considered likely that the weld heat cycle would produce a similar effect within the HAZ. Fig 4.3 shows the severe extent of coring in the VSEL casting at higher magnification where some grain boundary migration is apparent.

Chemical segregation in the APV, VSEL and WBL alloys was measured by EDAX for those elements whose bulk analysis values were greater than 0.2% wt. A region was selected in each alloy where a clearly discernible dendrite arm centre, etched to dark appearance when viewed in the SEM, was adjacent to a grain boundary. A series of spot analyses were then taken between these two positions. The results, listed in Tables 4.1.1, 4.1.2 and 4.1.3 give the bulk analysis data supplied by the manufacturers, the composition measured at dendrite core and grain boundary and the linear distance over which each spot survey was made. The percentage change in chemical composition, at both the dendrite core and grain boundary, with respect to the bulk analysis values are given in brackets and this indicates the propensity for each element to segregation. Fe, followed by Cr showed the greatest tendency to segregation and this result was consistent in all three alloys. This behaviour has been observed previously by Sahoo [35]. The full segregation data for each alloy is plotted in Figs 4.4, 4.5 and 4.6. The maximum rate of

change of chemical composition with respect to distance was calculated from these graphs. These data are included at the final column of each of Tables 4.1.1, 4.1.2 and 4.1.3.

4.2 Microstructural observations

Specimens from the APV, VSEL and WBL alloys were ground, polished and lightly etched in dilute (10%) alcoholic ferric chloride, then examined using the SEM. Apart from the severely cored microstructure noted above, four distinctive microstructural features were observed and are defined as Types A to D.

Type A

The Type A feature is illustrated in Figs 4.7 and 4.8. These are equi-axed grain boundary particles of approximately 0.8 um in size, evident on all grain boundaries at an average spacing of 4um in the APV, VSEL and WBL alloys. Type A particles were found to be rich in Cr and Si and, to a lesser degree, Zr. Fig 4.9 shows the range of compositions measured in this type of particle found commonly in all three alloys.

The spacing of this type of particle in the Rosyth Dockyard alloy appeared to be very much closer, ie. <1 um, but this observation is based on a rather limited examination of casting RD 466.

Type B

The Type B feature is illustrated in Fig 4.7 and 4.8. These are larger, zirconium rich particles, of average size 3 um or greater, observed usually at the grain boundaries but also occasionally within the grains. They were far less widespread than the very frequently observed Type A particles, but nevertheless were easily discernible due to their large size. The measured Zr

content in these particles ranged between 33% and 92% with the analyses less frequently also indicating Ti. Fig 4.10 shows the range of composition measured in them.

Titanium and zirconium are added to the melt as a final deoxidising treatment immediately prior to pouring and after all other checks and adjustments of the composition have been made [36]. Additionally, Zr is considered to improve the hot ductility of wrought HSCN and is therefore included in the cast alloy to produce a similar effect. If this element remains undissolved, as is shown throughout this work, it is unlikely to fulfil this function. The Type B particles are assumed to be alloy additions which did not dissolve into liquid solution during manufacture of the alloys.

Type C

The appearance of the Type C feature, in two different alloys, is shown in Figs 4.11 and 4.12. This grain boundary feature was observed very rarely, and in the APV and VSEL alloys only. It is distinguished by its long slender shape (10 um x 0.3 um) and is rich in Si and Zr. Fig 4.13 shows the range of compositions measured in two of these particles.

Type D

The Type D feature is illustrated in Figs 4.7, 4.8 and 4.14. It is observed frequently in the interdendritic regions and especially near to grain boundaries, often leading from a Type A particle. Having a narrow vein-like appearance, of width approximately 0.1 um, the feature is rich in silicon; Fig 4.15 shows the range of compositions measured in this feature although the accuracy of the data is limited due to the very narrow size of this feature.

Although the Ni content measured in the Type D feature was similar to, or marginally lower than, the bulk analysis values measured in the three alloys, the coring

survey has shown the grain boundary regions to be denuded of Ni. In consequence this feature is considered to be rich in both Ni and Si and is probably a compound of these two elements.

4.3 Hardness observations

4.3.1 Macro-hardness

The castings were sectioned, polished and etched prior to taking hardness readings using a Vickers machine with a 10 kg load. Measurements were taken commencing adjacent to the edges, then traversing the centres of the cast plates and one flange of the APV valve body. No wide variations in hardness were observed between these two regions. The mean average of at least 10 hardness readings taken on each alloy were calculated and these are listed in Table 4.2.1. On the APV alloy, two hardness readings of 190 and 197 measured very close to the outside edge of the casting were discarded as they differed considerably from all other hardness values measured throughout the main volume of the alloy. The macro-hardness mean average values were found to be similar in all three alloys with the WBL 3794 material being marginally harder than the other two.

4.3.2 Micro-hardness

The microhardness measurements were taken using a 50 gram load applied for ten seconds. This was found to produce consistent hardness results in each region examined, while making an impression small enough to distinguish between the dendrite cores and grain boundaries. The mean average microhardness results for dendrite centres and grain boundaries are listed in Table 4.2.2. It was not possible to measure the hardness of the grain boundary particles observed in the SEM with confidence due to their small

size.

The range of microhardness values further illustrates the degree of chemical segregation and consequent wide variation in strength within individual grains. In particular, the WBL 3794 alloy mean average macro-hardness value of VPH 174 (Table 4.2.1) is very similar to the micro-hardness value of 177 (Table 4.2.2) measured at the dendrite cores. The combination of these two measurements indicates that the matrix of this alloy has uniform fairly high strength. However, the narrow grain boundary region, with mean average VPH 140 (Table 4.2.2), is by comparison very weak.

The maximum of all hardness values (measured at the dendrite centres) and minimum of all values (measured at the grain boundaries) are listed in Table 4.2.3. These clearly indicate the existence of an intrinsic weak potential fracture path at the grain boundaries of these alloys. In particular this is suggested by the minimum micro-hardness value of VPH 98 measured in the WBL 3794 alloy.

4.3.3 Weld test micro-hardness survey.

The WBL 3794 alloy weld test plate was sectioned, polished and etched. A series of micro-hardness measurements was taken commencing in the weldmetal then traversing the fusion and heat affected zones as shown in Fig 4.16. The results are given in Table 4.3.1. Fig 4.17 shows the fusion zone where partial melting of the interdendritic regions has occurred. Subsequent chemical analysis of this region by EDAX, combined with the micro-hardness results, confirmed that the copper rich interdendritic regions melt before adjacent regions rich in nickel in this zone. The four micro-hardness impressions are, from left to right, points 6,7,8 & 9 listed in Table 4.3.1.

The chemical analysis of the weld metal was found to be similar to the bulk analysis of the alloy. The weld root run hardness was greater than that of the subsequent weld runs. This hardening effect was considered to be a consequence of the root run weld metal being reheated by subsequent runs, thus enhancing operation of the spinodal decomposition hardening mechanism [37].

4.4 Grain size.

The grain structure of all three alloys was coarse, with regions close to the casting surface being clearly of columnar structure. This condition, in addition to the severe chemical segregation, is a result of the high pouring temperature. The WBL alloy had a central region of more equi-axed microstructure due to having been cast in thicker section than the VSEL alloy. The average grain size measurements are listed in Table 4.4.

RYG	3.0mm x 3.0mm	
VSEL	10mm x 2.5mm	
WBL	15mm x 2.5mm	near to the surface
	2.5mm x 2.5mm	in the central region

Table 4.4 Average grain size

A major detrimental effect produced by coarse grain size is to reduce the total grain boundary area existing throughout the casting. Impurity atoms, present in a homogeneous liquid solution, will be concentrated to this region during the solidification process, as they will remain dissolved in the last liquid to freeze. Hence, the reduction in total grain boundary area resulting from coarse grain size will have the effect of increasing the thickness and concentration of any impurity film which may

be present.

4.5 Weld tests

The cast plates and a flange from the APV valve body were skimmed to remove surface defects and weld preparations, with 90° included angle, were machined into the new surfaces. The castings were clamped to a steel beam to ensure restraint during welding and the initial test welds were made with the material at room temperature using electrodes baked before use to remove moisture.

In these tests, weld cracking was not evident in either the APV or VSEL castings. Surface breaking cracks were clearly evident in the WBL alloy adjacent to and on both sides of the final run. This test plate was sectioned at positions selected to include weld cracks.

4.5.1 Weld crack profiles

The specimens were polished, cleaned ultrasonically to remove polishing debris from the cracks, etched and examined using the SEM.

All weld induced cracks observed by this method were found to propagate along grain boundaries and none were observed commencing in the fusion zone. Fig 4.18 shows a convoluted crack at a grain boundary approximately 1 mm from the fusion zone, discernible at the right of the photograph. The crack initiation points were always observed to be distant from the fusion zone, usually by approximately 0.5 to 1 mm. as is illustrated in Fig 4.19. A weld crack propagating towards the fusion zone from an initiation point remote from this region is shown in Fig 4.20. This suggests that the melting of a thin impurity film during the weld cycle is unlikely to be the fundamental cause of cracking. The region close to the

fusion zone, observed to be free from weld cracks, will be heated to a greater temperature during the weld cycle than the point where cracking is seen to commence. In consequence, if a low melting point film were the cause, cracks would be expected to propagate from the fusion zone into the parent plate. This was not observed.

Chemical analysis, including detailed spot surveys across the regions ahead of the advancing crack tips, occasionally indicated normal and marginally high Ni content in addition to regions of high Cu content as expected, due to coring. This suggested grain boundary migration had occurred, either during welding or the prior stress relieving heat treatment.

Particles observed both in cracks and on the grain boundary ahead of the advancing crack tip were examined. Fracture usually took place at these by de-cohesion of the particle/matrix interface Fig 4.21, but occasionally occurred across the particles themselves.

The etching treatment revealed a region adjacent to the grain boundary with a variable width of approximately 0.5 to 1.5 um, where the surface appeared to be featureless Fig 4.21, 4.22 and 4.23 illustrate this. Analysis of the particles on the grain boundaries indicated enrichment in Cr, Ni and Si. This suggests a reaction takes place at elevated temperature during welding, whereby the matrix immediately adjacent to the grain boundary is denuded of those elements intended to stiffen it, as growth of the grain boundary particles takes place, thus further weakening this intrinsically weak region.

4.5.2 Weld crack fracture surfaces

Specimens containing weld induced cracks were sectioned to 2.5 mm thickness and opened mechanically to expose the

fracture surface. These were mounted and examined in the SEM.

The exposed undulating interdendritic fracture surfaces were scaled and discoloured by oxide near to the original plate surface, Fig 4.24. Within this scaled region, the surfaces of shrinkage pores were clearly thermally etched and did not exhibit the scaling evident in immediately adjacent regions, Fig 4.25. Thermal etching indicates that a surface, such as a shrinkage pore or newly fractured region, was present at, and exposed to high temperature.

Closer to the weld crack root, in the mechanically opened specimen, a region was evident where thermally etched undulating surface, free from scaling, surrounds smaller regions of dimpled ductile failure Fig 4.26. It is concluded that the thermally etched region is a new surface, fractured during the welding process and that the regions of ductile failure were produced when mechanically opening the weld crack. Fig 4.27 shows the crack root region at the commencement of the ductile fracture through the remainder of the specimen thickness. No trace of a fused impurity film is visible, nor was a film detected by EDAX. It is acknowledged that this EDAX equipment is an accessory to the Cambridge SEM and not a dedicated microprobe analysis system. It is possible that a very thin impurity film existed and may have been detected by a more sophisticated and accurate analytical method such as Auger spectroscopy.

4.5.3 Weld preheat tests

Weld test blocks were prepared as described previously. The plates were clamped to a steel beam to ensure restraint during welding and welds were made with initial preheat and interpass temperatures of 0°C, 20°C, 100°C and 200°C. After cooling, the plates were cropped to remove

surplus material, the weld bead reinforcement was removed and the length of the weld ground, polished and etched. Cracked regions were revealed using dye penetrant and the total length of cracks was measured. This process was repeated at 2mm and 4mm below the original plate surface summing the total crack length observed.

A cracking susceptibility index was calculated for each preheat temperature using the expression :-

$$\text{Cracking susceptibility index} = \frac{\text{Total length of cracking}}{\text{Length of weld test block}}$$

The results, which are listed in Table 4.5, indicate the possibility of a reduction in cracking susceptibility with increasing weld preheat and interpass temperature although they are inconclusive. The tests conducted at 20°C and 100°C preheat temperature were both repeated with widely differing results being recorded in the similar tests. Additionally, it is known that the Fleet Maintenance and Repair Authority Laboratory at Portsmouth Naval Dockyard have conducted tests with 450°C preheat without detecting a reduction in weld cracking [31].

The weld test block used for the 200°C preheat test was given a pre-weld stress relief heat treatment at 450°C for two hours. This treatment was found to have produced crack like defects in the surface before welding. A similar effect was observed during the post weld heat treatment of a niobium hardened HSCN by Scott [5].

4.6 Dilatometer tests

A Theta dilatometer was used to heat specimens under a vacuum of 10^{-4} Torr or greater. Two types of test were conducted :-

1. A variable temperature test in which a hollow specimen of 1mm wall thickness was heated and held, during a continuous sixty minute period, at a series of temperatures in the range 500°C - 1080°C. This test was designed to reveal the presence of a thin, low melting point, intergrannular impurity film by detecting a sudden reduction in the specimen length, as such a film melted.

2. A series of tests in which a polished specimen was heated and held for an extended period at a set temperature in the range 500°C - 1180°C. The specimens were then examined in the optical microscope and SEM both on the previously polished surface and on subsequently sectioned internal surfaces. The aim of these tests was to detect changes in microstructure occurring at elevated temperature.

For the best resolution of changes in length caused either by thermal expansion or some other phenomenon, it is desirable to use the full span of the chart recorder. This was achieved, when testing 7 mm long HSCN specimens in the temperature range 20°C to 1180°C, by setting the pen movement magnification to 1000 times. At this setting, a 1 um change in specimen length produces 1 mm of pen recorder travel. This sensitivity was considered adequate to detect a 3 um step reduction in length, such as may have been produced by the action of the support rod spring force, if an intergrannular film had melted. No such abrupt reduction in length was observed during the variable temperature test which encompassed the known

ductility dip range of temperatures. It was therefore concluded that an impurity film with low melting point was not the cause of cracking during welding in WBL 3794 HSCN.

The initial isothermal dilatometer tests established that Cu evaporates from solution at the specimen surface, especially from the grain boundaries, at temperatures greater than 800°C. This is illustrated in Fig 4.28. Subsequent EDAX analysis indicating the substantial loss of copper from the specimen and coating of the HF furnace specimen support quartz rod surfaces with copper confirmed this. Solid dilatometer specimens were subsequently sectioned after heat treatment to enable accurate chemical analysis to be conducted free from error due to this surface effect. The silicon rich vein-like feature (Type D in section 4.2) began to break up at 800°C and was not observed in specimens heat treated above this temperature. Grain boundary migration, illustrated in Fig 4.29, occurs during the stress relief heat treatment conducted at 450°C. The boundaries traverse the old cored matrix and may become pinned by shrinkage pores which are common throughout the structure. This is illustrated in Fig 4.30. Numerous grain boundary voids, shown in Fig 4.31, developed in the specimen heat treated at 900°C causing further weakening of this potential fracture path.

The chromium rich grain boundary particles (Type A, section 4.2) contain approximately 4%Cr when the alloy is in the as cast condition. These particles became enriched in Cr at elevated temperature and with prolonged time at temperature in the range 700°C to 1000°C. A typical Cr content of the enriched particles was 30%Cr with the maximum Cr content measured being 48.5%Cr in a specimen heat treated for 15 minutes at 1000°C. The enrichment of grain boundary particles in Cr took place by denuding adjacent regions of this element. Fig 4.32 shows the thermally etched external surface of a specimen heat

treated at 970°C for 15 minutes including a migrated grain boundary where particles averaging 13% Cr content are embedded in a matrix of 2% Cr content. Fig 4.33 illustrates the acid etched internal surface of a specimen heat treated at 800°C for 15 minutes. Grain boundary particles, averaging 14% Cr have developed, the richest concentration measured in these being 28% Cr. The Zr and Ti rich particles (Type B, section 4.2) remained insoluble in a specimen heated to 1150°C for 15 minutes, as shown in Fig 4.34, despite partial melting of the matrix occurring at this temperature shown in Fig 4.35. This is considered to clearly indicate the inherent difficulty in causing Zr to become dissolved into solid solution in this alloy.

Element	Bulk chemical comp. wt%	Dendrite core comp. wt%	Grain boundary comp. wt%	Max. rate of change of comp. wt% um^{-1}
Cu	66.6	60 (-10)	76 (+14)	+167
Ni	29.6	35 (+18)	21 (-29)	-152
Cr	1.82	2.22(+22)	1.17(-36)	- 11
Fe	0.7	1.5 (+114)	0.42(-40)	- 6
Mn	0.8	0.8 (0)	0.68(-15)	- 1
Si	0.2	No segregation of Si was detected. The average Si content measured was 0.38%		

Table 4.1.1 Alloy APV RYG coring survey.
Survey distance :- 123 um.

In table 4.1.1, the figures in brackets indicate the percentage change in composition with respect to the bulk analysis data.

Element	Bulk chemical comp. wt%	Dendrite core comp. wt%	Grain boundary comp. wt%	Max. rate of change of comp. wt% um^{-1}
Cu	65	54 (-17)	75.6 (+16)	+517
Ni	31	40.2 (+30)	21.7 (-30)	-361
Cr	1.92	2.9 (+51)	1.06(-45)	- 47
Fe	0.74	1.18(+59)	0.3 (-59)	- 34
Mn	0.84	0.91(+8)	0.66(-21)	- 15
Si	0.29	No segregation of Si was detected. The average Si content measured was 0.6%		

Table 4.1.2 Alloy VSEL 4710 coring survey.
Survey distance :- 80 um.

In table 4.1.2, the figures in brackets indicate the percentage change in composition with respect to the bulk analysis data.

Element	Bulk chemical comp. wt%	Dendrite core comp. wt%	Grain boundary comp. wt%	Max. rate of change of comp. wt% um^{-1}
Cu	65.7	55 (-16)	72 (+10)	+670
Ni	30.4	39 (+28)	25 (-18)	-875
Cr	1.83	3.03(+66)	1.22(-33)	- 63
Fe	0.79	1.35(+71)	0.43(-46)	- 27
Mn	0.76	0.97(+28)	0.6 (-21)	- 10
Si	0.33	No segregation of Si was detected. The average Si content measured was 0.56%		

Table 4.1.3 Alloy WBL 3794 coring survey.
Survey distance :- 65 um.

In table 4.1.3, the figures in brackets indicate the percentage change in composition with respect to the bulk analysis data.

Alloy	APV RYG	VSEL 4710	WBL 3794
Mean average	HV.	HV.	HV.
hardness	165	167	174

Table 4.2.1 Macro-hardness test results - 10 kg load.

Alloy	APV RYG	VSEL 3710	WBL 3794
Average for:-	HV.	HV.	HV.
Dendrite cores.	171	180	177
Grain boundaries.	135	142	140

Table 4.2.2 Micro-hardness test results - 50 g load.

Alloy	APV RYG	VSEL 4710	WBL 3794
	HV.	HV.	HV.
Maximum value	183	192	188
Minimum value	96	134	98
Hardness range	87	58	90

Table 4.2.3 Maximum and minimum micro-hardness values.

Point No.	HV.	Point No.	HV	Point No.	HV.
1	137	11	160	21	161
2	137	12	124	22	167
3	143	13	127	23	101
4	161	14	125	24	100
5	157	15	137	25	164
6	153	16	144		
7	145	17	160		
8	127	18	156		
9	126	19	133		
10	104	20	177		

Table 4.3.1 Weld test microhardness survey results.

Weld Preheat temperature	Cracking susceptibility index		
	Test 1	Test 2	Combined results Tests 1 & 2.
0°C	3.96	----	3.96
0°C	0.2	2.2	1.2
100°C	0.012	4.45	2.33
200°C	0.56	----	0.56

Table 4.5 Results of weld preheat tests.

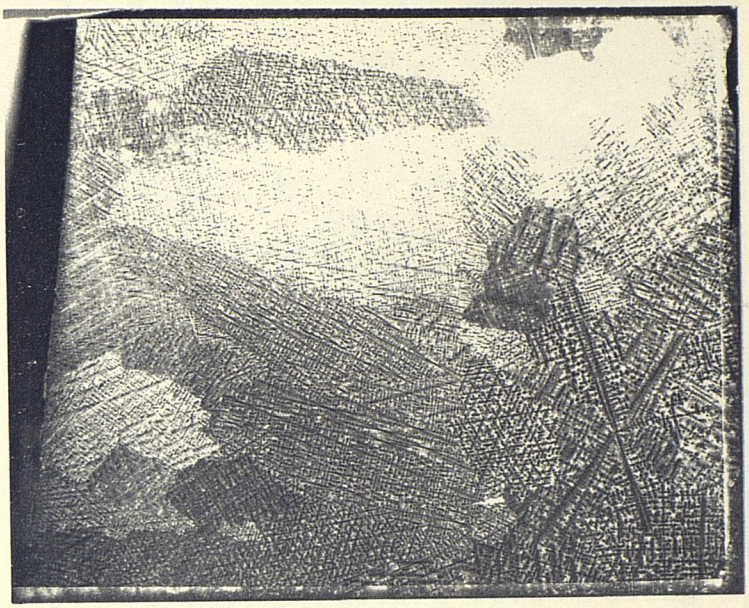

Fig 4.1 As cast structure typical of the alloys used. VSEL-4710. x6

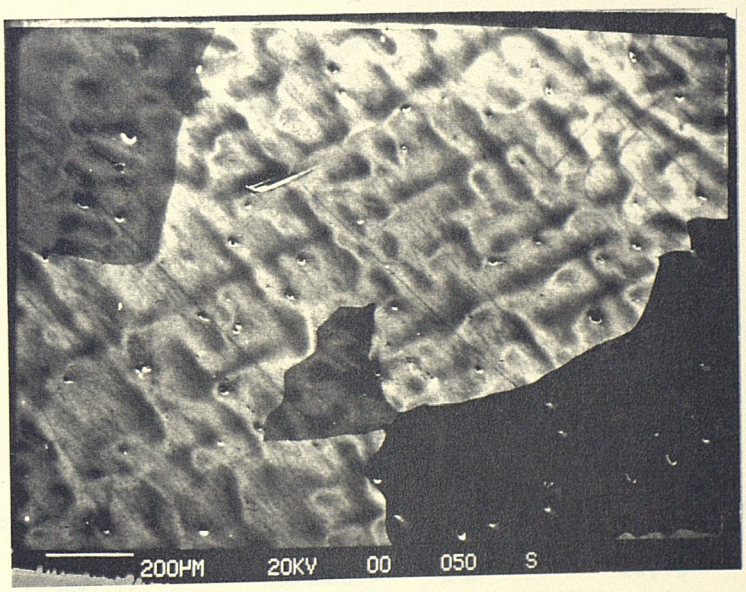

Fig 4.2 As cast structure illustrating widespread shrinkage porosity. APV-RYG. x60

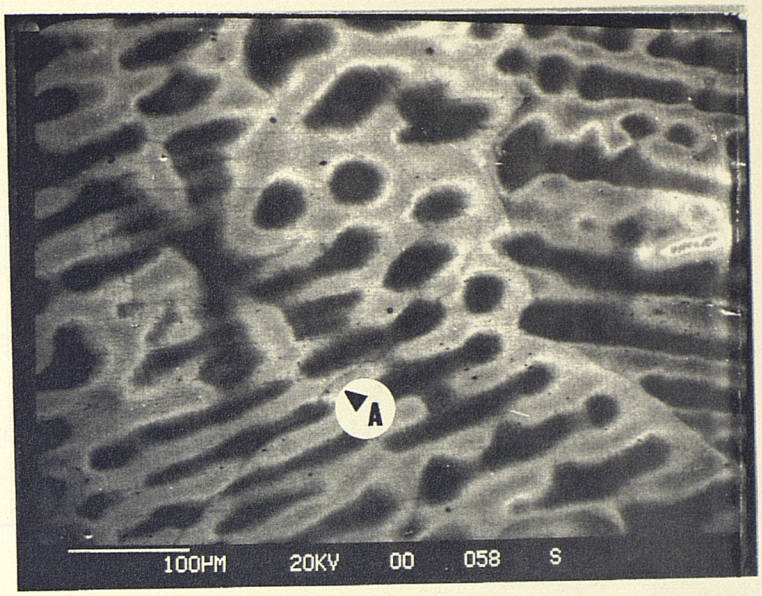

Fig 4.3 As cast structure illustrating dendritic segregation (coring). VSEL-4710. x160

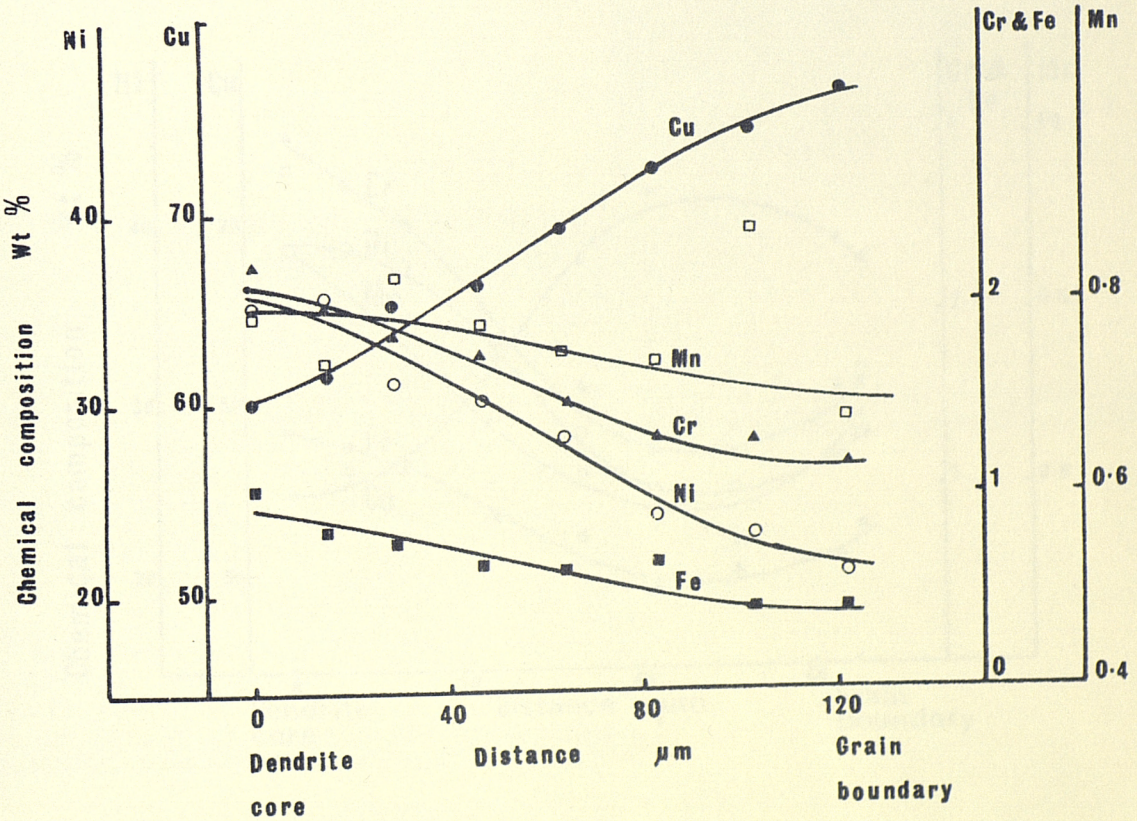

Fig 4.4 Chemical segregation graph for APV-RYG.

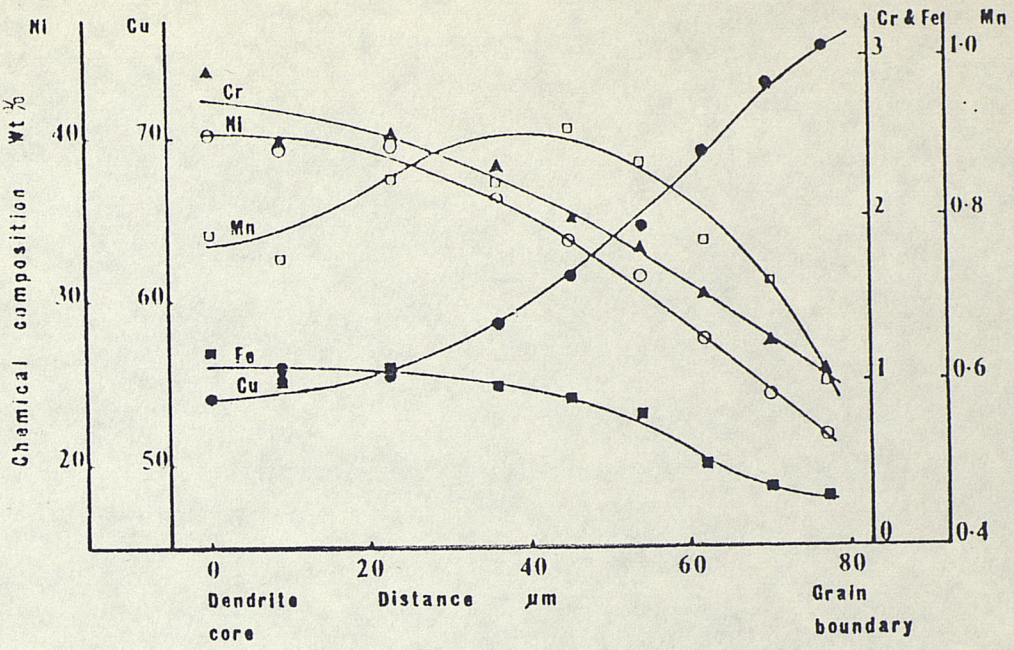

Fig 4.5 Chemical segregation graph for VSEL-4710.

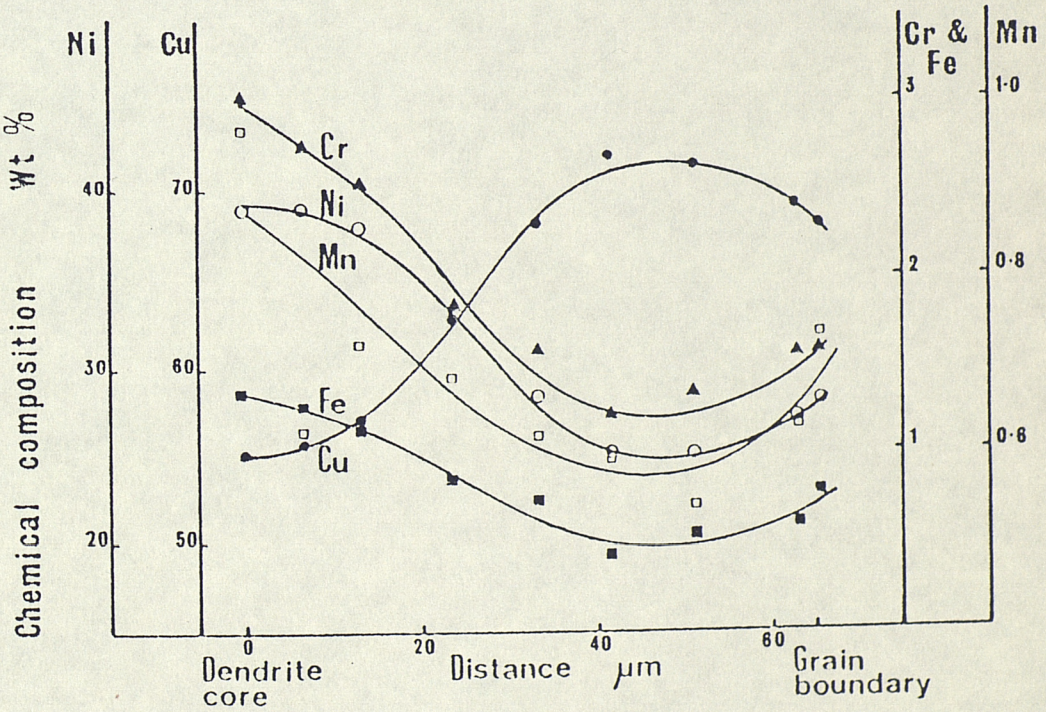

Fig 4.6 Chemical segregation graph for WBL-3794.

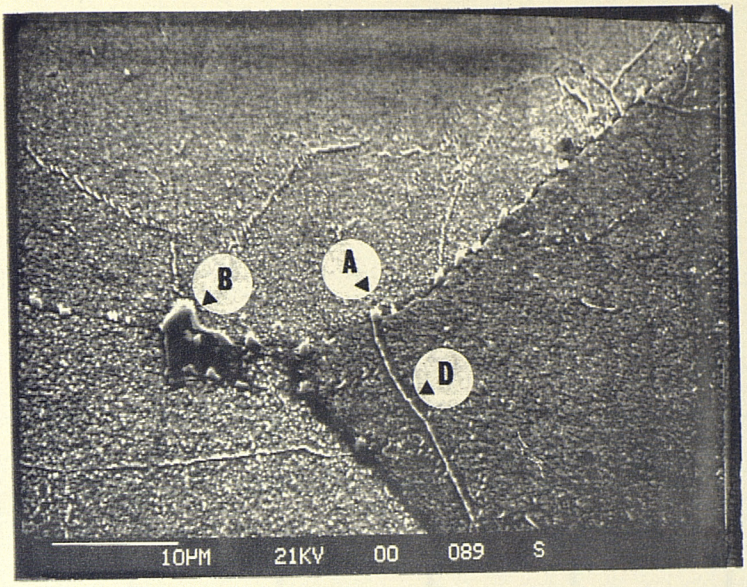

Fig 4.7 Microstructure of APV-RYG illustrating type A, B and D features. x1650.

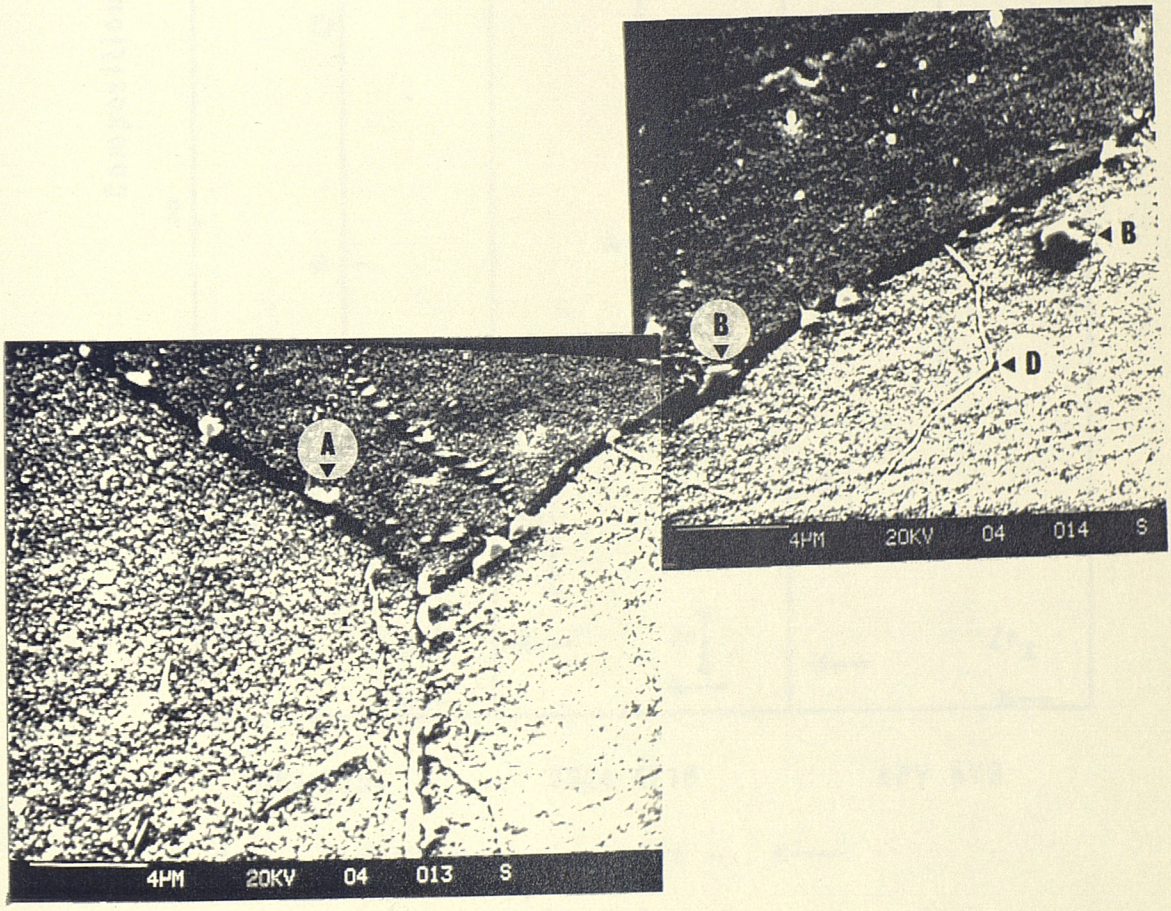

Fig 4.8 Microstructure of WBL-3794 illustrating type A, B and D particles. x3800.

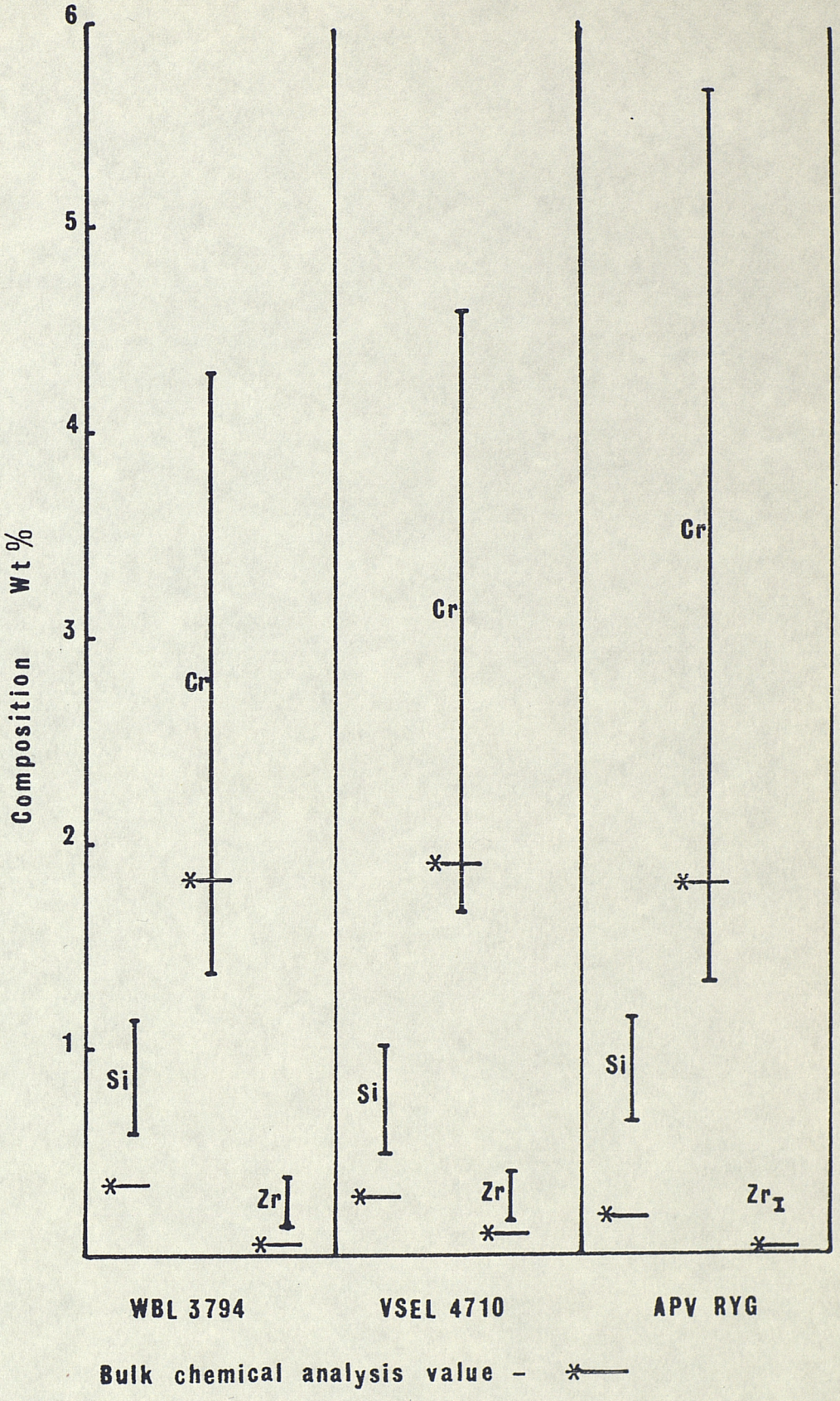

Fig 4.9 Chemical composition chart for Type A particles.

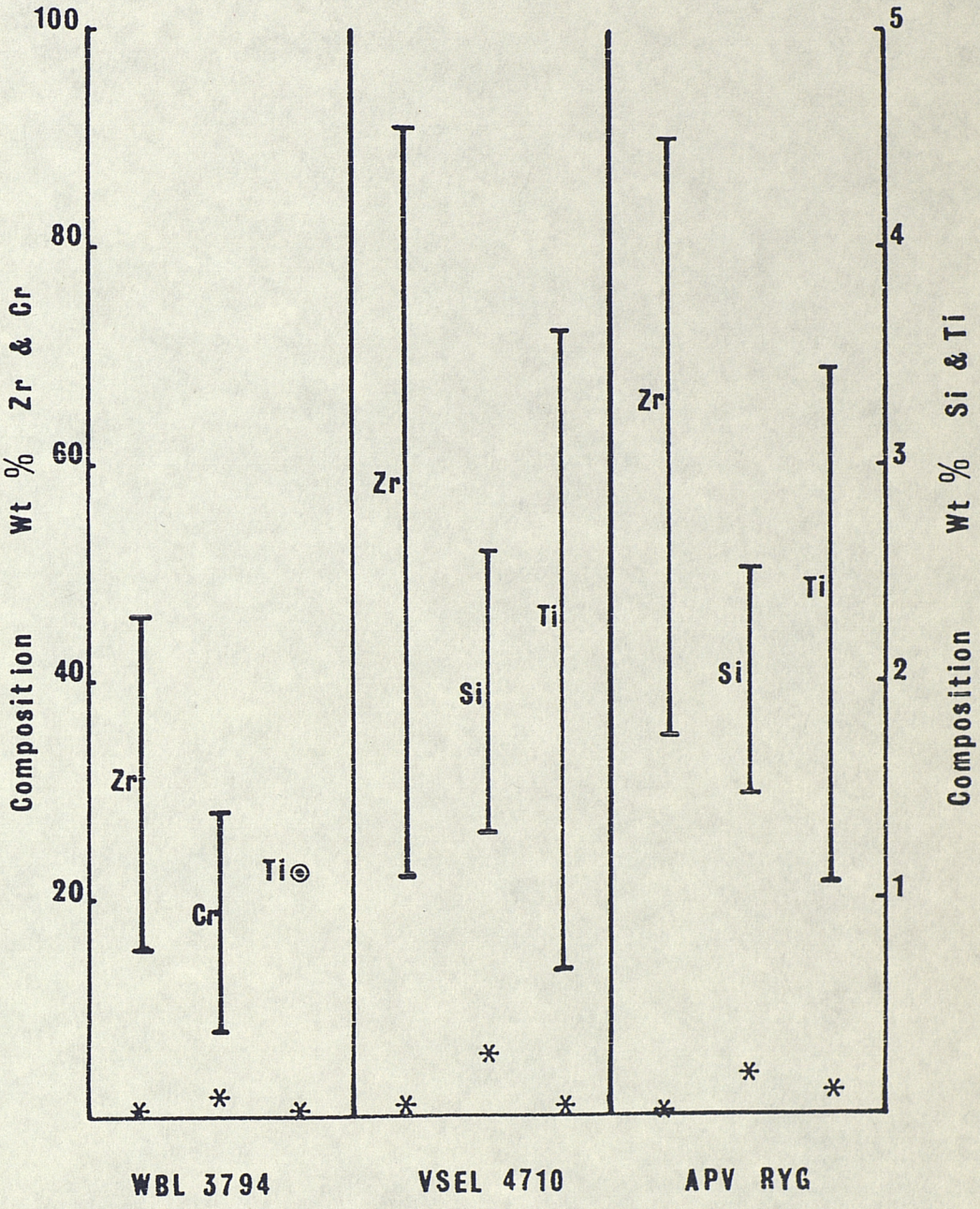

Fig 4.10 Chemical composition chart for Type B particles.

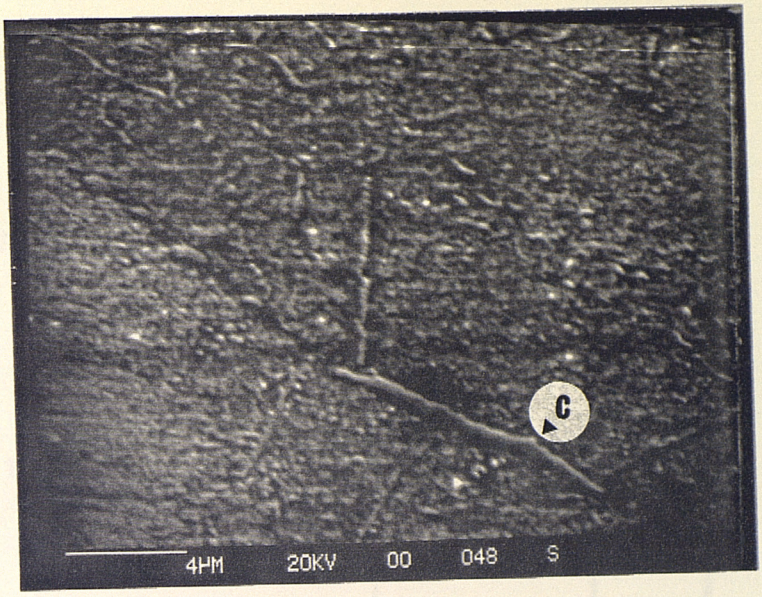

Fig 4.11 Microstructure of VSEL-4710 illustrating the Type C feature. x4000.

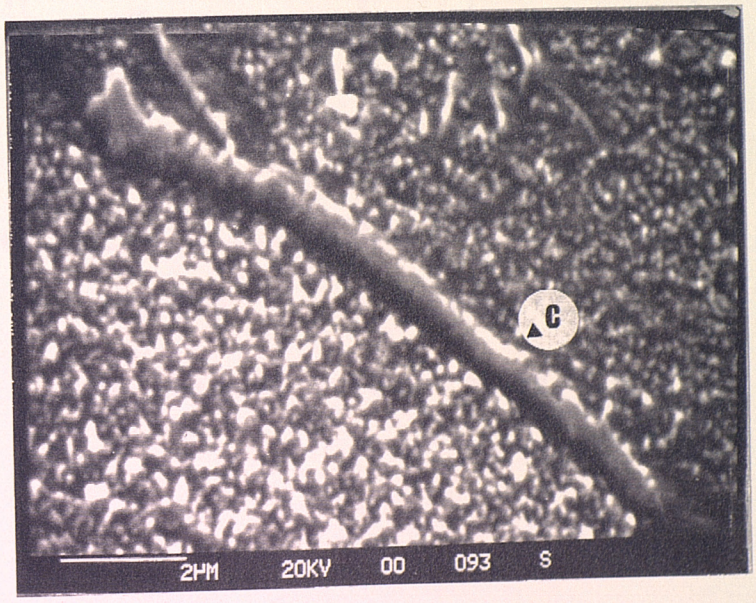

Fig 4.12 Microstructure of APV-RYG illustrating the Type C feature. x8500.

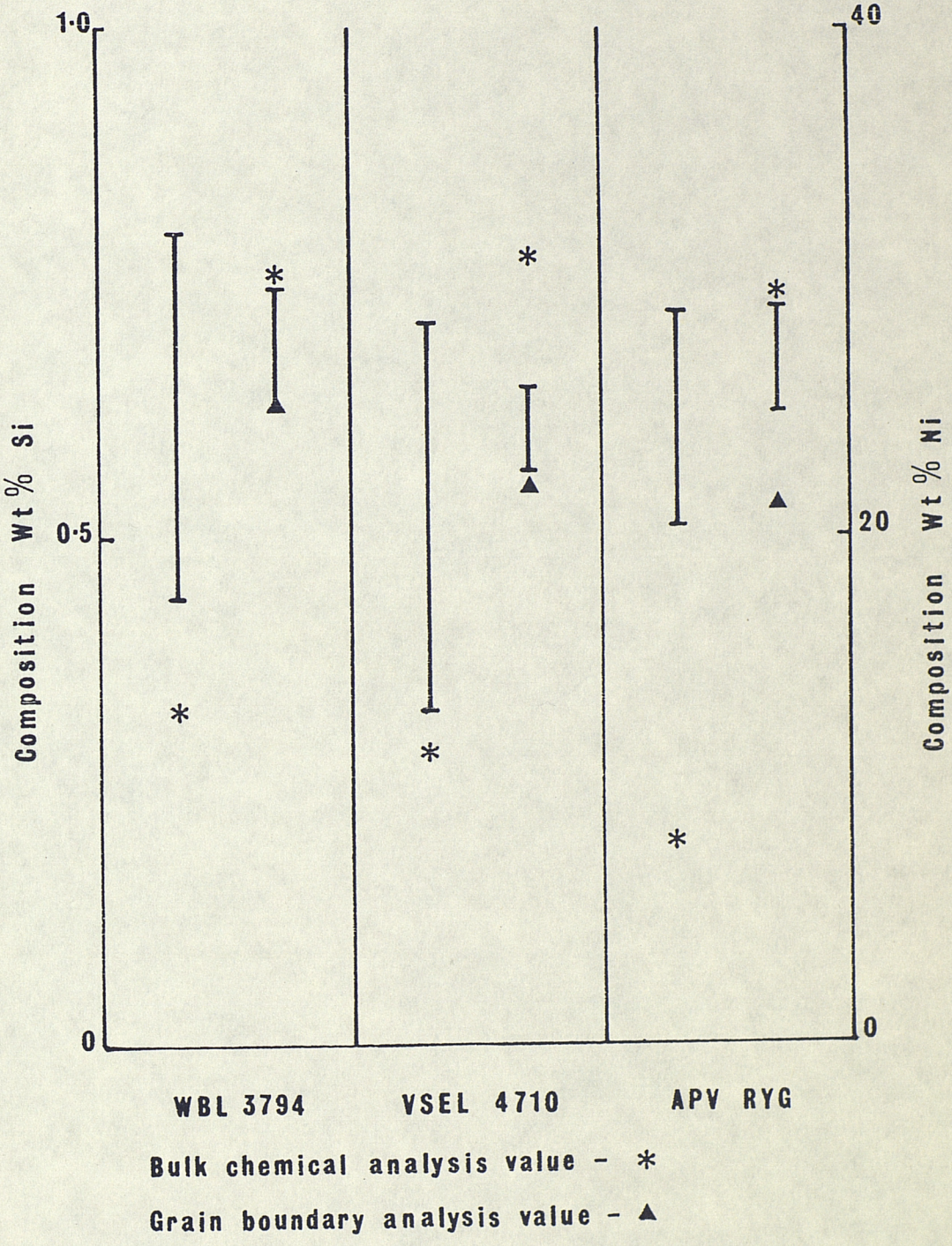

Fig 4.15 Chemical composition chart for Type D feature.

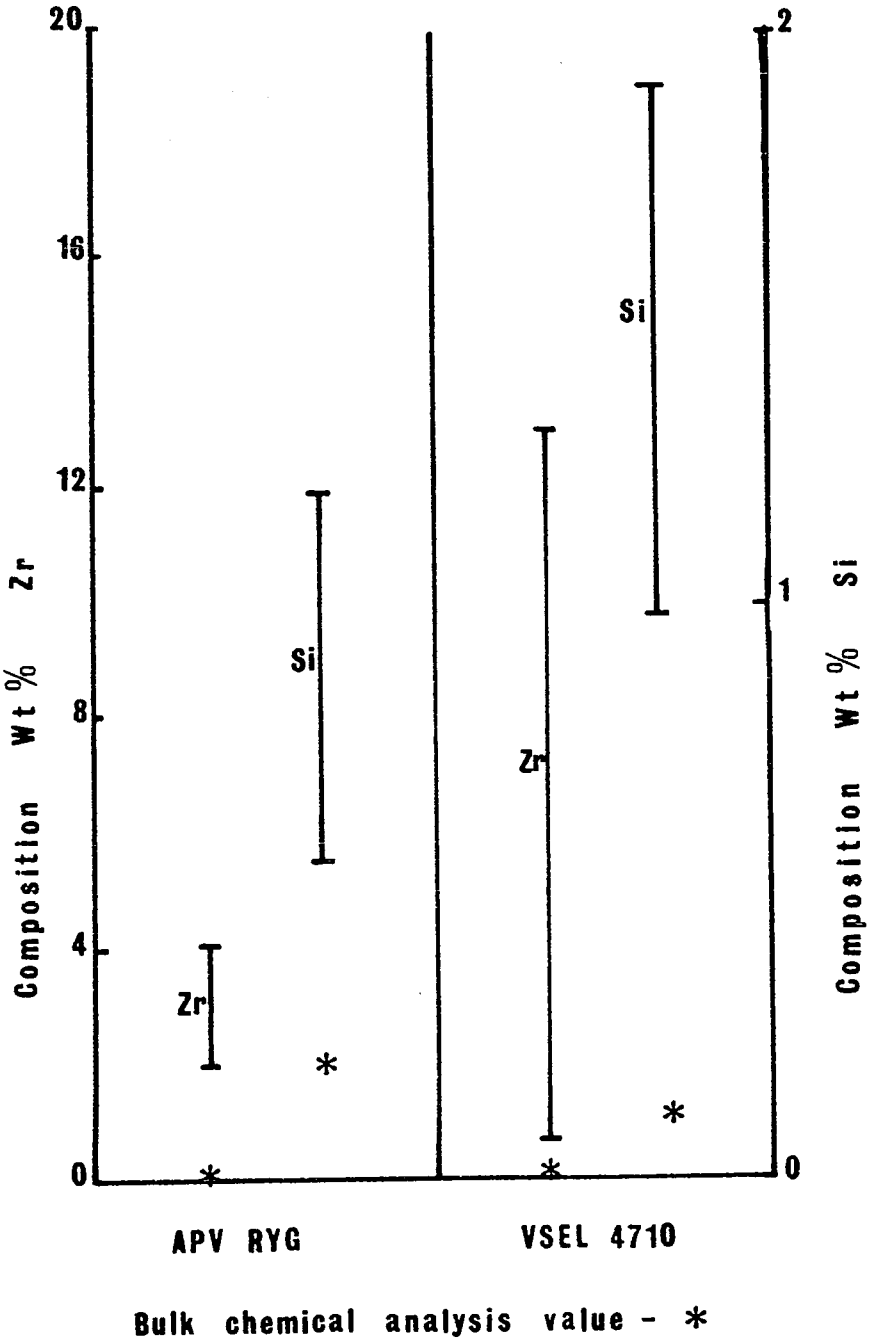

Fig 4.13 Chemical composition chart for Type C particles.

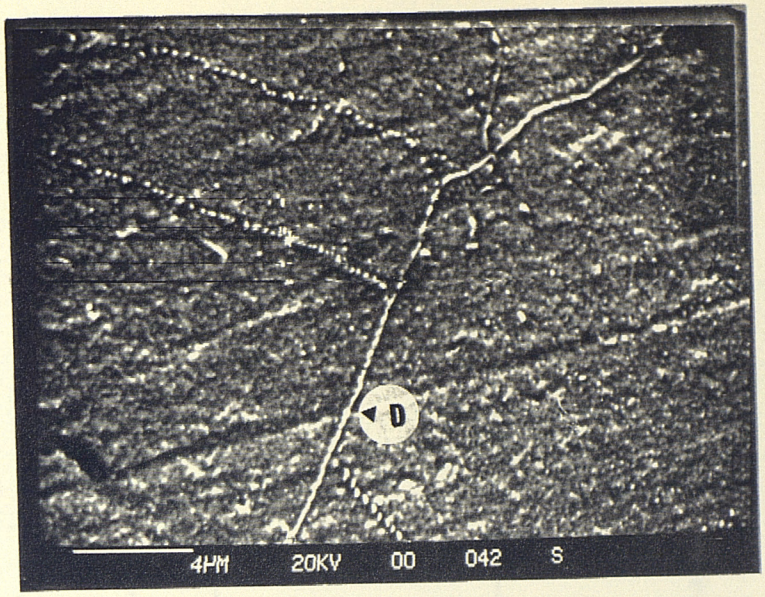

Fig 4.14 Microstructure of WBL-3794 illustrating the vein-like Type D feature. x4000.

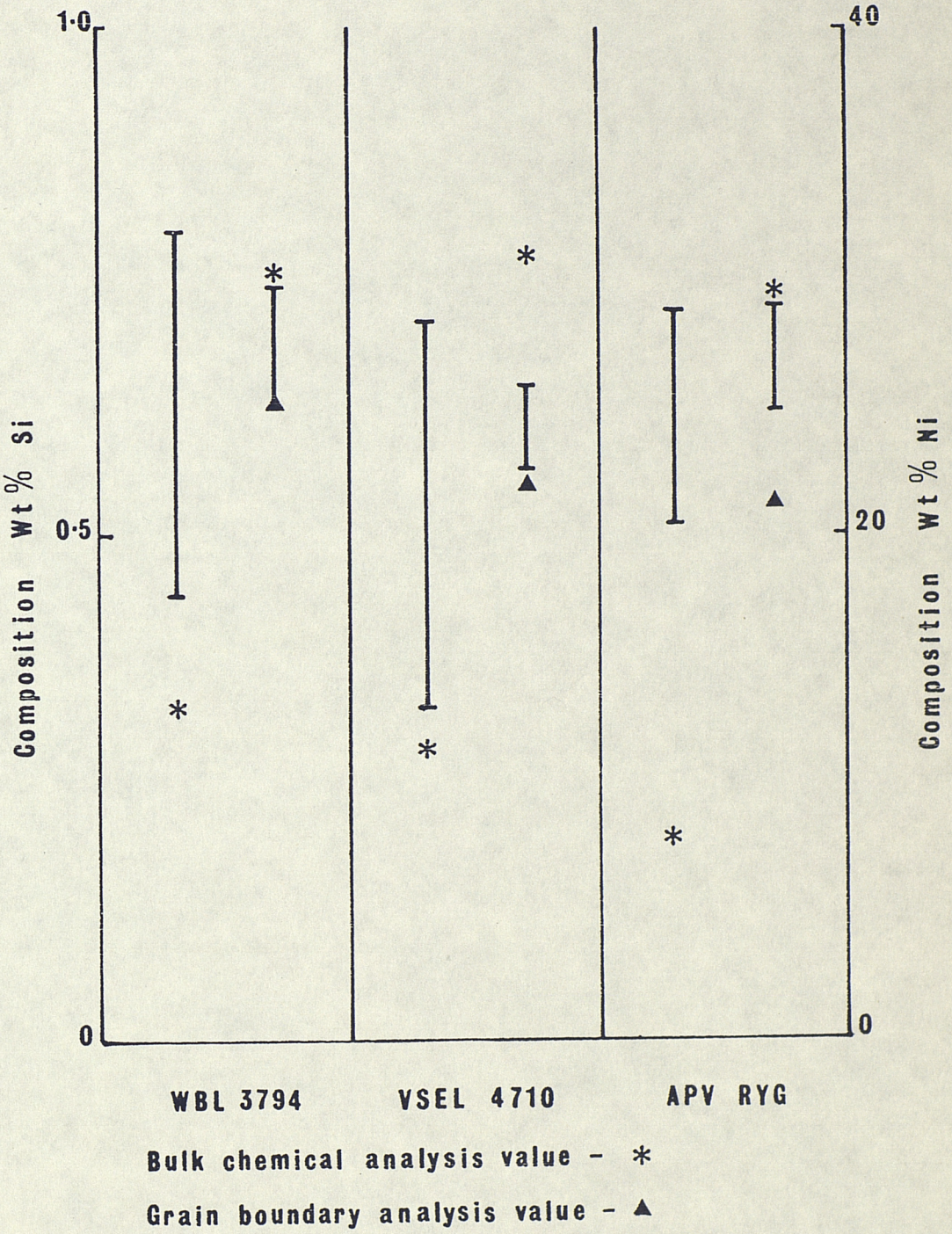

Fig 4.15 Chemical composition chart for Type D feature.

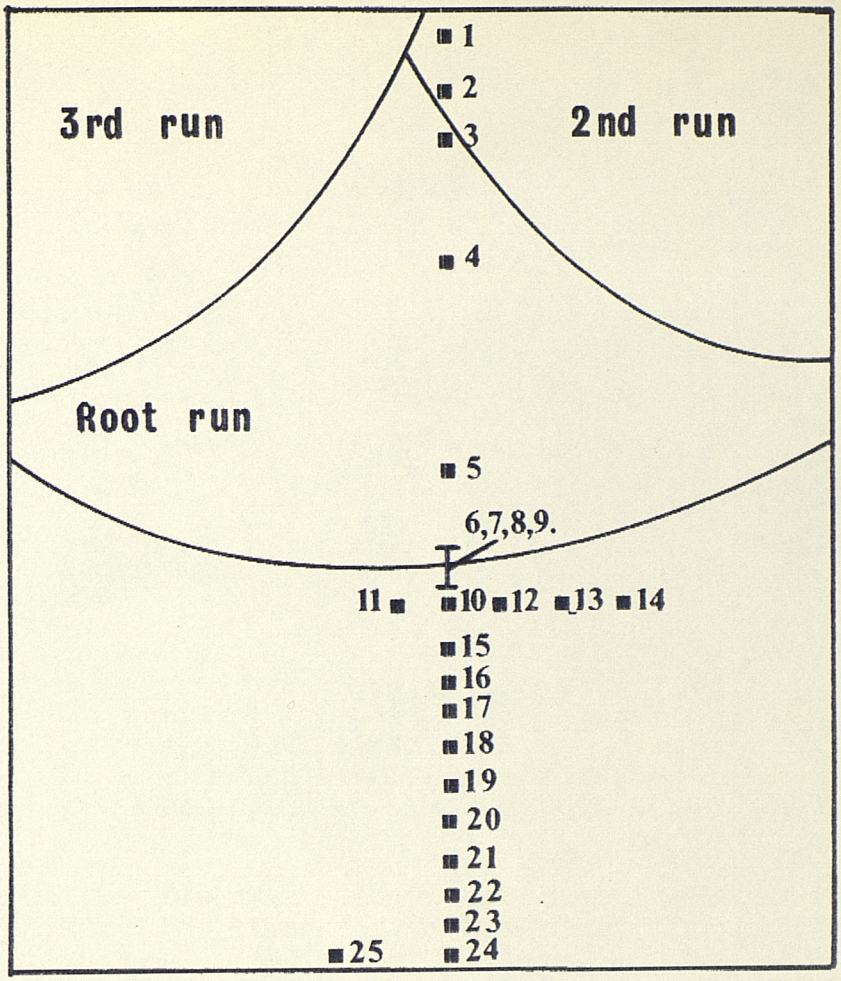

Fig 4.16 Weldment micro-hardness survey indentation points.

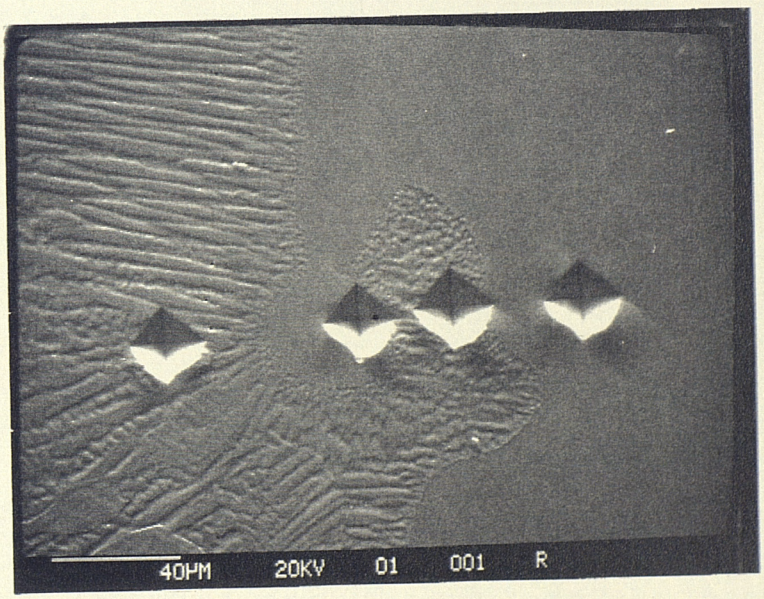

Fig 4.17 Weldment micro-hardness survey indentation point Nos. 6,7,8 and 9 across the fusion zone. x420. (Hardness values are listed in Table 4.3.1)

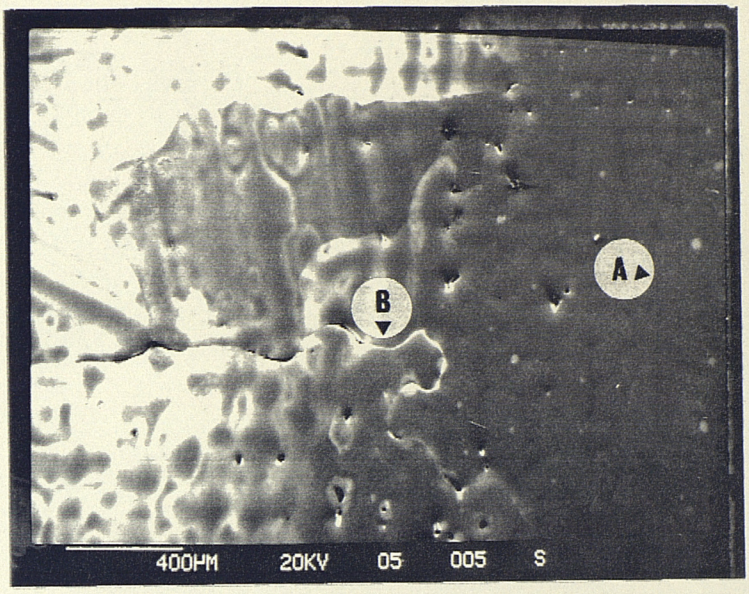

Fig 4.18 Weld induced crack in WBL-3794. x40.

A :- Weld fusion zone.
B :- Crack.

Fig 4.19 Surface-breaking weld induced crack in WBL-3794. The grain boundary crack path and crack position approximately 1.5mm from the fusion zone are illustrated. x50.

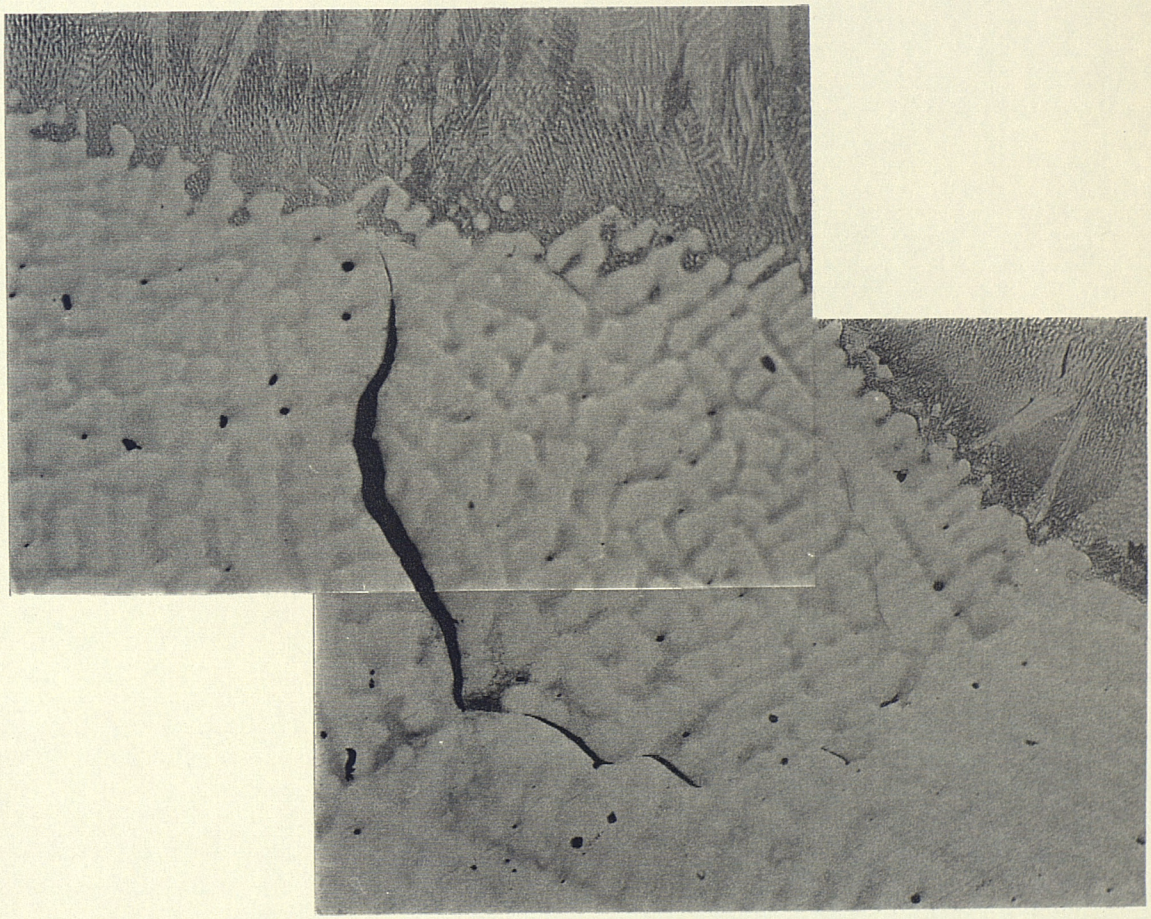

Fig 4.20 Sub-surface weld induced crack in WBL-3794. x50.

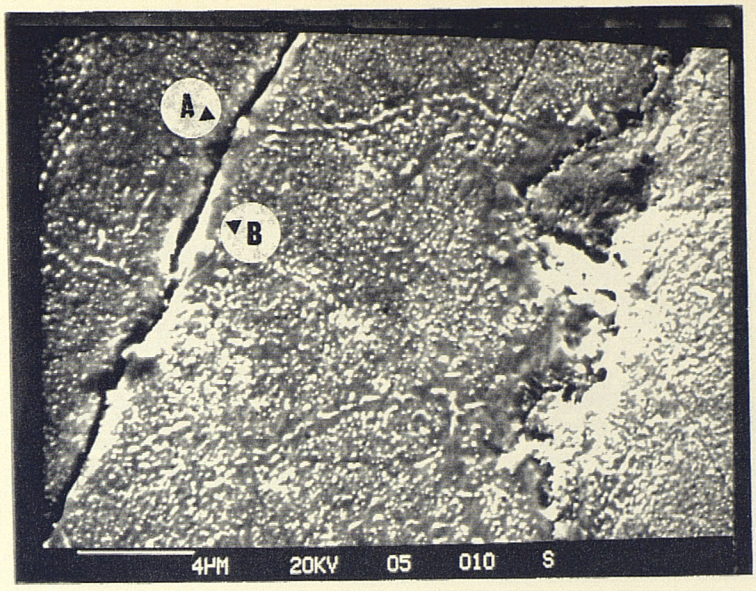

Fig 4.21 Weld induced crack in WBL-3794 illustrating the fracture path, at the interface between a grain boundary particle and matrix (A), and the precipitate free zone (B). x4000.

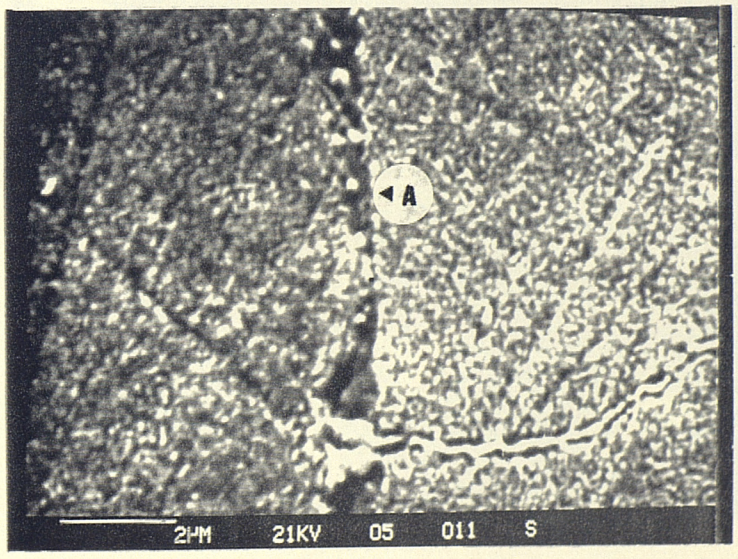

Fig 4.22 Grain boundary precipitate free zone in WBL-3794 (A). x7500.

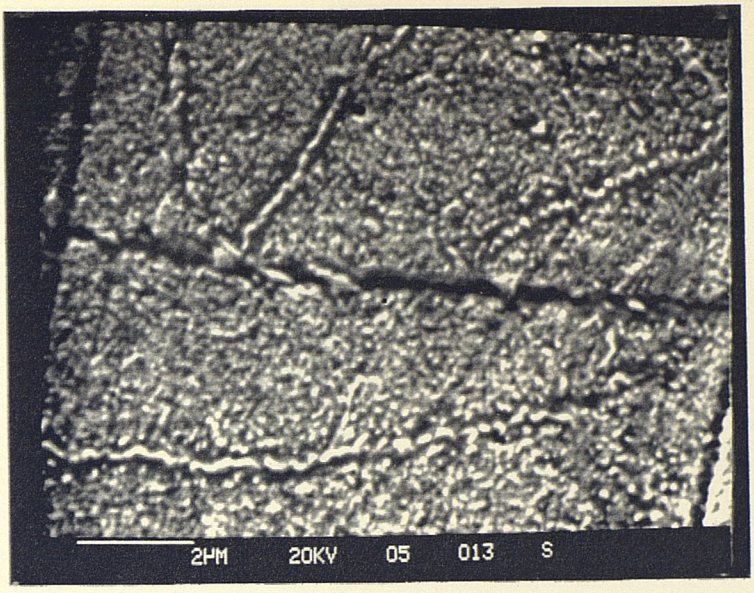

Fig 4.23 Grain boundary precipitate free zone in WBL-3794. x7500.

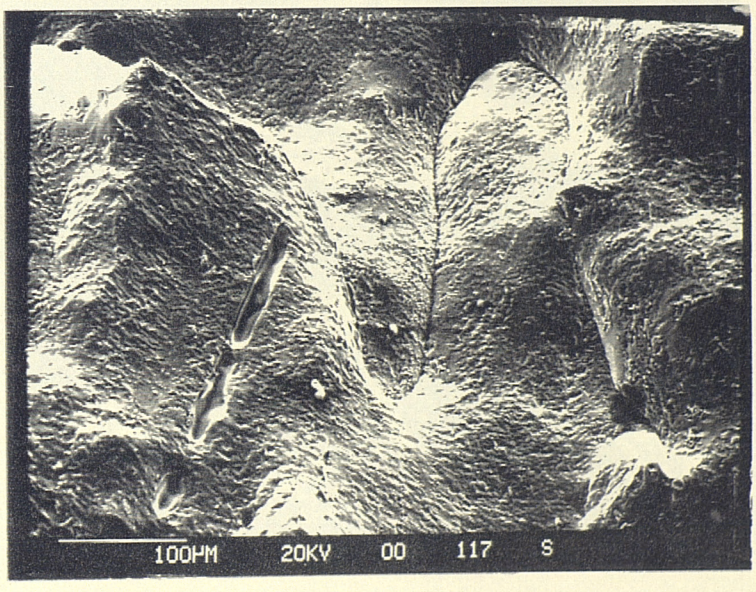

Fig 4.24 Weld induced crack fracture surface in WBL-3794 illustrating shrinkage pores and dendritic structure. x170.

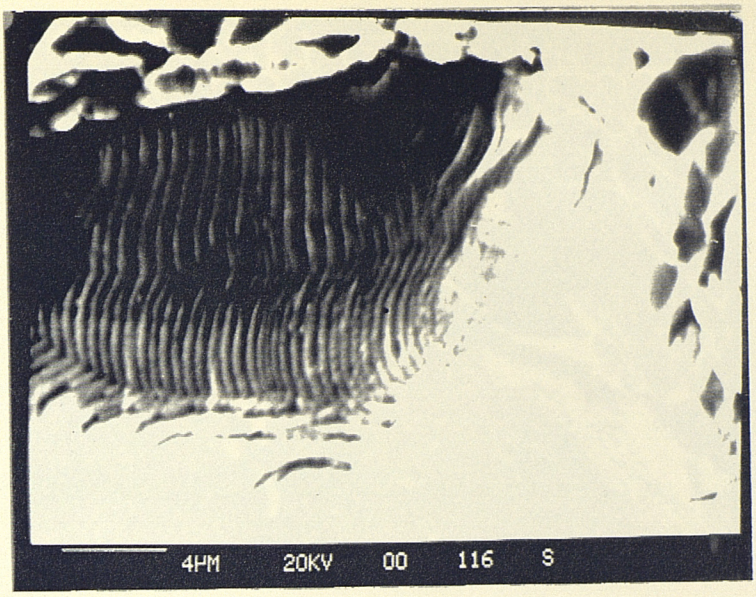

Fig 4.25 Thermally etched shrinkage pore surface in a weld induced crack fracture surface. x3500.

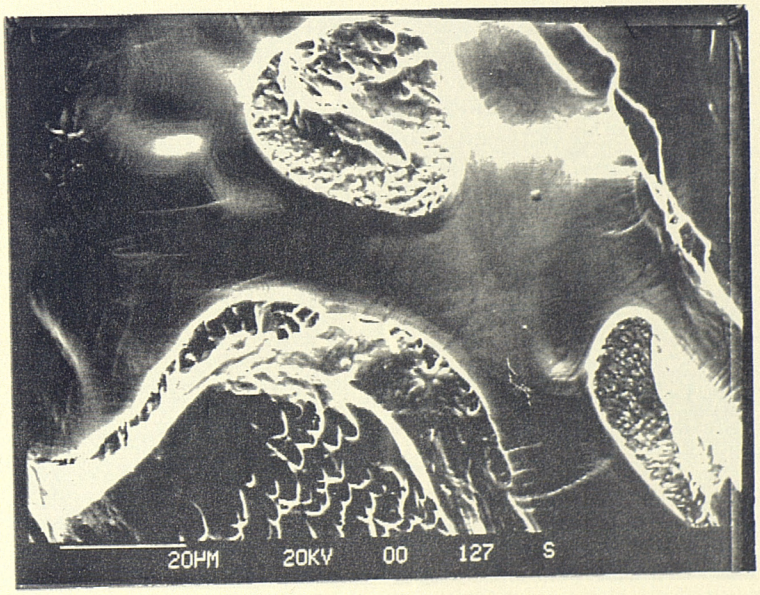

Fig 4.26 Thermally etched weld induced crack fracture surface surrounding regions of dimpled ductile rupture. x850.

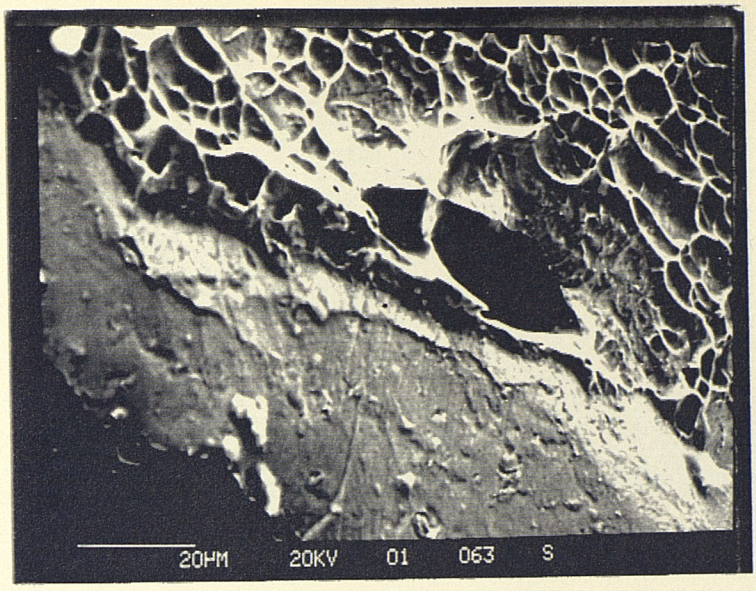

Fig 4.27 Weld induced crack root in WBL-3794. x750.

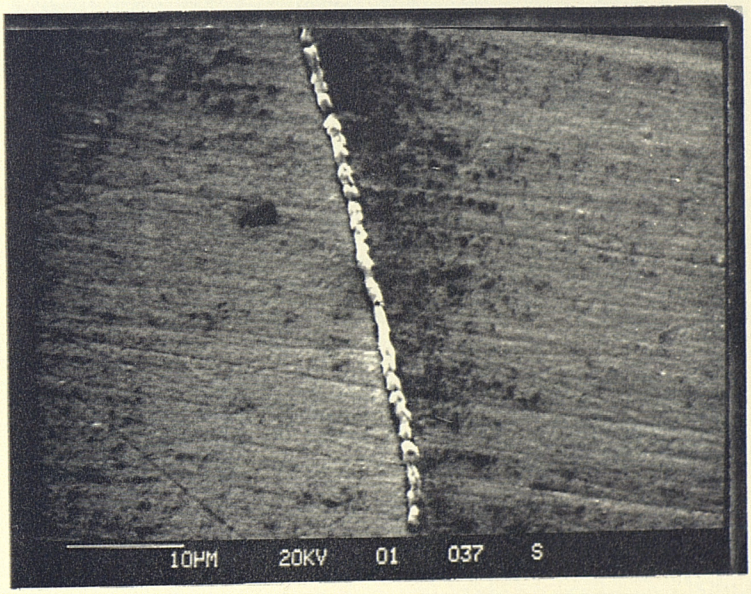

Fig 4.28 WBL-3794 dilatometer specimen heat treated at 800°C for 4 minutes, illustrating a Cu-rich substance at the grain boundary. x1500.

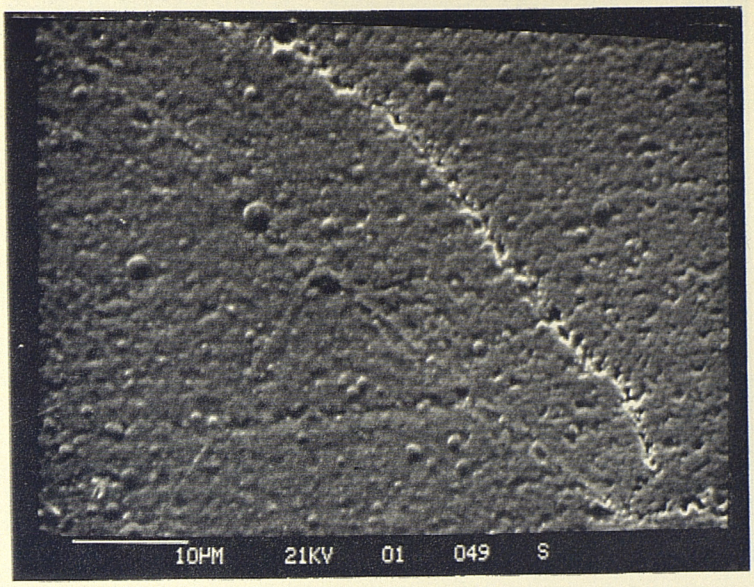

Fig 4.29 WBL-3794 dilatometer specimen heat treated at 900°C for 10 minutes, illustrating grain boundary mobility pinned by shrinkage pores. x190.

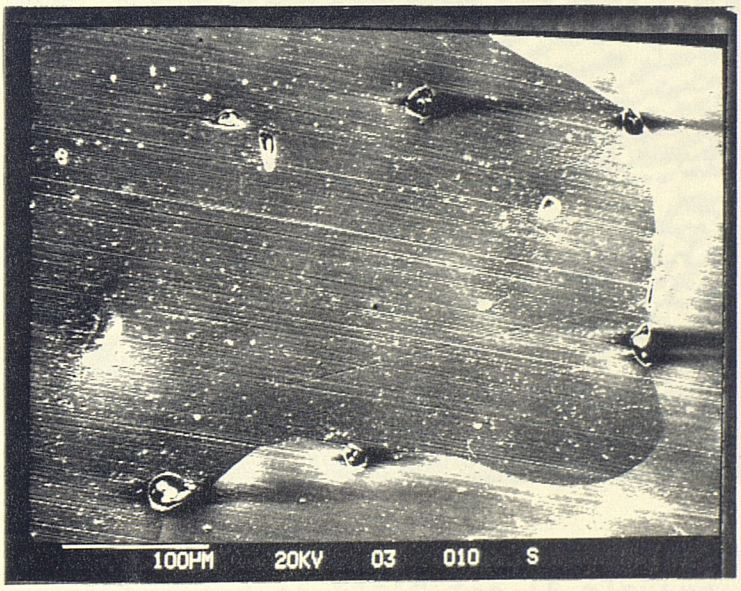

Fig 4.30 WBL-3794 dilatometer specimen heat treated at 1030°C for 15 minutes, illustrating migrating grain boundary. x190.

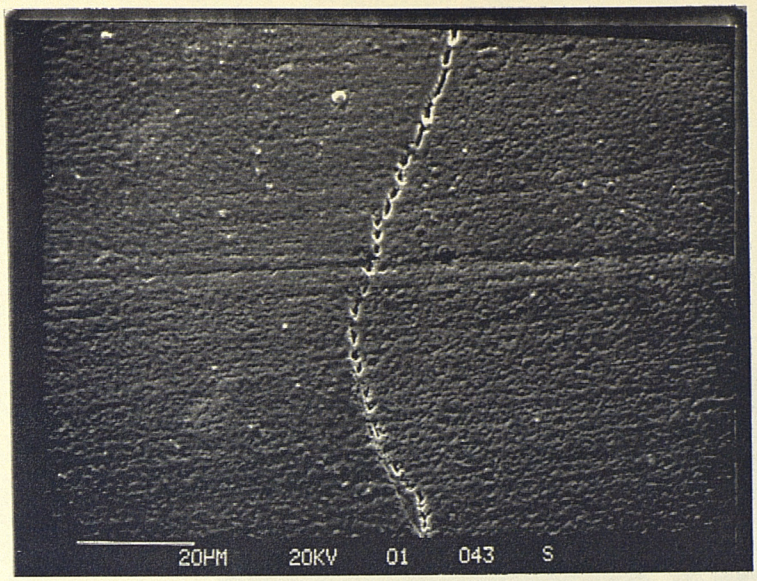

Fig 4.31 WBL-3794 dilatometer specimen heat treated at 900°C for 10 minutes, illustrating grain boundary voids. x770.

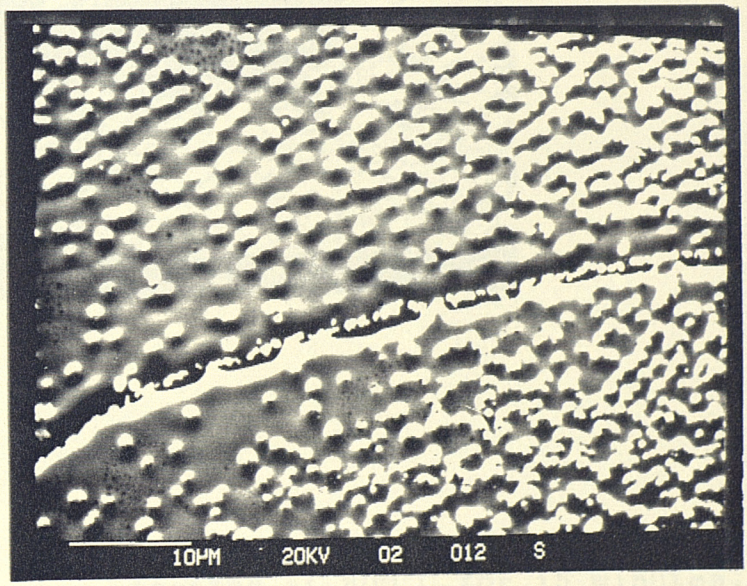

Fig 4.32 WBL-3794 dilatometer specimen heat treated at 970°C for 15 minutes, illustrating the thermally etched surface normally occurring in this test. The average chromium composition is 13%Cr in the particles and 2% Cr in the matrix. x1600.

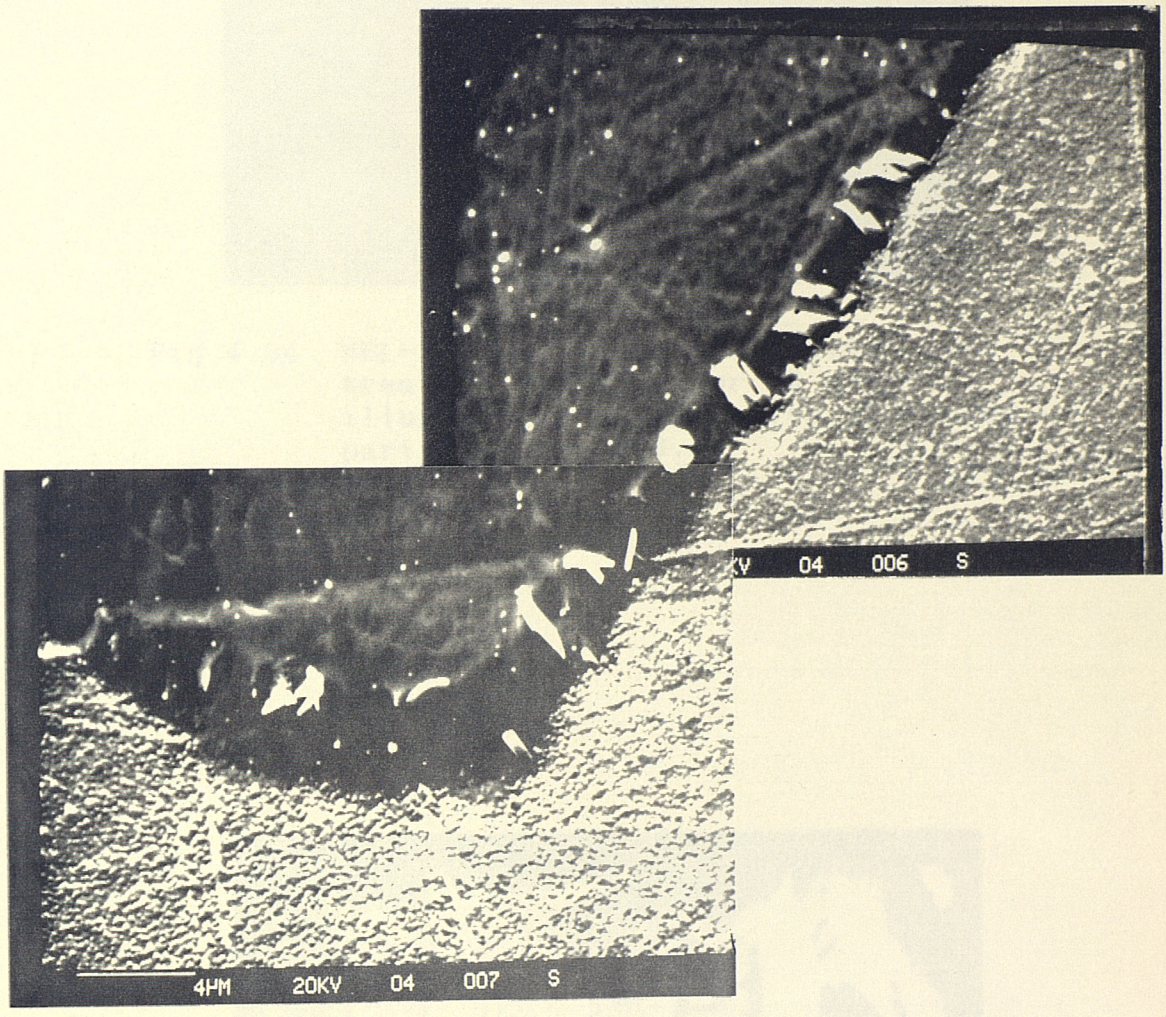

Fig 4.33 WBL-3794 dilatometer specimen heat treated at 800°C for 15 minutes, illustrating enriched grain boundary particles containing up to 29% Cr. x3800.

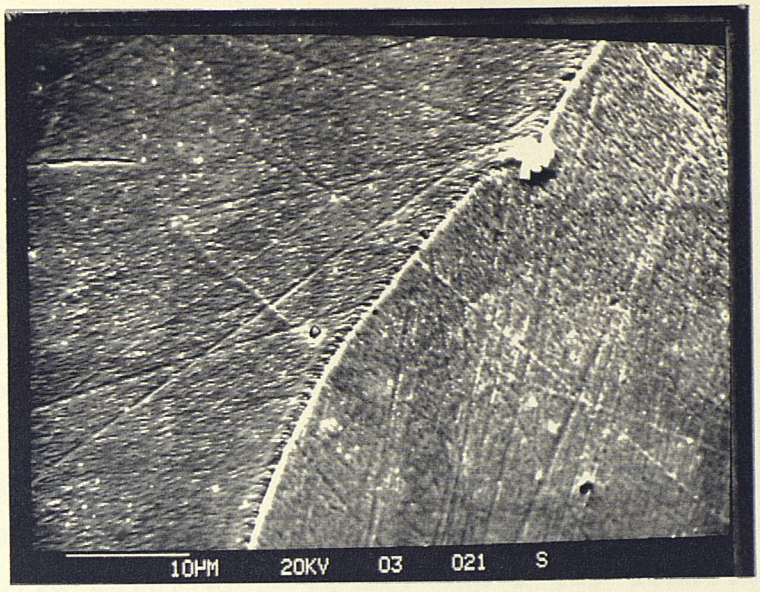

Fig 4.34 WBL-3794 dilatometer specimen heat treated at 1150°C for 15 minutes, illustrating un-dissolved zirconium particles. x1000.

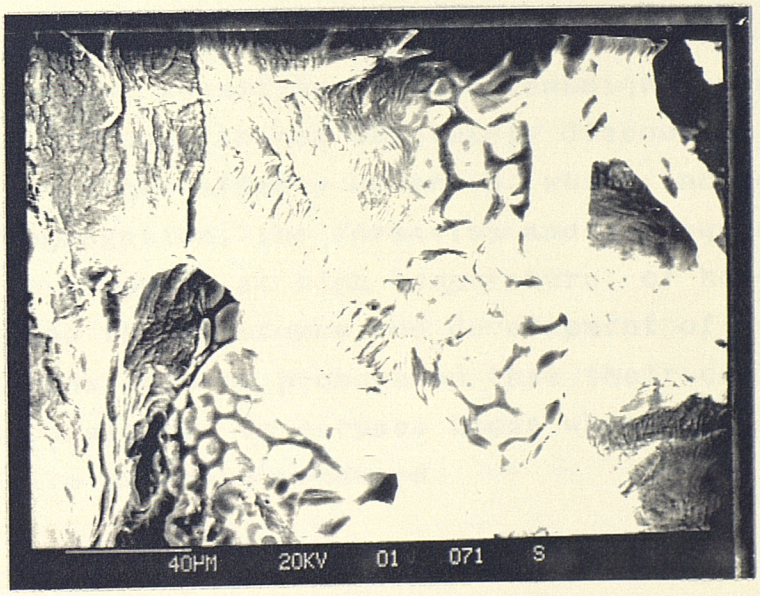

Fig 4.35 WBL-3794 dilatometer specimen heat treated at 1150°C for 15 minutes, illustrating partial melting. x400

5 Discussion

The development of HSCN to replace nickel aluminium bronze (NAB) was initiated due to corrosion problems associated with the complex microstructure of NAB. Problems of this type, such as preferential corrosion of the Kappa II phase in the heat affected zones of weld repairs, would not be expected in a cupronickel alloy which is normally assumed to be a solid solution with uniform mechanical properties. The present work has shown that as cast HSCN is not a simple solid solution with all the alloy constituents distributed homogeneously throughout the structure. It has been found that the combination of several observed effects leads to a gross reduction in strength at the grain boundaries. Cracking on welding was found to occur along grain boundaries, which had become embrittled, in the cast parent metal. Although embrittlement of the grain boundary region in metals and alloys is often associated with a film of impurities existing at the boundary [38], no such segregated films were detected throughout all of the observations made in this work.

The existence of a very fine impurity film, observable using sensitive surface techniques such as Auger spectroscopy, is not completely discounted. However, the other effects observed, which include gross chemical segregation, the formation and subsequent enhanced development at high temperature, of hard particles and the existence and development of grain boundary voids, are so pronounced that their combined effect is considered to surpass those which any such impurity film may have produced.

5.1 Grain boundaries

Grain boundaries in metals may be regarded as internal surfaces or interfacial regions of atomic mismatch approximately three atoms wide. They may be considered to

resemble a three dimensional dislocation network or, where the misorientation between adjacent crystals is large, as a region of more highly disturbed lattice. Grain boundaries raise the total energy of an alloy system, and are present in single phase metals only because they take an extended period to anneal out. It is the nature of these internal surfaces, the forces between them and the change in crystallographic orientation across them which are ultimately responsible for the mechanical behaviour of the material. They obstruct the glide of dislocations and thus cause the operation of several slip systems within a grain to become necessary in order to accommodate strain; this produces an increase in the rate of work hardening. They serve as dislocation sources, paths for enhanced diffusion, sites for the segregation of impurities, for chemical attack and the accumulation of dislocations leading to the nucleation of cracks. Grain boundaries are thus invariably a region of weakness, due to the atomic mismatch there and consequently they provide an easy fracture path for the propagation of cracks.

At elevated temperatures the grain boundaries become glissile, enabling individual grains to slide or shear over each other. This provides an important additional deformation mechanism at high temperature which often leads to the formation of cavities of the type that lead eventually to creep failure [39,40].

When the chemical bond across the grain boundary interface is weakened, the material becomes brittle. Solute atoms which differ considerably in size from those of the solvent, are likely to segregate to this region of irregular structure, where they may be accommodated with a reduced degree of lattice strain.

All metals and alloys contain impurities to some degree and these are often difficult to remove; although present only in trace amounts, their effect may be severe.

McLean [40] found that solute segregation to the grain boundaries can reduce the energy required to form new (fracture) surface and hence cause embrittlement. He measured this effect in copper containing the impurity, Antimony, and his results are shown in Fig 5.1.

Where fracture is brittle with little or no plastic strain occurring, as is observed in HSCN, the surface energy of the new fracture surfaces must be critical in determining the fracture path. Once a crack has been formed, its tip will advance when the tensile stress there is the same as the cohesive strength of the atoms immediately ahead of the tip; this strength is a function of the fracture surface energy. If the new surface energy is low, then the stress required to produce it is decreased as is the amount of plastic work done. In metals, this surface energy can be reduced by the presence of dissolved atoms in a similar manner to that in which a detergent lowers the surface energy of water [40].

During the annealing and recovery processes, grain boundary migration enables the structure to reform with reduced internal stress. Smallman [41] showed that in two-phase alloys, the presence of precipitate particles on grain boundaries affects recrystallisation behaviour. Such alloys are particularly sensitive to the dispersion of the second phase as this inhibits the nucleation rate of new grains when the particle spacing is small. In as cast HSCN, the grain boundaries are found to be decorated with chromium rich second phase particles, undissolved particles of zirconium and titanium (which come from the original alloy additions) and also micro-shrinkage pores.

This contamination of the boundaries will inhibit grain boundary mobility during the welding heat cycle. The formation of chromium rich second phase particles (Type A Sect 4.2) will weaken the intrinsic strength of the grain boundary interfacial region by denuding it of

the dissolved chromium which is intended to stiffen the matrix.

5.2 Microstructure

Simple Cu-Ni alloys are strengthened by solid solution hardening whereby atoms of Cu and Ni occupy sites on the same face centred cubic (fcc) space lattice. The difference in atomic diameter between the two species of atom produces elastic strain in the lattice, thus obstructing the glide of dislocations and so causing an increase in strength. Chromium hardened HSCN increases in strength in a non linear manner, especially in the presence of silicon [42]. It is additionally strengthened by the precipitation of nickel silicide, chromium silicide and the solid phase decomposition, during cooling, of a high temperature fcc phase into two fcc phases of similar lattice parameter but with slight differences in composition. Badia et al [37] proposed that, in slowly cooled alloys, Cr is dissolved in the Ni rich (Cu lean) regions and this initial precipitation of Cr may provide nucleating sites for decomposition of the solid solution. In the early stages of decomposition, solute segregation occurs to produce a wavelike composition variation. The parameters normally of interest in this type of morphology are the composition amplitude and the wavelength or phase periodicity, because this gives a clear indication of the progress of coarsening in such interconnected phase structures. This has been found to be in the range 12.5 nm to 250 nm, depending on the rate of cooling. The coarser periodicity was measured by Badia et al [37] in material cooled from 950°C to 150°C during a 4 hour period. In the equilibrium condition, these are a Cu rich phase of lattice parameter $\underline{a}$ = 0.3589 nm and a Cu depleted phase with lattice parameter $\underline{a}$ = 0.3567 nm [43]. Hardening is caused by coherency strains between these two phases and
takes place during continuous cooling from 950°C. The

reaction is thought to be controlled by diffusion rather than being nucleation controlled, as in a conventional precipitation hardening process. The hardening mechanism occurs during continuous cooling from the annealing temperature and occurs uniformly over distances of the order of atomic dimensions. It is considered to be an example of spinodal decomposition [43] and, due to the very short distances involved, occurs rapidly in the range of temperatures between 760°C-540°C. The hardening process has been shown to be essentially completed after ten seconds in this temperature range [37,44].

Although the tensile properties of a homogeneous, fine grained HSCN would be dominated by the spinodal decomposition, in practice the actual strength and hardness properties of cast HSCN are primarily controlled by its coarse, over aged microstructure. There are large grain boundary precipitates and precipitate free zones adjacent to the grain boundaries. Starke [45] associated this type of structure, in age hardenable high strength aluminium alloys, with reduced ductility, reduced tensile strength and a susceptibility to cracking. He noted its existence in most commercial alloys of this type, where narrow precipitate free zones are the result of solute depletion. Solute may be lost from the region adjacent to the grain boundary due to :-

i) the nucleation of heterogeneous precipitates on the boundary during cooling. (This becomes possible at temperatures below the normal solidus temperature).
ii) preferential segregation of solute occurring at the grain boundary during cooling.

In each of these cases a solute profile, as shown in Fig 5.2, will be established; the precise form of this profile, and hence the width of the precipitate free zone, will depend on the misorientation between adjacent grains and the structure of the boundary because these factors

will affect the formation of grain boundary precipitates.

A typical microstructure of as cast HSCN is shown in Figs 4.2 and 4.3. Chemical segregation takes place during solidification on both a macroscopic and microscopic scale causing localised wide variations in solidification temperature and mechanical properties. Similar acute levels of segregation have been measured by Savage et al [46] in the fusion zones of welds. The tendency for chemical segregation to take place is enhanced by the rather high pouring temperature (1400°C-1500°C) specified in NES 824 Part 2 [36], which is required to achieve good fluidity in the Cr hardened alloy and the wide variation in melting point, T_m, of the constituent elements, given in Table 5.1.

Element	T_m °C	Element	T_m °C
Cr	1887	Ni	1453
Zr	1852	Si	1407
Ti	1675	Mn	1244
Fe	1535	Cu	1083

Table 5.1 Melting points of HSCN alloy constituents.

The liquidus and solidus temperatures for HSCN are approximately 1230°C and 1180°C respectively [36], depending on the bulk composition. Thus the freezing range is 50°C, but this range will be broadened where pronounced chemical segregation occurs. This was confirmed by the partial melting which is clearly evident in a WBL 3794 specimen heated in the dilatometer to 1150°C (some 30°C below the nominal solidus) for 15 minutes and subsequently fractured mechanically Fig 4.35. Cu is segregated to the grain boundaries while Ni,Cr, Fe and Mn are concentrated at the dendrite cores. Although the coring survey clearly showed this (Figs 4.4, 4.5 & 4.6),

evidence of the effect was more pronounced in the aluminium extraction work where material, considered to be from the core of a dendrite, averaging 21%Cu, 60%Ni, 10%Cr, 4%Fe and 2.6%Mn was removed from the heavily etched surface of VSEL 3794 Fig 5.3 and 5.4. Segregation of Si was not observed, although material with 17% Si content, assumed to be silica, was removed using this aluminium extraction technique. Particles of high Zr content and, less frequently, Ti were observed in the bulk alloy using the SEM. Additionally 2.5 um diameter particles of almost pure Zr were extracted from a heavily etched surface Fig 5.5. These particles were assumed to be final alloy additions which had failed to dissolve, either due simply to their high melting points or possibly due to inadequate agitation when mixing them into the melt. The presence of such particles indicates clearly the highly heterogeneous nature of the commercial alloys.

The microprobe analysis gave consistent chemical segregation results for the three alloys although both the degree of segregation and rate of chemical change with respect to distance from dendrite core to grain boundary were found to be lower in the APV cast number RYG. This was considered to be a direct consequence of the stress relief heat treatment given to this alloy, i.e. heating to 450°C and holding at this temperature for one hour per inch of casting section thickness. In order to approach true homogenisation of the alloy constituents, it was necessary to heat to 1150°C for 15 minutes in the dilatometer furnace. Although the Cu-Ni-Cr profile was now homogenised, this heat treatment caused partial melting shown in Fig 4.35. Even so, particles of Zr remained undissolved, both in the matrix and at grain boundaries, despite this heat treatment. The presence of these particles is considered to be relevant to the final cracking mechanism to be discussed in section 5.8.

Chemical segregation will cause wide variations in

strength with position across a dendrite; in particular it will result in a reduction in strength at the grain boundaries in comparison with the dendrite cores. The increase in solid solution strengthening, due to Ni, Cr, Fe and Mn enrichment at the dendrite interior regions, will not be as pronounced as that due to the spinodal hardening effect. However, the contrasting reduction in strength, due to loss of Cr in the vicinity of the grain boundaries, will be of greater importance. This will enhance the intrinsic tendency of the grain boundary region to provide a weak path for the propagation of cracks. The matrix strength of HSCN is assumed to be high and considerably in excess of the grain boundary strength, as was indicated by the microhardness results Table 4.2.2 and 4.2.3. These revealed wide variations in hardness with position, the maximum variation being found in the WBL 3794 alloy where hardness at the dendrite core was VPH 188 with VPH 98 at the grain boundary.

The relationship between the indentation hardness and the flow stress of a material is well known [47]. When consistent units are used, the VPH closely approximates to three times the compressive flow stress. Under the highly localised deformation, and consequent strain hardening conditions taking place during a microhardness test, it may be assumed that the flow stress is equivalent to the UTS. Thus, the hardness data above indicates strength of ~615 MPa at the dendrite cores, but of only ~320 MPa at the grain boundaries.

The coring survey and aluminium extraction observations illustrate the intense degree of chemical segregation, but this work does not explain the undoubtedly brittle type of fracture surface exhibited by the weld cracks. Although the grain boundary region was found to be very rich in Cu, (commonly approaching 80% Cu) it cannot be exclusively of this element because this would result in a very pronounced ductile mode of failure.

Ductile failure was not observed on the fracture surfaces caused by weld induced stress; this is considered to be a consequence of the contamination on the boundaries. Shrinkage pores, second phase particles and undissolved particles of original alloy additions will each contribute to reduction in the ability of the grain boundary region to accommodate strain.

5.3 Cr enriched Grain boundary particles.

As was observed in the survey of microstructural particles (Fig 4.9), chromium rich, second phase precipitates were seen to be present on all grain boundaries. The typical appearance of these is illustrated in Fig 4.7 & 4.8.

Cylindrical specimens for heat treatment tests in the dilatometer were initially manufactured in both the VSEL and WBL alloys. Early tests using the VSEL alloy produced specimen surfaces significantly obscured by an opaque grey film. In consequence, all subsequent dilatometer tests were conducted using WBL 3794 alloy which retained a brighter cleaner surface after testing. This enabled the effects produced by the various heat treatments to be more clearly observed. The cause of this prominent difference in surface appearance was not determined. However, it was considered to be a strong indication of the complexity of the HSCN alloy system and the difficulty in producing the alloy with consistent high quality, both alloys having been produced in different foundries, to comply with the same specification.

The small grain boundary particles (Type A, Section 4.2) were found to contain a mean average of 3.8% Cr and 1.1% Si in the as cast material. These values are 2.1 and 3.4 times the bulk analysis values for Cr and Si respectively. The Cr content of this feature increased substantially at elevated temperature and with prolonged time at temperatures greater than 700°C. This is

considered to be a consequence of the path for enhanced diffusion at the grain boundary enabling dissolved Cr to be supplied from the original Ni rich spinodal regions.

The greatest enhancement of Cr content in an individual instance was observed in a specimen heat treated at 1000°C for 15 minutes where the composition measured was 48.5% Cr in a particle 1.5 um x 0.5 um x 0.5um. The average Cr content calculated for all the grain boundary particles chemically analysed after this heat treatment was found to be 40% Cr. The results of the programme of dilatometer tests are shown in Fig 5.6. and these observations of chromium enrichment indicate that the as cast structure of WBL 3794 alloy is intrinsically unstable.

The Cr rich particles were observed to be considerably reduced in size in a specimen tested at 1080°C for 15 minutes Fig 5.7. Final dilatometer tests were conducted at 1150°C with specimens held at this temperature for 4 and for 15 minutes. The Cr enriched grain boundary particles were no longer observed in these test specimens and it was concluded that heat treatment at this high temperature caused them to dissolve into solid solution in addition to producing a very small amount of selective partial melting Fig 4.35.

It is clear that the welding heat cycle will not maintain a casting at high temperature for the extended time periods used in the dilatometer tests. Study of particles on the grain boundaries, in advance of the tips of cracks produced by welding, did not reveal their enrichment in Cr content to the same high degree as produced by prolonged heat treatment in the dilatometer furnace. However, particles with 6.7% Cr and 2.1% Si content were observed. These values are 3.7 and 6.4 times the bulk analysis values for Cr and Si respectively and therefore clearly exceed the compositions found to be typical in these particles in the as cast material.

Fig 5.8 shows particles of this type, 25 um in advance of a weld crack tip. Fig 5.9 illustrates, at lower magnification, a weld induced crack tip propagating on a grain boundary. Migration of this grain boundary has clearly taken place although pinning by shrinkage pores is also apparent (point A). Material at the triple point (point B) was found to be rich in Cr(29%), Mn(7%) & Zr(16%), thus again indicating the heterogeneous nature of the cast material.

It is believed that the presence of these Cr rich and Zr rich particles have three distinctive effects.

Firstly, enrichment of the grain boundary particles by Cr will denude the region immediately adjacent to the boundary of this element, consequently producing a highly localised reduction in strength in this already weakened region. Denuded regions adjacent to the grain boundaries can be observed in Figs 4.21, 4.22 & 4.23. The effect of coring causes a reduction in the chromium content in the boundary region when the alloy is in the as cast condition and this largely remains after stress relief heat treatment at 450°C. Thus, subsequent enrichment of grain boundary particles with chromium will cause the matrix in the narrow band, immediately adjacent to the grain boundary region, to become even leaner in active hardener content. This was observed by Saunderson et al [48] who noted a well established and clearly denuded zone extending approximately 2 um to each side of the grain boundaries in a 3.8% Cr Cu-Ni alloy heat treated at 900°C for 24 hours.

A second effect which the boundary particles may produce is a reduction in cohesive strength at the particle / matrix interface of the type normally observed in the cusps where ductile failure begins. This is indicated by the path of the weld cracks usually observed circumventing the particles on this interface, as shown in

Fig 4.21. Such a strength reduction will provide a weak path at the particles for easy crack propagation.

A third effect caused by the grain boundary particles occurs when grain boundary sliding takes place. Any discontinuity on the boundary such as a triple point, a particle or a shrinkage pore will produce a severe stress concentration as adjacent grains begin to move with respect to each other. Where the concentration of stress exceeds the cohesive strength of the particle / matrix interface, a micro-crack or void will form on the boundary. The formation of such defects at many of the numerous grain boundary particles would further reduce the strength of this region.

It is considered significant that enhancement of the grain boundary Cr content was observed to commence within the same temperature range as the ductility dip ie, at approximately 700°C. This will be considered further in Section 5.8

5.4 Grain boundary voids.

The development of voids at the grain boundaries of metals during creep has been well documented. Under the action of a fairly low level of stress, small cavities appear at points along the grain boundaries, the voids increase in size, coalesce and subsequently fracture takes place along the weakened grain boundary. Gittings and Williams [49] have shown that this takes place, due to grain boundary sliding, on boundaries which are orientated at approximately 45° to the applied stress when the creep rate is large.

When grain boundary sliding takes place, cavities will tend to nucleate at any protuberances on the boundary such as a ledge or particle. Movement of adjacent grains will cause concentration of stress at such a point and

this may exceed the cohesive strength. Reduction in the grain boundary surface energy, caused for example, by the segregation of impurities, will enhance the formation of cavities as this is effectively equivalent to a reduction in the cohesive strength.

Although the fracture of HSCN due to the weld heat cycle occurs within a very short time scale in comparison to creep, the elements of both applied stress and high temperature are common. Voids were observed to develop in HSCN during heat treatment in the dilatometer furnace. Fig 5.10 shows such voids in a specimen treated at 1030°C for 15 minutes. Figs 4.29 and 4.31 show a similar effect in a specimen treated at 900°C for 10 minutes. Grain boundary sliding at the triple points in a specimen treated at 900°C is apparent in Fig 5.11. Both the void development and boundary sliding have occurred under the action of residual stress within the specimen and the dilatometer support rod spring force only.

In addition to the development of micro-voids, shrinkage pores are also often positioned on the grain boundaries. These larger scale defects will tend to pin the boundaries preventing their migration and consequent relief of internal stress. Fig 5.12 illustrates an example of this in a specimen heat treated at 1000°C for 15 minutes.

It is believed that both types of voids are significant in controlling the mechanical properties of the alloy and this will be further discussed in section 5.8.

5.5 Titanium and Zirconium.

The NES 824 Part 2 specification [36] gives brief guidance on the method of adding the elements Ti and Zr to HSCN. They are stirred into the melt immediately prior to

pouring, both elements being intended to act as deoxidisers. Ti is additionally intended to refine the grain structure but was not found to be successful as, in all three casts investigated, the grain size was rather coarse. This is largely a consequence of the high pouring temperature used to produce adequate fluidity, but may also indicate a fundamental difficulty in the melting practice resulting in failure to dissolve Ti. The importance of grain size is exemplified by the work of Evans [18] who showed that the minimum ductility value decreased with increasing grain size in a Mg - 0.8% Al alloy. This alloy displayed ductility dip behaviour in the temperature range 200°C to 350°C.

The work conducted by Ansuini and Badia [42] at the International Nickel Company, in the original development of HSCN alloy, and by Petersen [44] to develop welding filler metal for the alloy, determined that zirconium is necessary to improve the hot ductility. This property is intrinsically poor in Cu-Ni alloys. Zr is known to produce this improvement in wrought HSCN and therefore was included in the equivalent cast alloy [50].

In the current work, large Zr particles were found to exist in the structure, usually at the grain boundaries. This indicated a problem in foundry practice, in failing to dissolve zirconium into the liquid solution. This failure was common to all the four alloys examined, each of which were manufactured at a different foundry. Similar difficulty in controlling the Zr content was reported by Sahoo, Wang and Edwards [35]. These workers proposed both a failure to dissolve the Zr master alloy addition initially into the melt and also the subsequent loss of Zr from the liquid solution, in the form of ZrO_2, to be possible causes for low Zr content.

The WBL alloy, on which most of the weld tests were conducted, was chemically analysed by the Admiralty

Laboratory at Holton Heath, Dorset and found to contain 0.005% Zr. This result both fails to comply with the alloy specification and is below the 0.07% Zr figure claimed by the manufacturers in their analysis which was conducted by an independent testing laboratory. The effect of this low bulk analysis value for Zr, combined with current observations that much of the Zr present in the alloys exists in the form of undissolved particles, indicates there will be almost no Zr in solid solution within the alloy matrix. In consequence, the improvement in hot ductility, intended to be brought about by the addition of Zr, will not take place.

In a comprehensive review of the literature concerning the casting properties and welding of cast HSCN, Dion et al [50] stated that the presence of Zr is considered necessary to produce adequate weldability. Kanno [28] conducted an investigation specifically into the effect of Zr. He used a simple Cu - 0.7% Cr alloy and compared it to a similar alloy to which 0.05% Zr had been added. Cast alloys were cold worked and subsequently heat treated such that the recrystallised grain size was very fine (approximately 40um). Tensile tests were conducted in a nitrogen atmosphere at various temperatures producing the results shown in Fig 5.13. This work showed the addition of Zr improved ductility by inhibiting fracture on the grain boundaries. The mechanism Kanno proposed as the cause for this improvement was the removal of a thin sulphur film, segregated to the grain boundaries, by the formation of zirconium sulphide particles, the presence of which were detected using Auger spectroscopy.

5.6 The effect of weld preheat temperature

The degree of stress induced during a weld cycle, and hence the tendency for cracks to form, will be affected by welding process parameters. Arc voltage, welding current, speed of travel and weld preheat temperature each

affect the rate of post weld cooling during which contractural stresses are developed.

Joint restraint, essential for the development of stress, will normally increase with the thickness of the casting being repaired. This restraint may be defined as resistance to the deformation which, if it occurred, would relieve the contractional welding stresses. Additionally, increased casting thickness will raise the post weld cooling rate, by providing a larger heat sink volume.

In the weld tests conducted, using the manual metal arc welding process, the single parameter which could be easily varied was the weld preheat / interpass temperature. The weld preheat temperature range proposed as suitable for Cu-Ni alloys is 20°C to 110°C [32,(Ch33)] and tests were conducted at temperatures encompassing this range. The initial weld test results indicated the possibility of a reduction in cracking susceptibility with increased preheat and interpass temperature. This would be expected as a consequence of the slower post weld cooling rate causing a reduction in internal stress by permitting more time for plastic strain to take place.

The results, recorded in the limited number of weld tests which were conducted, were inconclusive. These are shown in Fig 5.14 and Table 4.5. Although the initial test results, at each of the four preheat temperatures, showed the expected reduction in cracking susceptibility, a very wide variation in the cracking index values were found between tests subsequently duplicated at 20°C and 100°C. It was additionally noted, on one test plate, that crack like defects appeared during pre-welding stress relief heat treatment. It is therefore concluded that the cause of weld cracking is more complex than that associated with simple cooling rate effects.

5.7 Summary of observed effects

It is useful, at this stage, to summarise the known effects which have been observed in this alloy during the current work.

Brittle cracking during welding HSCN always occurs on the grain boundaries where the strength and ductility properties differ considerably from those of the matrix material. The brittle condition is caused by a number of factors, listed below, which combine to prevent the reliable weld repair of castings.

1. Recrystallisation, which would relieve internal stress, is inhibited by the decoration of grain boundaries with shrinkage pores, second phase particles and particles of undissolved original alloy additions.

2. Gross dendritic segregation causes severe weakening of the grain boundary regions, in comparison with the very strong matrix throughout the grain interiors.

3. Chromium denudation causes highly localised weakening in the grain boundary regions, on a microscopic scale, as the second phase particles form during cooling after solidification and, at elevated temperature, subsequently become enriched in chromium.

4. The impurities, shown to be present in the bulk analysis data, will be concentrated at the grain boundaries. This concentration is significantly enhanced by the massive reduction in grain boundary area resulting from having very coarse grain size.

5. Grain boundary cohesive strength is reduced at the interface between the matrix and particles of the

second phase and the original alloy additions.

6. The tendency for crack nucleation during grain boundary sliding is enhanced by the existence of discontinuities on the boundaries such as particles and pores.

7. Failure to dissolve the element zirconium into solid solution, which is intended to produce an improvement in hot ductility. This is caused by problems in foundry practice.

5:8 Model for cracking

A proposed model to explain the cause of cracking, found to occur in most as cast HSCN when welded, is set out below.

The inability to weld as cast HSCN, is caused by a combination of effects. These are almost all associated with the extreme heterogeneous nature of the alloy when in this condition. Due to this, the stress which is developed inevitably during the welding heat cycle, may be relieved only by strain which is highly localised within the structure i.e. the generally high strength of the matrix will cause any resulting strain to be concentrated in the grain boundary regions where the plastic yield strength is inferior to that of the matrix.

On a chemically clean boundary, this stress would be accommodated by plastic strain or shear, and cracking would not normally be expected to occur. However, the boundaries are not clean; they are decorated with numerous shrinkage pores and various types of particles.

The regions in which all positions containing cracked grain boundaries were observed, were always in the HAZ,

close to the fusion zone, but separated from it by a small distance (1 mm to 2 mm) Fig 2.3. Similar observations were also reported by Plumb [29] in his report of work conducted on thirty four individual HSCN casts. This indicates that the alloy becomes brittle within a specific range of temperatures and possibly also only when this is maintained for a necessary time period.

In the close vicinity of the fusion zone there is a region which is heated, during welding, to a temperature greater than that at which embrittlement occurs. At this higher temperature it is probable that the grain interior matrix rapidly looses strength and this will cause any strain taking place here to be much more evenly distributed throughout the whole structure, so cracking does not occur. Cracking also does not occur in the HAZ region which is most distant from the fusion zone. In this region, the temperature at which the brittle condition develops is either not achieved, or is maintained for a period of time which is too brief for the development to take place. It is also possible that cracking does not occur here because the weld induced stresses have already been relieved by brittle cracking occurring closer to the fusion zone, before this more distant region undergoes sustained heating to the required temperature.

There will be a minimum Threshold Stress, σ_{Th}, which must be achieved before cracking may occur. At low temperature, both grain boundary and interior strengths exceed σ_{Th} Fig 5.15. At higher temperature, the alloy strength is reduced and so weld induced stress is relieved by plastic strain before σ_{Th} is achieved. Thus brittle cracking is confined to the region, parallel to a weld, where the range of temperature ΔT in Figs 5.15 and 5.16 is maintained. It is proposed that the ΔT temperature range is in the region of 700°C - 900°C.

Contamination of the boundaries by particles

contributes in two respects to embrittlement of the alloy.

Firstly recrystallisation, which would partially relieve weld induced stress in this region, is inhibited. The work of Chubb and Billingham [6] has shown that the initial temperature at which this process commences in copper based alloys is increased by the addition of nickel Fig 2.4. Recrystallisation is further inhibited by gross contamination on the grain boundaries; shrinkage pores, undissolved Zr and Ti original alloy additions, a chromium rich second phase and silicon rich particles all decorate the grain boundaries reducing their mobility. It is also possible that grain boundary mobility is inhibited by impurity atoms segregated to this region. Cottrell [51] noted this effect, observed mainly in fcc metals, where impurities in trace amounts (10 to 100 ppm) reduce the mobility of some boundaries by two or three orders of magnitude when compared to those of zone refined metals.

Secondly, the easy path for crack propagation, provided by the more open structure at grain boundaries, is enhanced by the accumulation of shrinkage pores and particles there. These all reduce the ability of the boundary to accommodate strain and so favour development of a brittle condition. Sharp cracks, impinging on these hard particles, will cause either fracture of the particle or of the weak interface between particle and matrix.

Severe dendritic segregation, on a macroscopic scale, will cause very wide variations in mechanical strength within individual grains. Strengthening of the matrix in the dendritic core regions throughout the structure will take place with consequent weakening in the vicinity of the grain boundaries. The severity of this segregated condition is confirmed both by EDAX, where regions containing 79% Cu 20% Ni were observed at the surface of shrinkage pores, and by the aluminium extraction

observations which revealed material assumed to be from a dendrite core, composed of 68% Ni and 21% Cu. Further indication of the severity of chemical segregation is given by partial melting which took place at 30°C below the nominal solidus temperature. This extreme heterogeneity is caused by both the high pouring temperature, found necessary to produce adequate fluidity, and the wide variation in melting points of the individual alloy constituents. A further factor which may be significant, is the inherent degree of solid solubility which individual constituents have within each other.

This reduction in the strength of the grain boundary region in general, which develops during solidification, produces the base condition onto which further weakening effects are compounded.

Dissolved impurity elements are invariably concentrated at the grain boundaries during the process of solidification because they remain in solution in the final liquid to solidify. The bulk analysis data supplied for the WBL 3794 alloy by both the manufacturers and the Admiralty laboratory at Holton Heath indicate the total of all impurities present to be < 0.02%. Although this low value is within the NES specification, the coarse nature of the grain structure will result in a pronounced reduction in the total area of grain boundary present. This will cause the bulk of the impurities to be significantly more highly concentrated at the boundaries than if the structure were fine grained. This effect is a probable major cause of the observed embrittlement which can be brought about by reducing the energy required to produce new (fracture) surface [40].

A general manufacturing difficulty in producing HSCN alloy of consistent high quality is illustrated by the disparity in appearance between the VSEL and WBL alloys after initial heat treatment tests in the dilatometer.

This may be due to the low volume of HSCN alloy produced, i.e. approximately 200 tonnes annually, being insufficient to warrant the allocation of foundry equipment specifically dedicated to its production.

The subsequent dilatometer work revealed a proclivity for the second phase grain boundary particles to become enriched in chromium at temperature >700°C. This enrichment will produce a number of effects:-

1. The enhanced rates of diffusion, normally occurring at the grain boundaries, causes this region to be drained of solute. This will produce a narrow matrix region, adjacent to the boundary, to be denuded of Cr, the element intended to stiffen it. The effect will be particularly pronounced because the region is already lean in Cr due to the effect of coring on a macroscopic scale.

2. An easy path for crack propagation is provided by the interface between these hard particles and the matrix.

3. Cracks will tend to be nucleated at any stress concentration caused at a protuberance on the grain boundary when sliding occurs.

Denudation of Cr, on a microscopic scale, from the narrow matrix region adjacent to the grain boundary, will cause a pronounced and highly localised reduction in strength. This is confirmed by the microhardness results where hardness on the boundary of VPH 98 is compared with values of VPH 188 in an adjacent region. This effect will tend to concentrate all plastic deformation in this narrow region resulting in the initiation of cracks at the grain boundary triple junctions Fig 5.11.

The development of micro-voids, observed to take

place at high temperature, will further reduce the resistance of the grain boundary region to crack propagation; this will favour development of the brittle condition Fig 5.10.

It is clearly indicated in the literature that hot ductility, and hence improvement in weldability is brought about by the addition of zirconium. Chemical analysis by the Admiralty laboratory at Holton Heath has shown the bulk concentration of Zr to be very low. Further to this, the current work indicates the Zr which is present, exists mainly as undissolved particles, assumed to be the original alloy additions. In consequence, the amount of Zr dissolved in solid solution will be almost zero and so the intended improvement in hot ductility and hence also in weldability will not be achieved.

The inconsistencies in the results of the programme of welding tests showed that, although cracking was reduced with increased preheat temperature, the cause of cracking is far more complex than may be associated with the effects of simple cooling rates.

In conclusion, it is therefore suggested that cracking in this alloy system occurs in a narrow temperature range between 700°C and 900°C, due to the highly heterogeneous nature of the material.

It has been shown that the alloy is severely cored and in addition, the grain boundaries are decorated by pores and numerous particles. Thus, in the critical temperature band, the stresses developed produce strains which are concentrated along the boundaries. Here, both ductility and strength are inadequate to accommodate the strains and therefore cracking occurs.

It is believed that this effect is so significant that it outweighs any embrittlement effect caused by the

existence of films.

This model, based both on observations made during the current work, and on those reported in the literature by other workers, is considered to be a sound proposal.

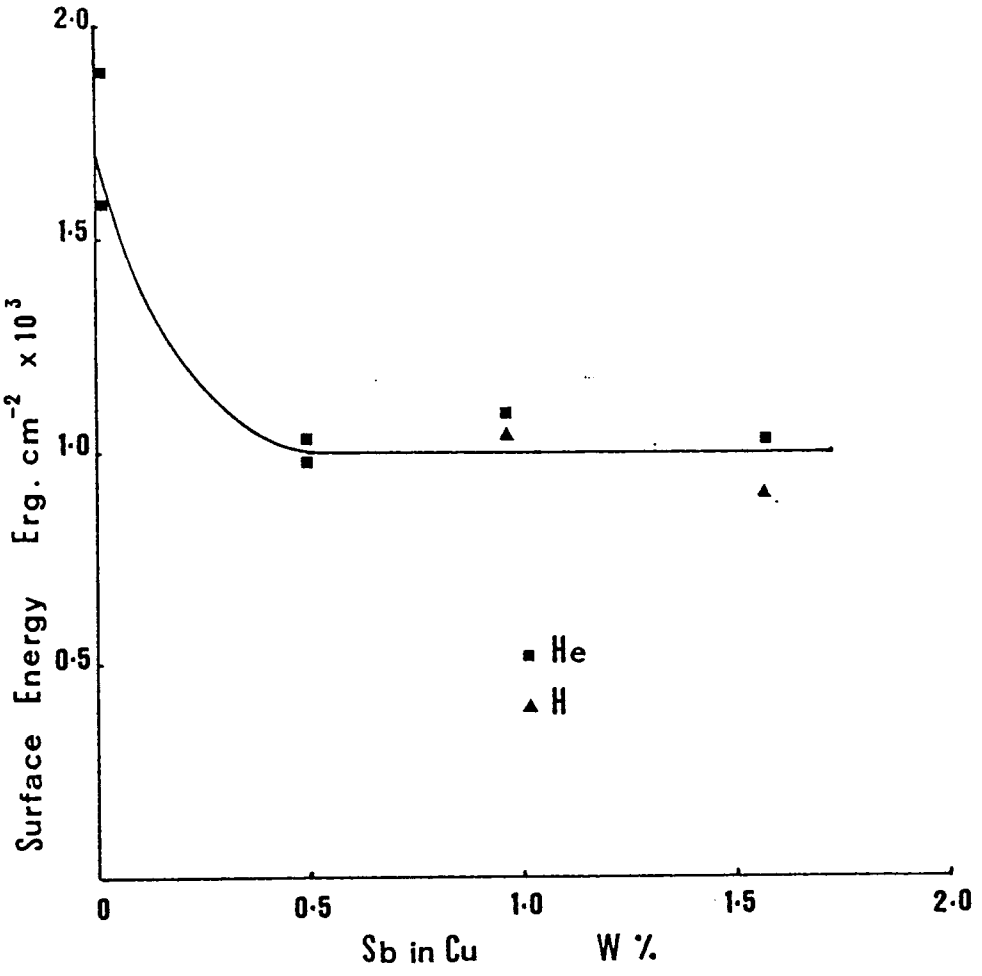

Fig 5.1 The effect of antimony in copper.(After McLean).

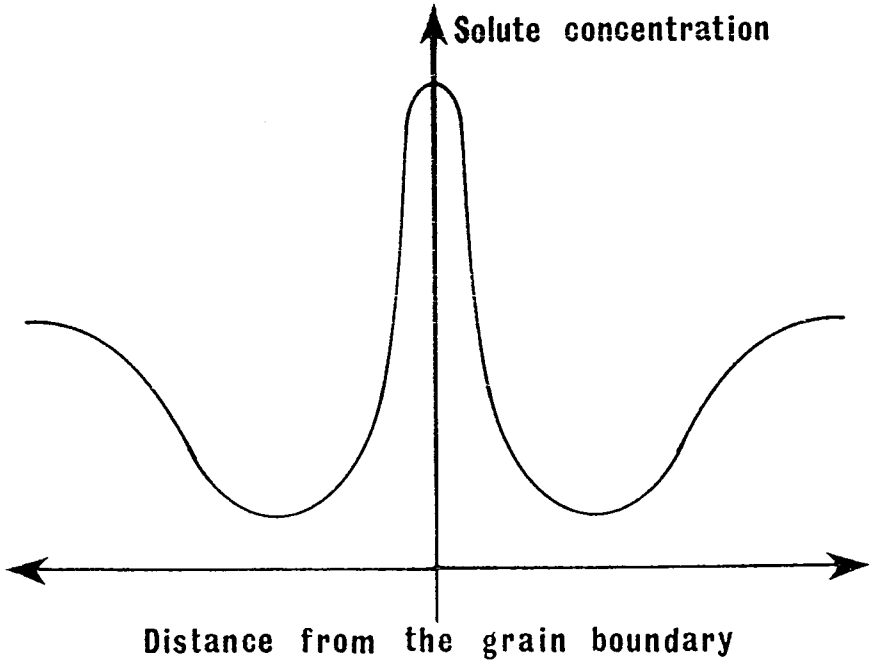

Fig 5.2 Grain boundary region solute concentration profile. (After Starke).

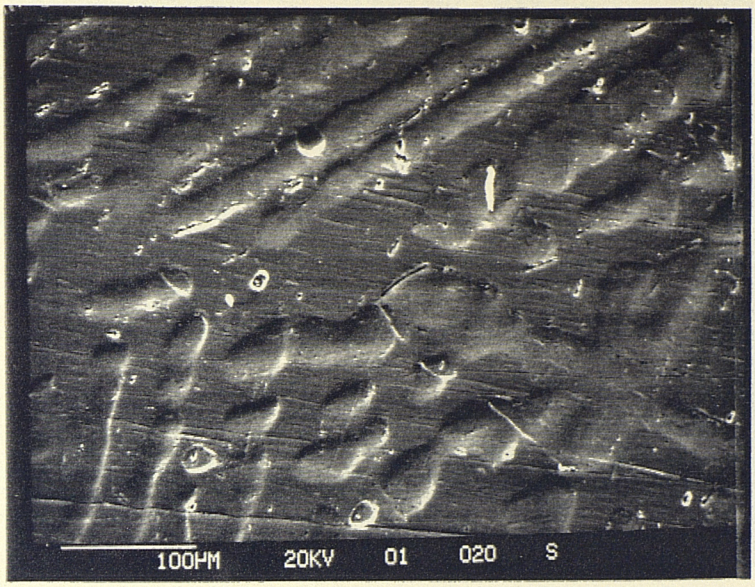

Fig 5.3 Aluminium extraction replica of the heavily etched surface of VSEL-4710. x180.

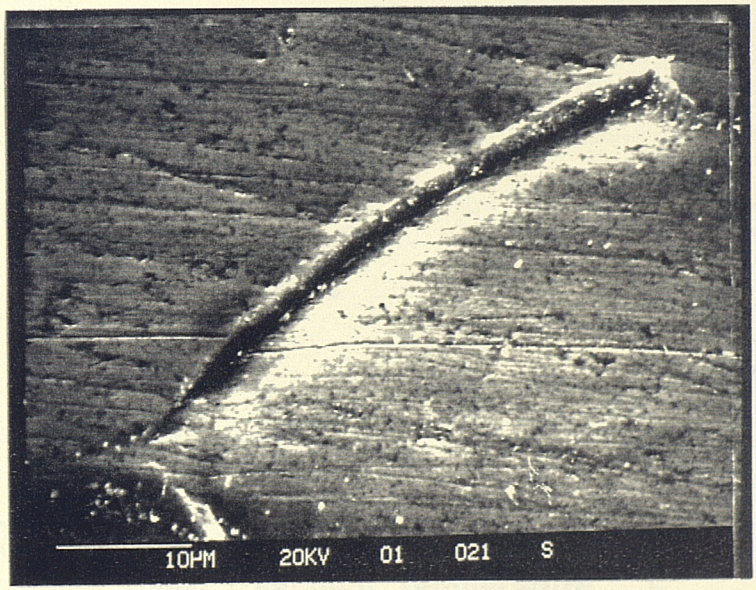

Fig 5.4 Aluminium extraction replica of the heavily etched grain boundary region of VSEL-4710. x1750.

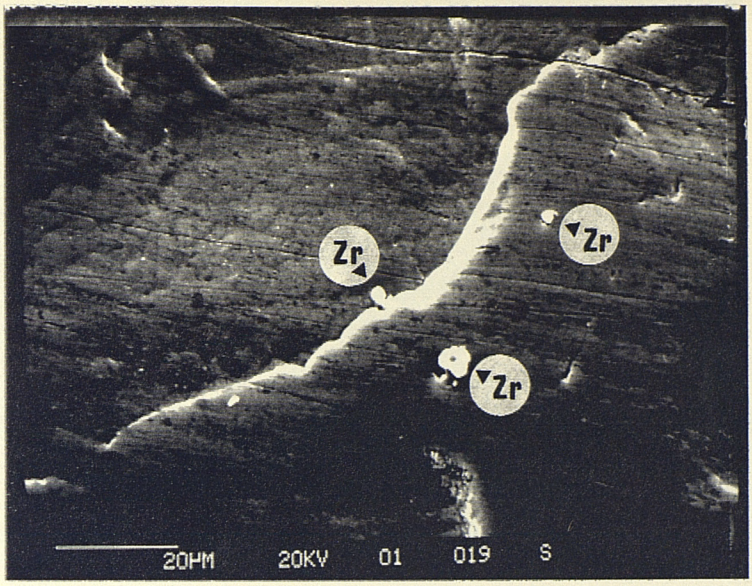

Fig 5.5 Aluminium extraction replica of the heavily etched surface of VSEL-4710 illustrating zirconium particles. x800.

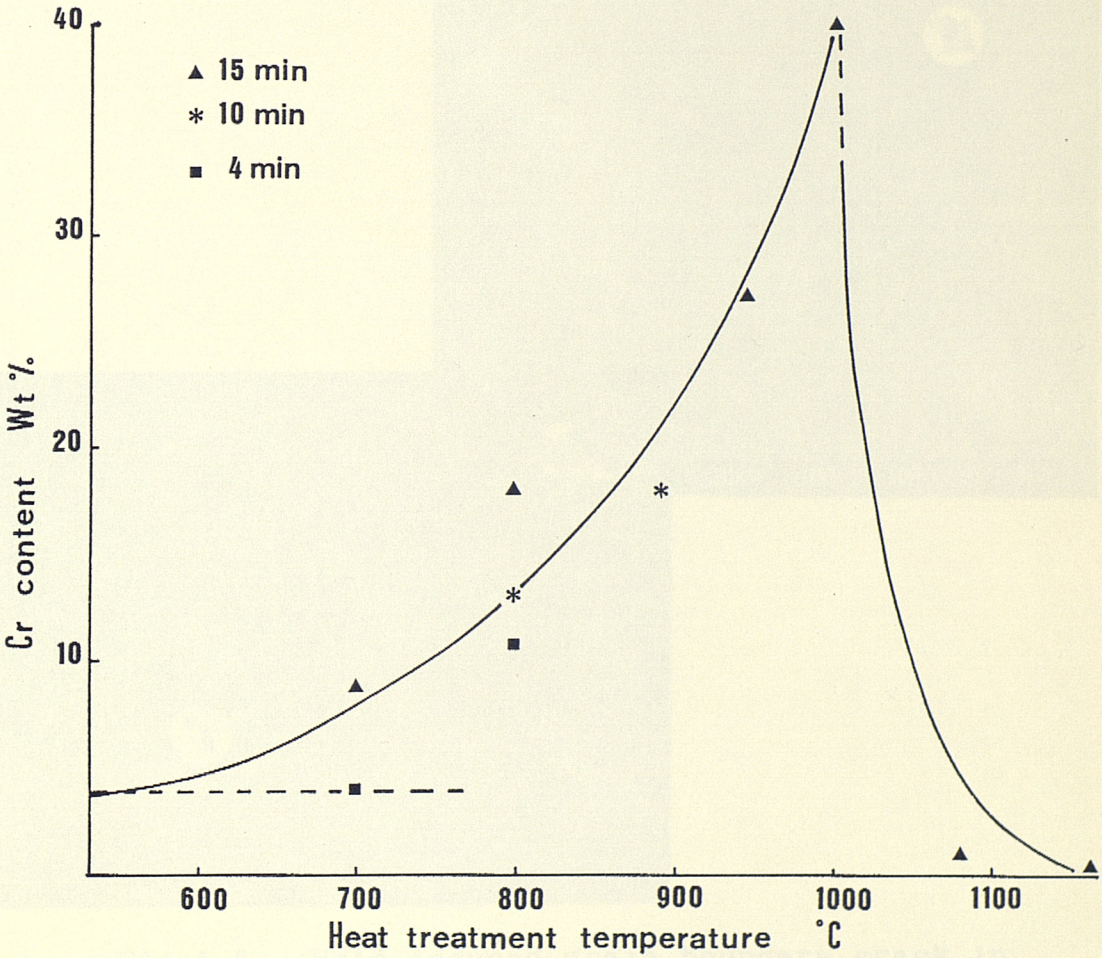

Fig 5.6 Chromium content of Type A grain boundary particles after prolonged heat treatment.

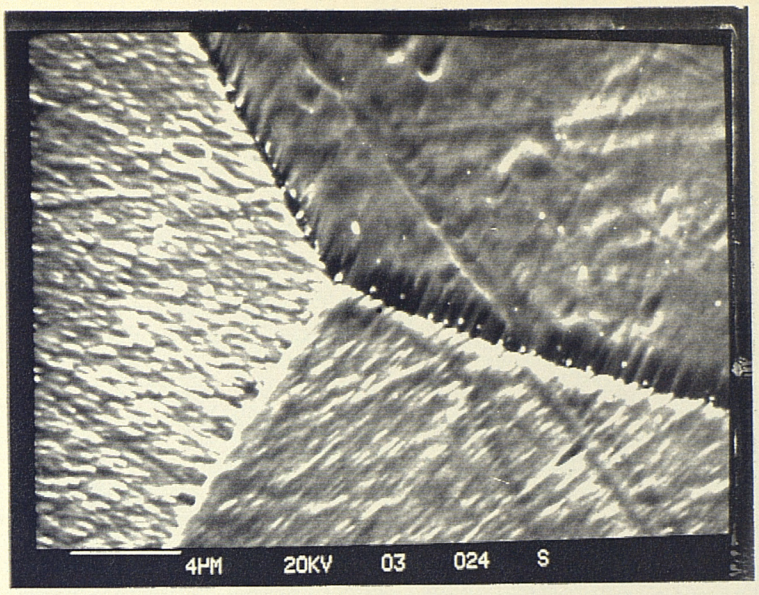

Fig 5.7 WBL-3794 dilatometer specimen heat treated at 1080°C for 15 minutes illustrating dissolution of the chromium rich Type A grain boundary particles. x3600.

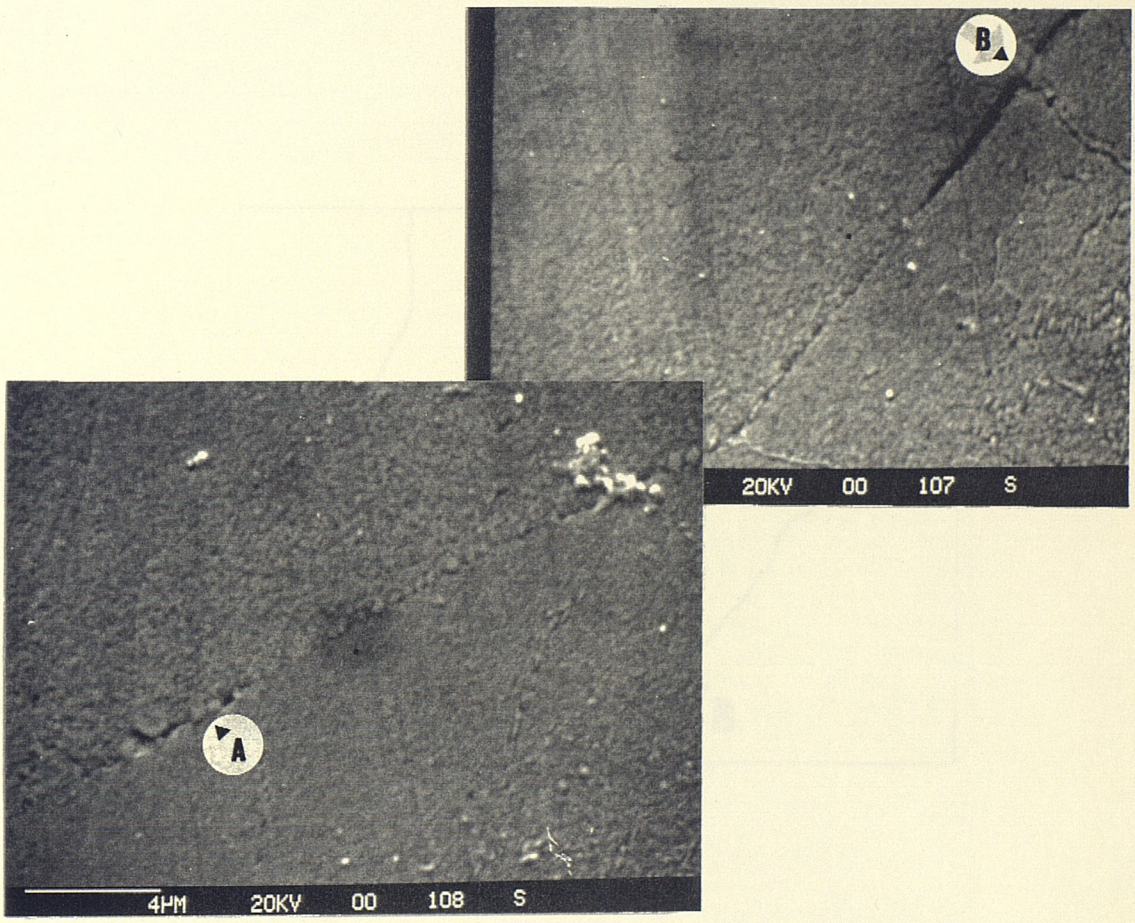

Fig 5.8 Weld induced grain boundary crack in WBL-3794 illustrating Cr and Si enriched particles 25 um in advance of the crack tip (A). The fractured particle within the crack contains 8% Cr (B). x4500.

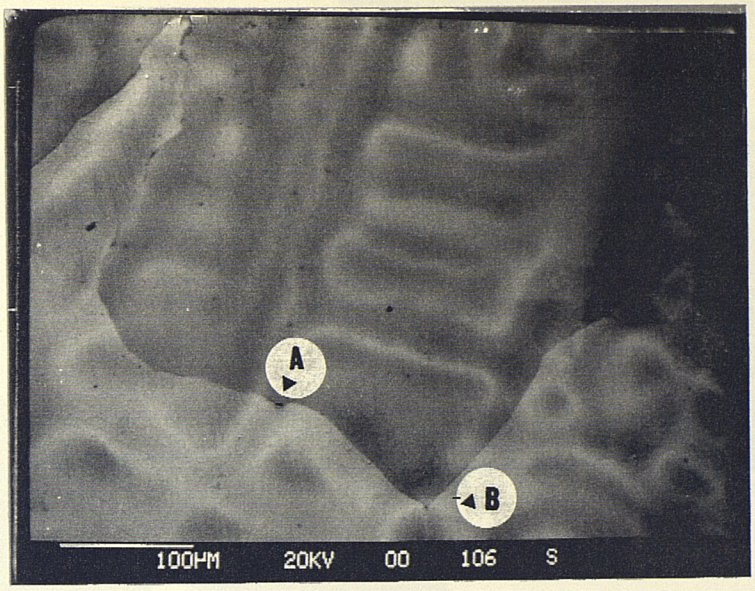

Fig 5.9 Weld induced crack in WBL-3794. x175.

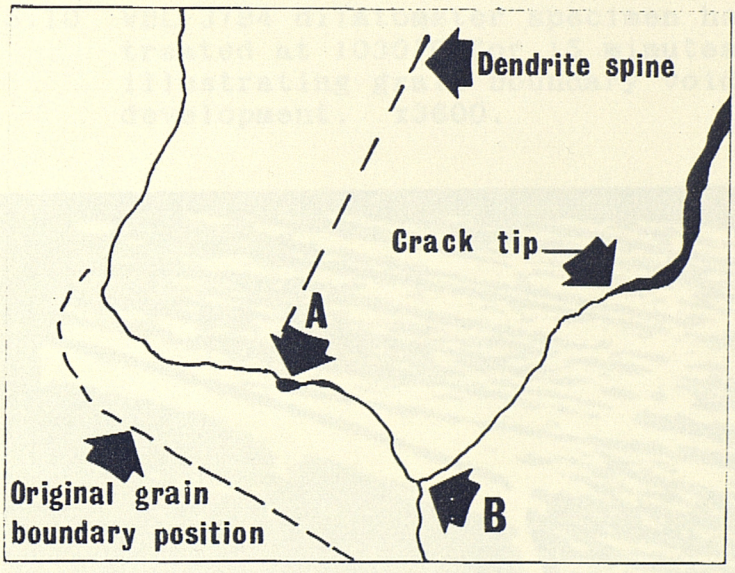

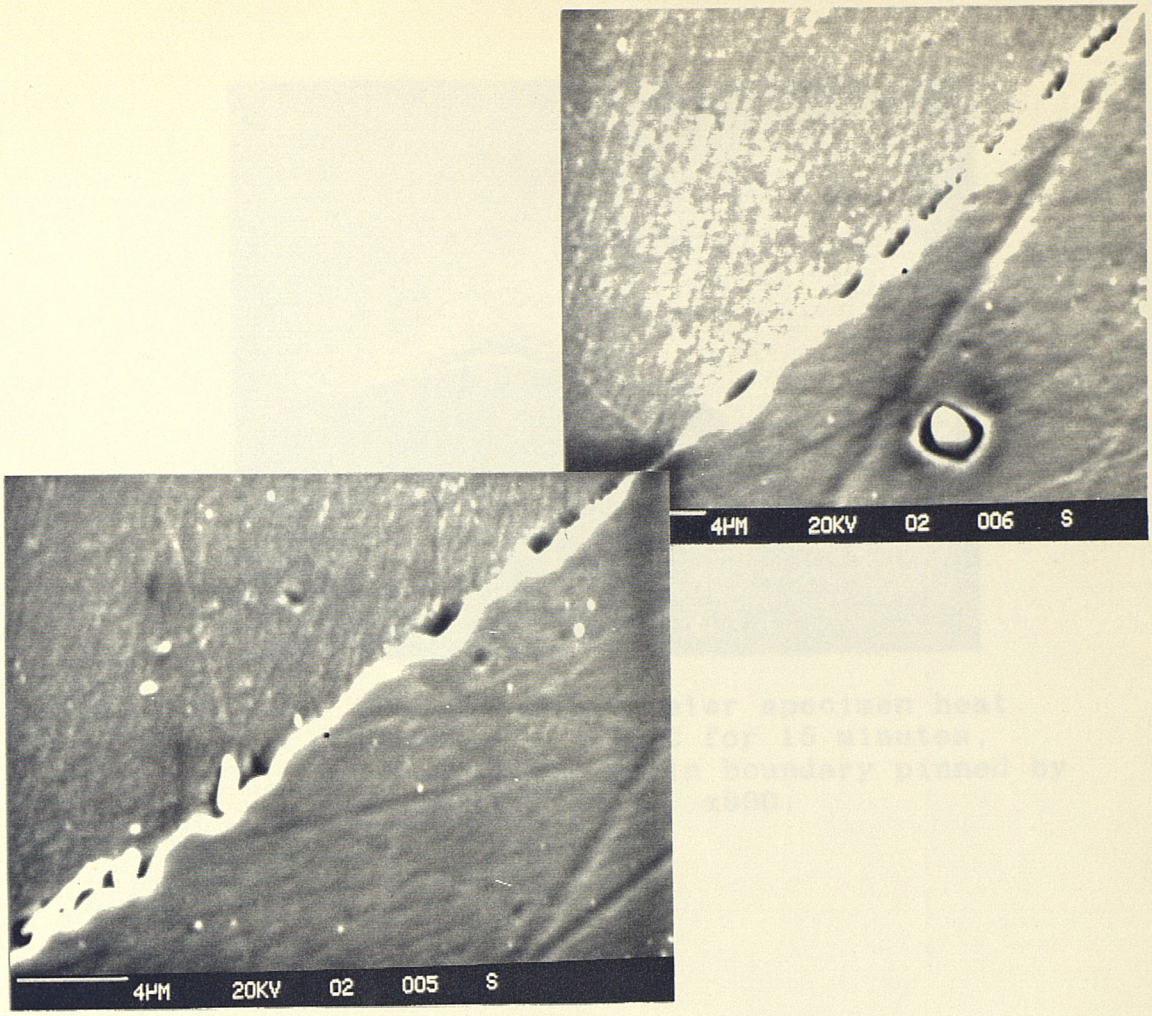

Fig 5.10 WBL-3794 dilatometer specimen heat treated at 1030°C for 15 minutes, illustrating grain boundary void development. x3600.

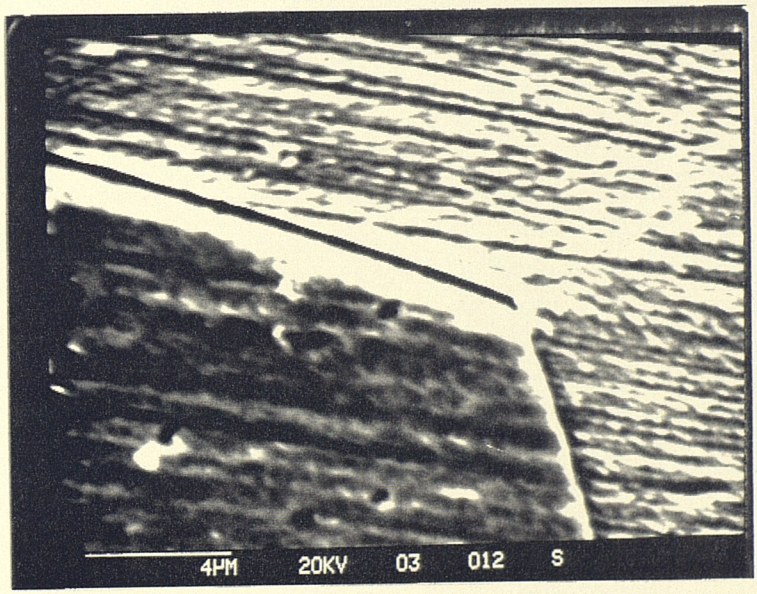

Fig 5.11 WBL-3794 dilatometer specimen heat treated at 1030°C for 15 minutes, illustrating grain boundary sliding at a triple point. x4750.

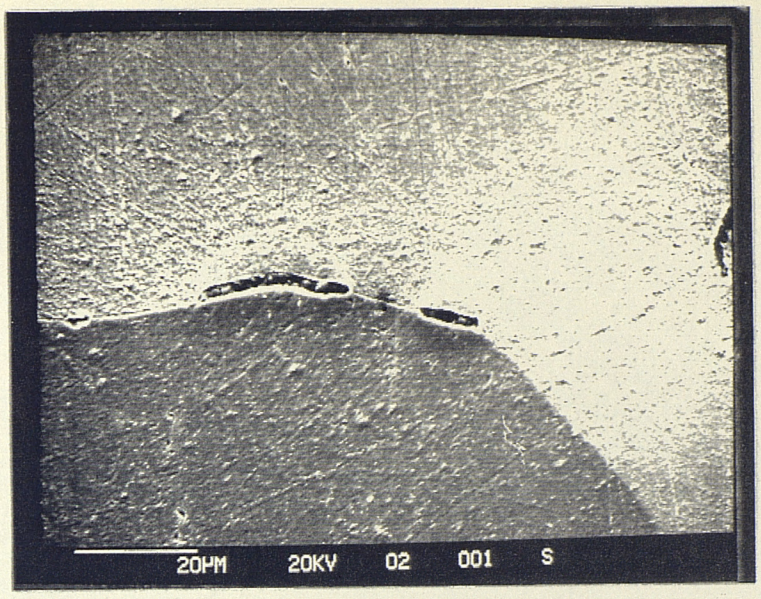

Fig 5.12 WBL-3794 dilatometer specimen heat treated at 1030°C for 15 minutes, illustrating grain boundary pinned by shrinkage pores. x800.

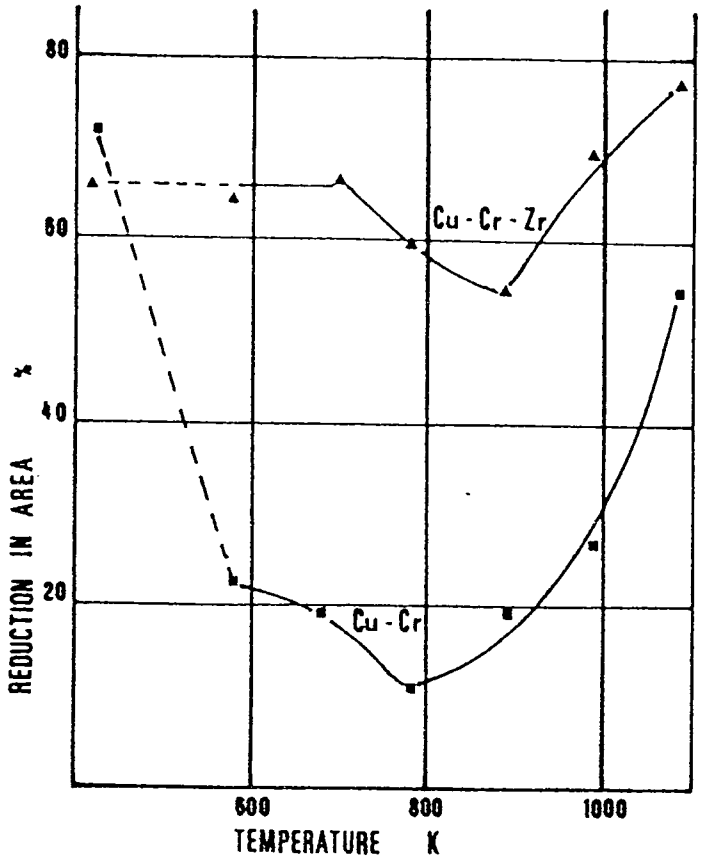

Fig 5.13 Graph illustrating the effect of zirconium on the hot ductility of a Cu-Cr alloy. (After Kanno).

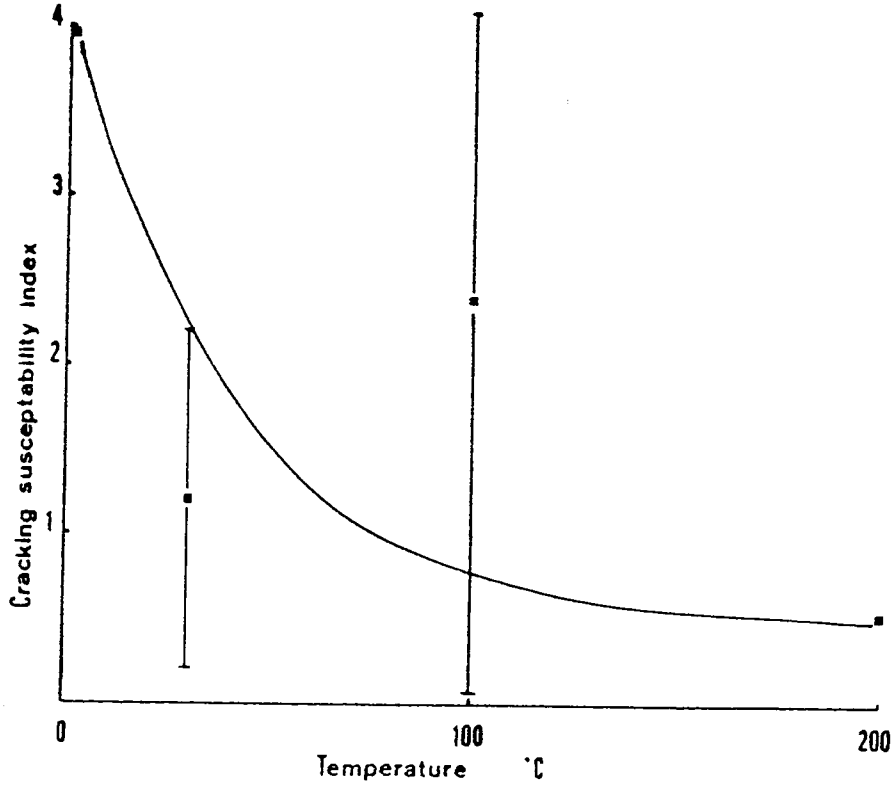

Fig 5.14 Graph illustrating the weld preheat temperature cracking susceptibility index results.

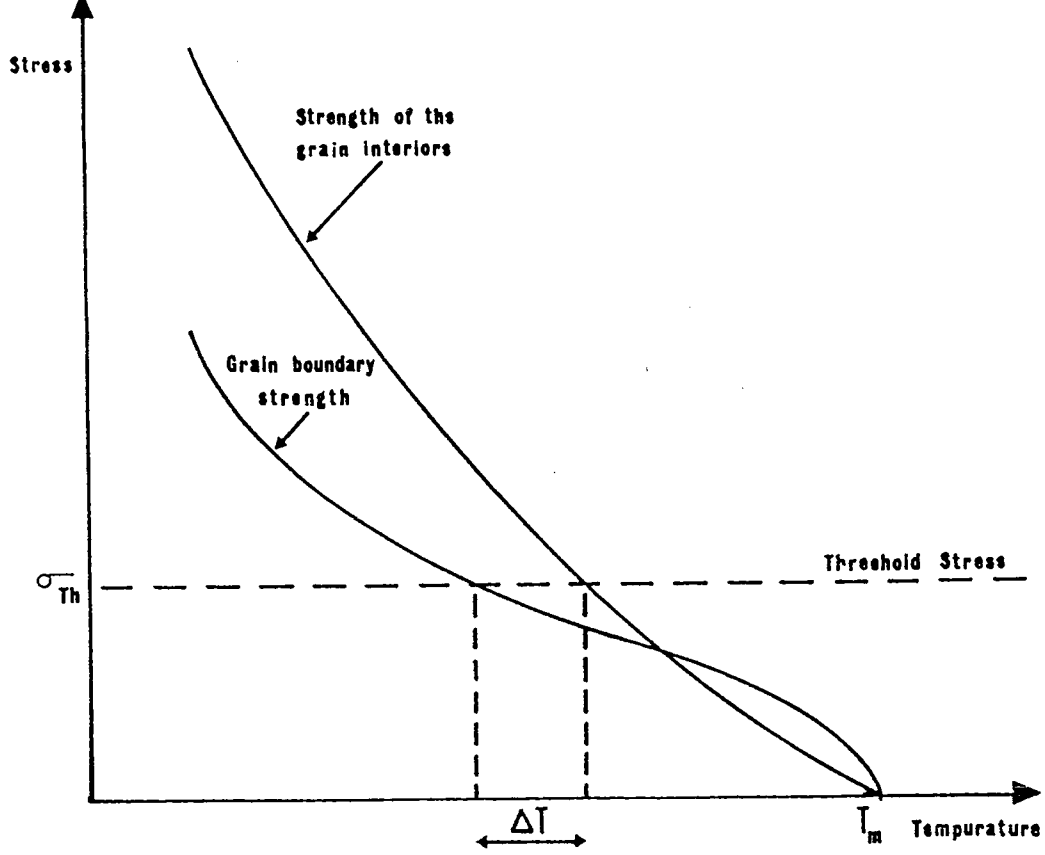

Fig 5.15 Cracking model diagram.

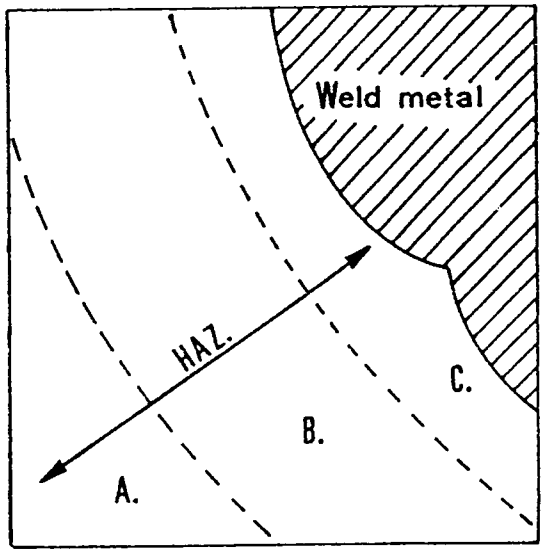

A - Lower temperature region where cracking does not occur.
B - Region in which the ΔT range of temperature is maintained producing embrittlement.
C - High temperature region where cracking does not occur.

Fig 5.16 Heat affected zone.

6 Conclusions

Four chromium hardened high strength cupronickel alloys have been studied, each manufactured at a separate foundry to comply with the MOD specification NES 824 [1]. The as cast and post welding microstructures and weld crack fracture surfaces were examined using microhardness, optical and scanning electron microscopy and EDAX techniques.

The following conclusions are drawn from observations made during this work :-

1. Cracking during welding occurs along grain boundaries in the parent plate because there is a very pronounced disparity in both strength and ductility between the matrix and grain boundary regions. This disparity, caused by a combination of factors, concentrates strain in the boundary regions.

2. Grain boundary mobility, enabling recrystallisation to occur, is inhibited by widespread shrinkage porosity, second phase particles and particles of undissolved Ti and Zr original alloy additions. These features decorate the boundaries, pinning movement and thus inhibiting the relief of lattice strain.

3. On a macroscopic scale, the grain boundary region is substantially weaker than the dendrite interiors due to very severe segregation of the alloy constituents developed during solidification.

4. Second phase particles, which decorate the grain boundaries, become enriched in chromium at elevated temperature during welding. This process denudes chromium atoms from the microscopic region immediately adjacent to the boundaries, further

weakening this narrow zone.

5. Impurities such as S,P,Pb and Bi, present in only very small quantities, will be concentrated at the boundaries during solidification. Severe reduction of the total grain boundary area, due to the very coarse grain size, will significantly increase the degree of this impurity concentration. These impurities reduce the energy required to create new fracture surface thus favouring grain boundary embrittlement.

6. Particles, and other discontinuities at the grain boundaries, promote the nucleation of micro-voids and cracks where boundary sliding at high temperature occurs.

7. Crack propagation is promoted by the reduced interfacial cohesive strength between matrix and the numerous boundary particles.

8. A foundry practice problem, consistent in all four alloys, exists whereby the alloy additions of Zr and Ti are not dissolved into solution. The improvement in hot ductility, intended to be produced by these alloy additions, consequently does not take place.

A combination of the factors listed above both weaken and embrittle the coarse grain boundaries of the cast parent plate within the temperature range ~700°C to ~900°C.

7 Future work

1. The Rosyth Dockyard alloy No. 466, reputed to be weldable [31], should be examined in similar rigorous detail, and compared with the other three alloys.

2. The techniques listed above have been extensively used to their useful limits making the observations described in this work. Further very detailed observations of the microscopic grain boundary regions, both before and after welding, now need to be made. In particular, attention should be concentrated on the region immediately in advance of weld cracking tips. A modern scanning and transmission electron microscope fitted with energy dispersive analysis equipment (STEM-EDAX) will enable fine detailed examination of the microstructure, the chemical segregation and the composition at intervals of a few nm across the grain boundary region. This treatment should reveal the cause of grain boundary embrittlement.

3. A programme of post weld cooling rate tests should be conducted to determine whether a reduction in crack susceptibility can be produced by control of this parameter. In particular, the distance between the fusion zone and position of any cracking should be closely monitored in these tests in order to more closely establish the temperature range in which cracking occurs.

List of references.

1. Naval Engineering Standard 824 Part 1 Issue 2 May 1989
2. CALCUTT VA, Conference report, Metals and Materials 1988 V4 No8 490.
3. PETERSEN WA Welding Journal 1969 V48 425s.
4. HOLSBERG PW ibid 1970 V49 554s.
5. SCOTT MH Metal Const. B Weld.J 1972 V4 292.
6. CHUBB JP & BILLINGHAM J Metals Tech. 1978 V5 100.
7. GAVIN et al ibid 397.
8. DICKERSON WC & ZANIS CA American Foundrymens Soc. Trans. 1973 V81 388.
9. SAHOO M & CAMPBELL WP ibid 1980 V88 727.
10. BAKER & NEWMAN Metal Const. & the Brit. Weld. J. 1969 V16 1.
11. HEMSWORTH B, BRONISZEWSKI T & EATON NF ibid. 5.
12. HADRILL DM & BAKER RG ibid. 1965 V 12 411.
13. ROLLASON & BYSTRAM J. Iron & Steel Inst. 1951 V 169 347.
14. DUVALL & OWCZARSKI Welding J. 1966 V 45 356s.
15. EVANS RW & JONES Metals Tech. 1976 V 3 494.
16. DAVIES PW & EVANS RW Acta Metallurgica 1965 V 13 353.
17. GITTINGS & WILLIAMS Philosophical Mag. 1967 V16 849.
18. EVANS HE Metal Sc. J. 1969 V3 33.
19. STEVENS Metallurgical Reviews 1966 V 11 129.
20. THOMAS & NUTTING J. Inst. of Metals 1959/60 V88 81.
21. STARKE J. of Metals 1970 V 22 54.
22. LEE, NICHOLS & GOODMAN Welding J. 1968 V 47 371 s.
23. SAVAGE & LUNDIN ibid 1965 V 44 433 s
24. HOLSBERG ibid 1970 V 49 554 s.
25. PETERSEN ibid 1969 V 48 425s.

26. SAVAGE, NIPPES & CASTERAS Welding J. 1978 57 375 s.
27. GAVIN, BILLINGHAM, CHUBB & HANCOCK Metals Tech. 1978 V 5 397.
28. KANNO Z. Metallkde 1988 V 79 No. 10 684.
29. PLUMB Fleet Maintenance and Repair Organisation HM Naval Base Portsmouth 1989 Report No 89021 (UK Restricted).
30. CHUBB & BILLINGHAM Metals Tech. 1978 V 5 100.
31. MOD Procurement Executive (Bath).
32. Smithells Metals Reference Book. 6th ed. Butterworths 1983.
33. BIRKS LS. Electron Microprobe Analysis. Interscience 1963.
34. REED JSB. Chapter 3, Analysis of High Temperature Materials, edited by O Van Der Biest. Applies Science Publishers 1983.
35. SAHOO M, WANG KC & EDWARDS JO American Foundrymens Soc. Trans. 1979 V87 529.
36. Naval Engineering Standard 824 Part 2. Issue 1 September 1987.
37. BADIA KIRBY & MIHALISIN Trans ASM 1967 V60 395.
38. HOPKIN LMT J Inst of Metals 1955-56 V 84 102.
39. STEVENS RN Metallurgical Reviews 1966 V 11 129.
40. McLEAN Mechanical Properties of Metals. J Wiley & Son 1965.
41. SMALLMAN RE Modern Physical Metallurgy. p 397 1970 Butterworths.
42. ANSUINI & BADIA AFS Trans 1970 V 78 165.
43. SAHOO & BOYD Canadian Metallurgical Quart. 1982 V 21 No3 281.
44. PETERSEN Welding J Supp 1969 V 48 425 s.
45. STARKE EA J Metals 1970 V 22 54.
46. SAVAGE, NIPPES & MILLER Weld J 1976 V 55

165s.

47. SCHEY JA Introduction to Manufacturing Processes 1977 McGraw - Hill.

48. SAUNDERSON RI, WILKES P & LORIMER GW Acta Metallurgica 1978 V 26 1357.

49. GITTINGS & WILLIAMS Phil Magazine 1967 V 16 849.

50. DION, EDWARDS & CAMPBELL AFS Trans 1977 V 85 143.

51. COTTRELL A An Introduction to Metallurgy Ch 21 -1975 Edward Arnold.